Rick Aster

Magnetic Gradiometry Applications in Unexploded Ordnance and Land Mine Detection

Joseph T. Duncan
Department of Earth and Environmental Sciences
Geophysics Program
New Mexico Institute of Mining and Technology
Socorro, N.M. 87801

Magnetic Gradiometry Applications in Unexploded Ordnance and Land Mine Detection

By:
Joseph T. Duncan
Department of Earth and Environmental Sciences
New Mexico Institute of Mining and Technology
Socorro, N.M. 87801
May 10, 1997

This Report is an Independent Study In Partial

Fulfillment of the Master of Science Degree in Geophysics

Research Advisor:
Dr. Allan Sanford
Department of Earth and Environmental Sciences
New Mexico Institute of Mining and Technology
Socorro, New Mexico 87801

Funded By:
Energetic Materials Research and Testing Center
New Mexico Institute of Mining and Technology
Socorro, New Mexico 87801

Technical Abstract

The current global proliferation of land mines and sources of unexploded ordnance (UXO) must be combated with rapid, accurate, and cost effective detection technologies. One such technology involves magnetometer sensors used to map lateral variations in the Earth's magnetic field. Using two cesium sensors as a differential gradiometer, the Geometrics G-858 magnetometer was used in the detection of magnetic and non-magnetic land mines and UXO. The EMRTC Counter-mine Test Site provided a survey area with a variety of buried land mine and UXO targets. An off-site test pad also served as a survey area for controlled gradiometric experiments.

The Control Test Pad yielded magnetic maps of background soil magnetism, gradiometric characteristics of buried voids and inert dummy land mines, and provided detectability limitation on metallic and non-metallic materials. The Counter-mine Test Site provided magnetic gradient signature anomalies for two Italian land mines, four U.S. land mines, and a variety of ordnance sources. The gradiometer accurately detected the location of magnetic anti-personnel and anti-tank mines and detected some non-magnetic mines due to susceptibility contrasts only in soils of low magnetic noise. UXO sources were detected based on their high metallic content.

Detection rates for land mine and UXO surveys were also determined using both initial and filtered gradient data. Spatial filtering removed long wavelength trends which provided higher detection rates for the sharp peak anomalies associated with shallow objects. False positives were encountered during detection surveys. The sources of false positives included induced magnetization from magnetite contrasts in sub-surface rocks and soil, metallic debris, and remnant magnetization from thermal and lightning activity.

Table Of Contents

Table Of Contents Continued

Table Of Contents Continued

Table Of Contents Continued

List of Tables

List of Figures

List of Figures Continued

List of Figures Continued

Figure Number — Page

Chapter 1

Introduction: Counter-Mine Operations

1.1 Global Land Mine and Unexploded Ordnance Crisis

1.1.1 Current Global Statistics

"The land mine has been called the 'perfect soldier'. It's ever courageous, it never sleeps, and it never misses" (Hurley, 1997). Today there are an estimated 110 million anti-personnel land mines in the ground around the world and another 100 million in stockpiles. Between 5 and 10 million more land mines are produced each year, earning their manufacturers hundreds of millions annually (Oneworld, 1997). Joining these staggering numbers are anti-tank mines and unexploded ordnance. Worldwide, these weapons have found their way onto the country side of more than one-third of the world's countries. Famous wars and obscure revolutions have contributed to the pervasive distribution of these unseen killers.

The degree of infestation varies, with countries like Afghanistan, Angola and Cambodia possessing the greatest numbers. In Africa alone, an estimated 20 million land mines are distributed through nearly half the countries of the continent. All tolled, over 60 countries are in need of mass demining projects, as their land mines are held responsible for the deaths of over 12,000 people every year, more than 1000 people every month, and nearly three times this number are maimed or injured. Of the over 130 people killed or injured by anti-personnel mines daily, half die either immediately from the explosion or from blood loss and exposure (Oneworld, 1996). The current number of severely disabled survivors, of whom over 300,000 are children, are

quickly becoming a significant demographic percentage of many third-world countries.

Land mines and unexploded ordnance do not recognize cease fires, or treaties; even after the end of hostilities, even decades afterwards, anyone who strays into a mine-field is at risk. Of the armies who have practiced land mine warfare, nearly all would not be capable of remediating their own deployments, for most mine-field are unmarked and no one remembers exactly where they buried them. Land mines, like those seen in Figure 1.1, do their job with chilling efficiency just waiting to be triggered, without any means of self-neutralization, but rather multiple means of detonation. Thus everyone is vulnerable, creating longer-term costs for communities, stretching resources, and permanently restricting access to land for agriculture, grazing, and trading.

Closer to home, the United States also suffers from some degree of infection. Unexploded ordnance (UXO) is one of the most serious and prevalent environmental problems at DOD facilities. This includes active sites and test ranges as well as the formerly used defense sites. UXO is generally considered to be artillery or bombs that failed to explode on impact, leaving armed explosive debris scattered or possibly buried. The U.S. military admits that this actually occurs nearly 5% of the time. However this residual UXO source is usually only found within countries the U.S. has battled or remote testing ranges. The chief source of UXO within defense facilities is comprised of lost, misplaced, or abandoned ordnance. Often the ordnance is left in road-side bunkers or dropped on test ranges to be buried by sediment and debris. Recent studies have shown that ordnance components are the second most frequently occurring contaminant at U.S. Army sites, and were reported at nearly 20% of the 1100 Army facilities surveyed (ESTCP, 1996).

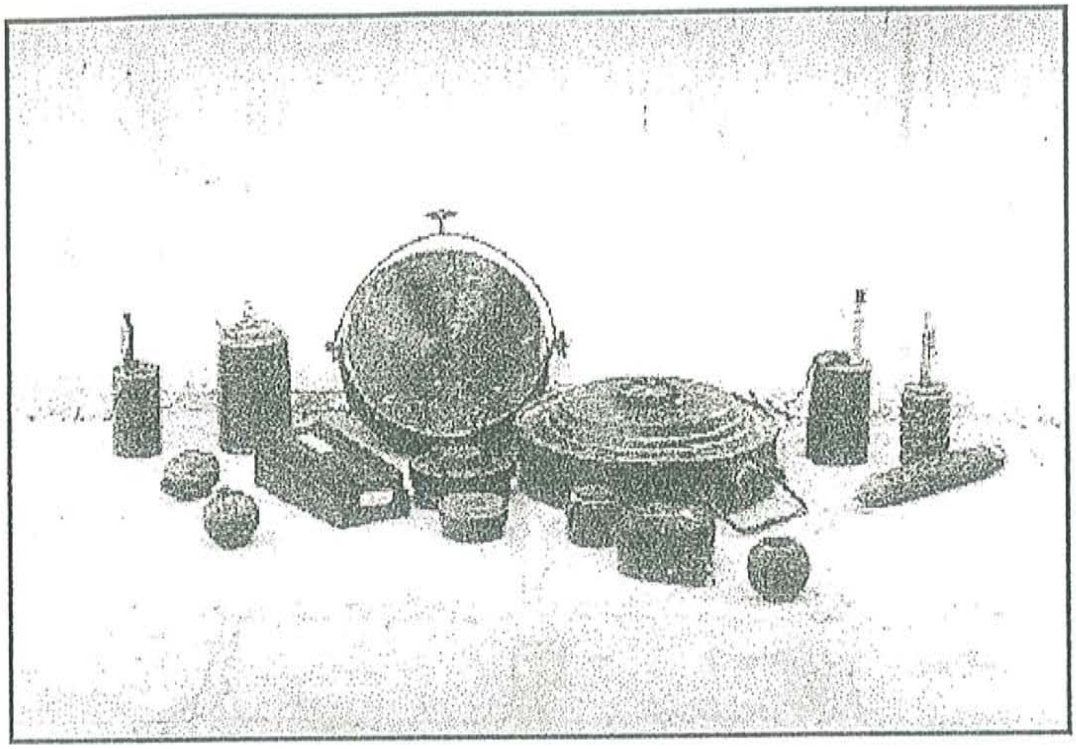

Figure 1.1: An assortment of widely used Anti-Personnel and Anti-Tank mines. The small objects are blasting mines designed to maim. The mid-size canisters are fragmentation mines lethal to tens of meters, while the largest mines are designed to destroy armored vehicles. (Dunlop, 1995)

The dangerous combination of incredible numbers and insufficient demining efforts has made the land mine crisis one of the greatest challenges facing politicians, scientists, and the world community. The global debate on banning land mine use may rage on, but the question of land mine and UXO remediation is one which has become increasingly important but equally difficult. The demining of former war zones and the UXO clean up of countless facilities will require the cooperation of not just Heads of State, but of competing technologic and scientific genres as well. For while it may be assumed that a land mine is a relatively simple thing to track down and neutralize in a world of high technology, it is far from the truth. The sheer number of mines scattered over endless search areas , combined with the vast

variability of composition, terrain, and climate, has made demining a formidable task.

1.1.2 Current Solutions for Land Mine and UXO Remediation

Obviously solving the land mine and UXO problem requires finding all possible sources and eliminating them. It is the detection part of this solution that has brought the scientific and engineering investigators to the forefront of demining projects worldwide. Their efforts, termed counter-mine operations, seek to create a rapid, affordable, but extremely efficient, technology to bring to the world market. These detection technologies are as vast in their scope and variety as the targets they seek.

Land mine detection methods are normally based upon two different strategies. The first may be employed when a land mine or UXO source, buried beneath the surface, disturbs the surrounding and covering soil from its original state. There then becomes a change in the soil properties that may be used as a means of identification. The second strategy is dependent on the properties of the source itself. A buried land mine will possess different properties (such as density, strength, thermal capacities, etc.) compared to the surrounding soil. Thus the variation in the physical properties of the soil, or the soil and the target, are the basis of all demining methods.

There are three categories into which present demining methods fall: hand-prodding, brute-force, and high-tech. Hand-prodding is the most reliable method of mine clearing, by which a probe is manually inserted into the soil at a 30° angle, approximately every five centimeters. When a solid object is detected, several more probings are conducted to get a feel for the shape and size of the object. If the object is determined to be a potential mine, a mine clearing team comes in to uncover the object. Figure 1.2 shows a

Cambodian explosive ordnance disposal (EOD) team member hand-prodding for land mines during an initial effort to clear a civilian foot path through a known mine field. Needless to say, this is a very slow, and extremely dangerous method of mine clearing, as a person performing this task will require frequent rests and is continuously at risk. On the average, this method takes about 4 minutes to clear about one square meter of land (Fyfe, 1996).

Figure 1.2: The hand-prodding demining technique employed by an EOD team member from Cambodia. The soil is explored with a probe very thoroughly until a mine is discovered. It is then uncovered, neutralized and removed, eventually leaving a safe, demined path through which farmers and children may travel. (Dunlop, 1995)

Brute-force demining is neutralization without detection. This method generally utilizes plows, rollers, and flails mounted on tanks, or explosives, to purposely detonate buried mines. These implements are generally effective in clearing paths for soldiers and vehicles through a mine-field in time of war, but in peace time these demining methods are of little use. The plows and rakes destroy the ground, or only push the mines out of the way, leaving them armed. The flails, heavy rollers and explosives are effective at destroying simple mines, but smart mines can avoid them, only detonating the second or third time they are triggered (Fyfe, 1996). These brute-force methods are also only practical in areas known to only harbor anti-personnel mine, as anti-tank mines or unexploded bombs would destroy most brute-force apparatuses or vehicles. Additionally, for peace keepers in a neutral zone between two opposing forces, it is required that mines be detected and removed without detonating them, as explosions in these fragile situations could be counter productive.

Low-tech methods, such as metal detection, have been around for decades. However, they have proven to be inadequate considering the current state of non-metallic mine technology and sheer numbers associated with all sources. High-tech methods of mine detection are just beginning to reach the world stage, but are still very expensive, have low accuracy, and a high false alarm rate. A false alarm is when a benign object is identified as a mine, such as a rock, tree root, or harmless metallic debris. This wastes time as an EOD team must assume it is dangerous and follow their standard demining procedures, during which time no other activity can take place in the area. This is again why accurate, but affordable, counter-mine technology has become the focus of many scientific, military, and humanitarian organizations around the world.

Of the wide array of proposed implements and instruments devoted to counter-mine efforts, a classification was put forth recently in a 1996 NATO Report on Demining Technology. Table 1.1 shows the variable sensor types and their developmental status and comparative cost (Oneworld, 1997).

Table 1.1: Classification of Potential Demining Technologies

Sensor technology	Developmental Status	Comparative Cost
Passive infrared	Near	Medium
Active infrared	Near	Medium
Polarized infrared	Near	Medium
Passive electro-optical	Near	Medium
Multi-hyperspectral	Far	High
Passive mm-wave	Far	High
mm-wave radar	Near	High
Ground penetrating radar	Near	Medium
Ultra-wideband radar	Far	High
Active acoustic	Mid	Medium
Active seismic	Mid	Medium
Magnetic field sensing	Near	Medium
Metal detection	Available	Low
Neutron activation analysis	Near	High
Charged particle detection	Far	High
Nuclear quadrupole resonance	Far	High
Chemical sensing	Mid	High
Biosensors	Far	High
Dogs	Available	Medium
Prodding	Available	Low

Of the promising new technologies in development, no single sensor will be reliable enough to find every mine in every situation, hence the need for sensor fusion, that is, the use of multi-sensor array platforms combining the data of several sensor technologies. It is of primary importance that scientists in each discipline share their knowledge and the result of their experiments in order to design solutions for humanitarian demining. War-time detection rates of 80% are not acceptable, for it is obvious that any suitable system have a detection rate approaching perfection. United Nations

specifications require better than a 99.8% detection rate for humanitarian applications (Fyfe, 1996). For this to come to past, new technologies must be developed to increase the detection rates and to automate the infield detection procedures whenever possible to preserve the life of the mine clearing personnel.

Research and development break throughs have occurred in several areas of detection, including ground penetrating radar (GPR), induction coil sensor imaging, infrared imaging, millimeter wave emission, and explosive detectors such as vapor sensors and thermal neutron activation (Fyfe, 1996). No single sensor has the capability of reaching a perfect detection rate while having a low false alarm rate, when considering the variety in the types of soil, mines and false targets encountered in the world. Rather, complementary sensor technologies should be used with the appropriate data fusion to increase their efficiency. Sensor fusion is currently in several stages of development and possesses the highest detection rates and possible applications. However, many of the individual sensor technologies are relatively embryonic with long strides left to fully understand their capabilities. Therefore, currently available technology should be explored to its limits. Instrumentation previously used in other disciplines may well be a link between what is already in use and what is still deep in development. One such instrument is used to explore the composition and structure of the Earth's sub-surface using the planets own magnetic field. The magnetometer is capable of measuring components of the magnetic field and thus providing indirect information as to the composition and geometry of objects in its vicinity.

1.2 Magnetic Applicability To Counter-Mine Efforts

1.2.1 Contributions to Counter-Weapon Technology

Metal detection devices have been used in counter-weaponry roles for over half a century (Telford, 1990). Arguably one of the first applications for magnetometers was in metal detection. Eventually a magnetometer was found to possess greater sensitivity, and wider detection threshold, to nearby metallic objects than induction type metal detectors. However, both types of detectors generally can not differentiate a metallic mine from metallic debris. In most battlefields the soil is contaminated by large quantities of shrapnel, metal scraps, and cartridge cases, leading to possibly hundreds of false alarms for each real land mine (Fyfe, 1996). Yet the magnetometer provides significantly more information on the target, such as scale and depth of burial. Thus the magnetometer has enjoyed some success for over 30 years in the detection of land mines, small arms, ammunition, booby traps, and vehicles (Cameron, 1967). It will become more successful with the advent of better sensor data fusion technology combining the best aspects of sensor spectra.

Having an equally extensive history in non-military applications such as geologic and forensic investigations, the magnetometer has undergone continuous evolution and development. Magnetometer instruments possess a wide variety of internal designs: Schmidt-type, torsion, flux-gate, proton procession, and vapor-type magnetometers (Telford, 1990). Each evolution leads to greater sensitivity, accuracy, and sampling speed. The current cesium vapor type is the state of the art in magnetometers (Geometrics, 1995).

1.2.2 Magnetic Research Purpose and Goals

The Independent Study encompassed within this report was initiated entirely for the purposes of exploring the applicability and limitations of a contemporary, state-of-the-art magnetometer in counter-mine operations, specifically the detection of land mines and UXO. The manufacturers' advertised specifications and capabilities of the Geometrics G-858 Cesium Magnetometer indicated that it was clearly an advanced remote sensing instrument in the field of magnetic exploration and thus it became the chief focus of this research endeavor. The instrument's sensor sensitivity, 0.1 nT per meter, and the use of differential measurements from two closely spaced sensors make it possible to detect magnetic disturbances arising from small objects, including voids, in the presence of a great deal of magnetic noise (Geometrics, 1995).

There are two chief problems addressed in this investigation; the magnetic signatures of iron and steel ordnance and those for non-magnetic ordnance. The magnetic anomalies detected from UXO are those arising from any ferrous material associated with the ordnance including projectiles, cartridges, casings, fuses, and fragmented debris. For detection of non-metallic UXO or mines, an examination of soil/target magnetic susceptibility contrast is applied. The anomalies produced by these objects arise from susceptibility variations existing after replacing the ground material, generally soil containing magnetic grains and possibly remnant magnetism, with objects of different or zero magnetic susceptibility. This is similar to detection of magnetic objects but anomalies of smaller intensity can be expected. The overall pattern of the magnetic anomalies produced by land mines and UXO, as well as their magnitude, may be used in the detection

process. Another goal of the study is the identification of natural conditions in the ground that might produce false alarms.

An accurate understanding of the intrinsic gradiometric properties of the test UXO and anti-personnel mines will only result from strict environmental and subsurface control. This control may be facilitated by the use of homogeneous soils of adequate depth and density, realistic stratigraphic profiles, and carefully measured positioning of true and dummy targets. All the physical variables needed to construct proper models and to develop methodologies useful in detection programs are best completed with a test pad in which the environmental and geologic conditions can be easily controlled. In addition to controlled environments, this study takes advantage of a land mine and UXO testing facility located on the Energetic Materials Research and Testing Center's (EMRTC) field laboratories. The EMRTC invitation extended to the New Mexico Tech Geophysics Program for on-site research, during U.S. Army regulated testing, provided vital real world data.

The following chapters of this Independent Study address the instrumentation and magnetic methods employed, provide control and field data, convey data analyses and survey results, investigate false target sources, and discuss the applicability of the cesium magnetometer and its gradiometric capabilities to counter-mine efforts.

Chapter 2
Methods: Magnetic Exploration

2.1 Magnetic Prospecting

2.1.1 Theory

One of the chief assumptions of geomagnetic theory is that the intrinsic magnetic behavior of our planet, to first order, can be approximated by a dipole bar magnet. This best-fit dipole aligns a magnetic south pole 11.5° from geographic north, and a corresponding magnetic north pole from the geographic south (Fowler, 1990). Thus the lines of magnetic flux that normally flow from a bar magnet's north to south poles, are also measured emanating from the Earth's geomagnetic poles with similar behavior, ascending latitudinally. Field lines exist over the entire surface of the earth, maintaining an angle of inclination with the vertical depending on the magnetic latitude. For example, the inclination of the field lines at the equator is horizontal while the polar regions have a vertical inclination.

The magnetic field lines, or flux, are vector quantities possessing both a magnitude and direction, termed intensity and inclination. These quantities vary both with latitude and longitude as seen in Figure 2.1. The distribution of magnetic inclination, or the angle between the field lines and the horizontal, changes with time at a predictable rate. The ambient strength of the magnetic field also varies proportional to inclination. The background field strength at the poles is nearly 60,000 nanoTesla, while that of the equator is only 30,000 nanoTesla (Steiner, 1977). This is consistent with the Earth's spatial density of magnetic field lines; the closer the field lines are to one another, the stronger the field. The ambient magnetic conditions at this location in Socorro, New

Mexico, consist of a field strength average of about 50,700 nanoTesla at an inclination of 61 degrees.

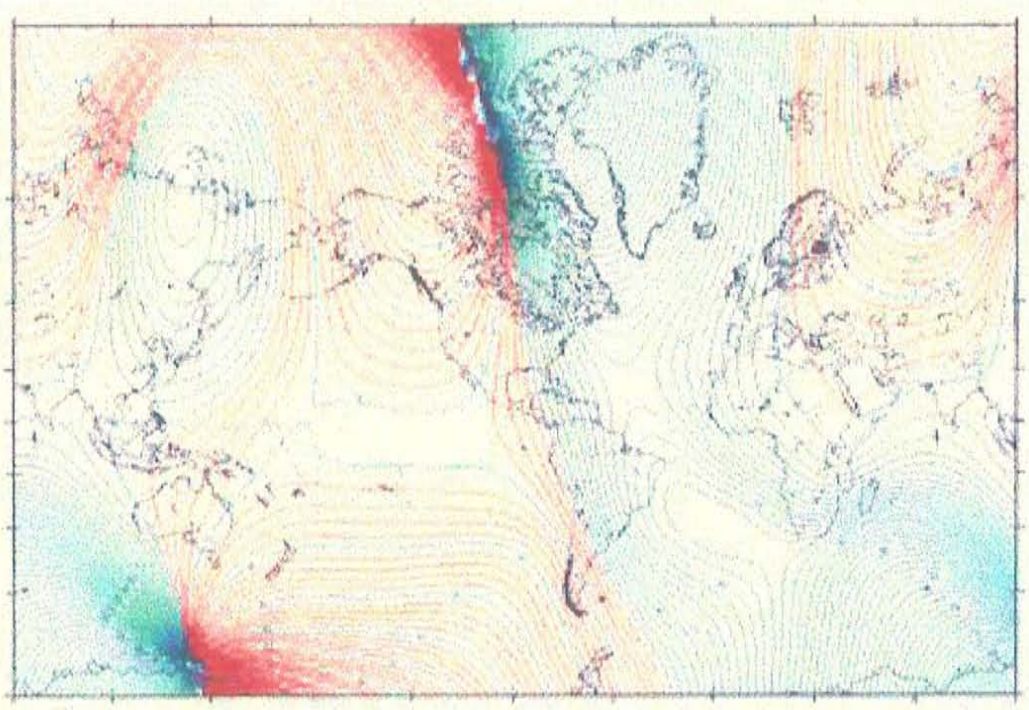

Figure 2.1: Map of the World Magnetic Inclination. Ambient magnetic intensity is inclination dependent and varies from 30,000 nT near the equator, to over 60,000 nT near the poles. Ambient intensity at survey locations within this study were on average 50,700 nT at an inclination of 61°.

Magnetic prospecting involves measuring some component of the Earth's magnetic field; either horizontal, vertical, or total. These measurements provide information on magnetic structures beneath the surface which influence the magnitude and direction of the ambient field locally. Non-magnetic structures within the sub-surface may also be detected because the soils that conceal them contain various iron minerals, some of

which are slightly magnetic. The variations in magnetic susceptibility between adjacent sub-surface material causes anomalies in the magnetic field. It is the resulting anomalies from susceptibility contrasts that provide insight into the materials' dimension and composition. The magnetic susceptibility of an object is its ability to be magnetized by an external field. Objects that behave magnetically in an applied field are considered to display induced magnetism. If the magnetism exists independent of the applied field, the material is considered to possess permanent magnetism (Sanford, 1994). Both types of magnetism create characteristically similar anomalies within the earth's field, and are difficult to distinguish during a magnetic survey.

There are several factors that contribute to a successful magnetic exploration. The distance from the field sensor to the intended target is of key importance due to the fact that the intensity is generally inversely proportional to the cube of the distance. The detectability of any target is also dependent on its constituent amount of ferromagnetic material in contrast with its surroundings (Steiner, 1977). In addition, it is vital that all possible sources of background noise be considered, including, geologic conditions, habitational objects and debris, and buried or suspended current lines. Finally, it should be remembered that the ambient magnetic field varies throughout the day, a phenomenon termed diurnal drift, and must be considered when analyzing magnetic data.

2.1.2 Survey Technique

The application of portable magnetometers is essentially the identification and description of spatial changes in the Earth's magnetic field (Steiner, 1977). A magnetometer is used to sample the earth's field at known heights above the surface, and at known lateral position within an area. This

sampling is continued at specific distance intervals until the desired coverage is completed. The two most common survey procedures are line surveys and grid surveys. A line survey consists of one or more lines running in a continuous direction, i.e. north to south, etc., with magnetic measurements taken at constant intervals depending on the desired resolution. The data generated are represented on two dimensional plots, termed magnetic anomaly curves, with field strength plotted against lateral position.

A grid survey consists of several line surveys run adjacent to one another, maintaining a line separation equal to the sampling distance interval with each line. Generally the distance spanned within each line is on the order of the distance spanned from the first line, laterally to the last, if not exactly the same. Thus the resulting data are plotted as contour maps with field strength magnitudes mapped onto surface positions. Both the anomaly curve and the contour plot are commonly used tools in the representation and analyses of grid magnetic data, and will be utilized in many sections of this study.

Magnetic data itself can take many forms, depending on the type and orientation of the sensor used, generally only one directional component of the earth's total field is recorded. The measurement recorded by most magnetometers is the total magnetic field intensity, that is the magnitude of the total magnetic field vector with directional information ignored. There exists several sources of naturally occurring spatial and temporal variations in this field that are treated as noise or interference in the data and must be dealt with accordingly. This phenomenon will be addressed in a subsequent chapter.

The traditional unit used in geophysics for the measurement of variations in the earth's magnetic field strength is the gamma (γ). In the S.I.

system 1γ equals 0.79 milliamp/meter of field strength, which also equals 1 nanoTesla of magnetic induction, and generally there is no distinction made between field strength and magnetic induction (Aitken, 1974). The data addressed in this paper will use the nanoTesla (nT) unit for magnetic field strength and nanoTesla per meter (nT/m) for magnetic gradient.

The sources of magnetic anomalies within any survey are complex. The anomalies mapped may occur over fractions of meters or thousands of meters and are usually caused by an anomalous distribution of magnetic minerals, iron objects, or cultural features. Naturally occurring rocks and minerals are often the principle sources of mapped anomalies due to the presence of magnetite (Fe Fe_2O_3), or its related minerals, ulvospinel, titanomagnetite, and maghemite. Collectively referred to as magnetite, these minerals are usually dark, heavy, hard, and resistant to mechanical or chemical erosion. Common forms of iron oxide are not usually magnetic and are seldomly related to the source of magnetic anomalies (Steiner, 1977).

All rocks contain some magnetite from very small fractions of a percent up to several percent, and even several tens of percent in the case of magnetic iron ore deposits. The distribution of magnetite or certain characteristics of its magnetic properties may be utilized in magnetic surveys to aid in the detection of objects buried naturally or intentionally planted. Furthermore, cultural features associated with man's habitation can frequently be detected through magnetic surveys owing to the contrast in sedimentary magnetite distribution. This includes man-made structures, voids, or the enhanced magnetic effects of fire and baking (Steiner, 1977). The various types of magnetism will be address in a subsequent chapter.

When performing a magnetic survey, several concerns must be addressed to ensure the integrity of the data. First there is the magnetic

cleanliness of the operator and the survey site. To accentuate the targeted sub-surface's magnetic signature, it is necessary to reduce data contamination resulting from magnetic materials, electrical equipment, magnets, compass, iron tools, etc. Care should also be taken to maintain consistent sensor height and lateral position for accurate mapping correlation. Sources of high magnetic interference such as large metallic surface objects, power lines, fences, and vehicles should be avoided as they will corrupt the data if in close proximity.

As stated in the introduction, a motivating factor of this research project was the availability of a state-of-the-art magnetometer. The field surveys conducted during this project were facilitated by the capabilities of a cesium-vapor magnetometer chosen for its high sensitivity, infield durability, and nearly instantaneous response.

2.2 The Geometrics G-858 Cesium Magnetometer

2.2.1 Physical Parameters

The Geometrics G-858 Portable Cesium Magnetometer/Gradiometer is comprised of a belt-mounted display/logging console connected to cesium sensors mounted on a hand-held counterbalanced staff (Geometrics, 1997). Figure 2.2 shows the components of the G-858 disassembled.

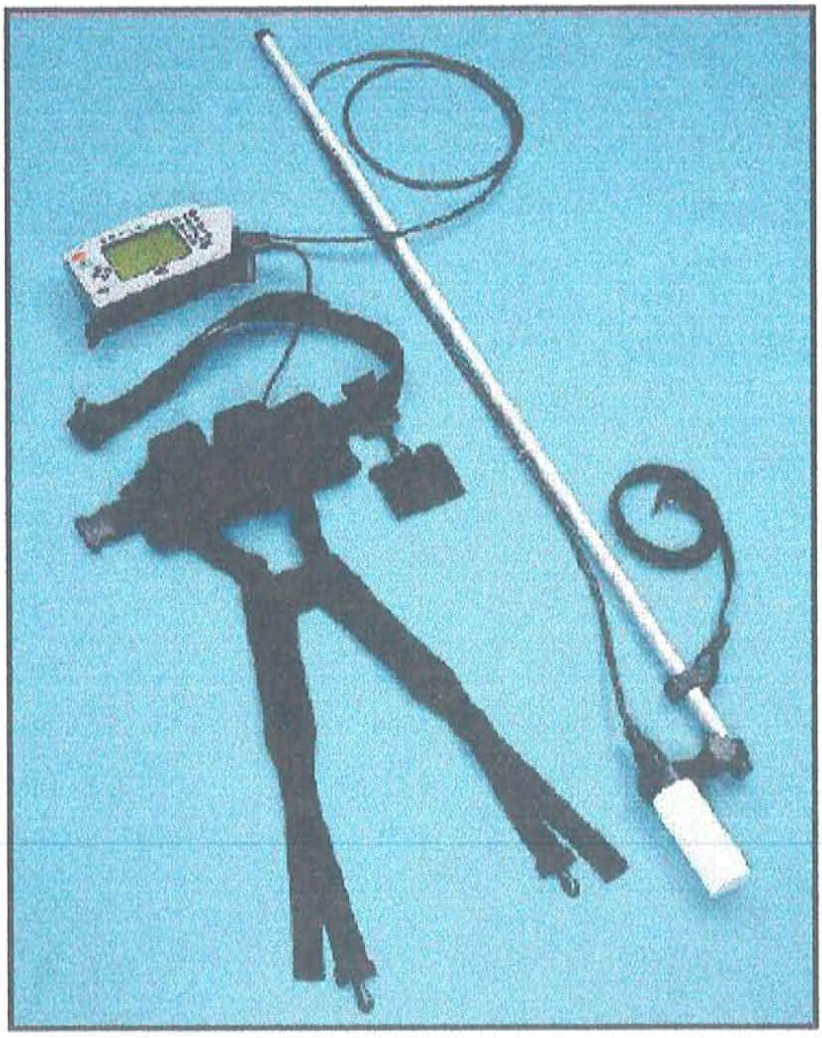

Figure 2.2: The Geometrics G-858 Portable Cesium Magnetometer instrumentation. The G-858 is comprised of a belt-mounted display console connected to a cesium sensor on a hand-held counterbalanced staff. (Geometrics, 1997)

The G-858 console, shown in Figure 2.3, contains electronics to acquire magnetic field data and position information, and display it on an real time LCD screen for review and edit, with sufficient memory to store high volumes of data up to more than 250,000 readings. The magnetometer has a port for input of GPS data so that the location of the observations can be logged simultaneously with the magnetic readings (Geometrics, 1995). Large areas may be surveyed at a rapid pace while real-time analog display provides immediate location and scale of the field strength or gradient. Both the plotted scale and audio tone representation of the magnetic data is completely adjustable, as are cadence beats for pacing, and signal quality warnings.

Figure 2.3: The CPU console of the G-858 acquires magnetic field data and displays it on an LCD screen for review and edit. The internal memory stores high volumes of data, and also allows input logging of differential GPS positions. (Geometrics, 1997)

The G-858 has a maximum sampling rate of 0.1 seconds and is programmable for both continuous and discrete recording. The four survey modes of operation include: a SEARCH MODE, for performing a random search or system test without recording data; a SIMPLE SURVEY, for non-coordinate complex surveys or line surveys; a MAPPED SURVEY, for defined coordinate systems and position tracking; and BASE STATION mode, for recording data used for diurnal corrections. The power supply of the G-858 consists of dual lithium cell batteries within each belt pack. Their field life is about 6 hours with a single sensor and 3.5 hours with dual sensors (Geometrics, 1995). The use of two alternate belts allowed continuous field operation of the magnetometer.

2.2.2 Field Operation

The G-858 may be used as a simultaneous vertical or horizontal gradiometer. The majority of the magnetic recording done during the course of this research project involved using the G-858 in the vertical gradiometer mode. This was accomplish by placing the cesium sensors in the dual configuration shown in Figure 2.4. The resulting data measurements taken in the field consist of total field strength readings at two heights above the ground simultaneously, as well as a vertical magnetic gradient based on the readings from the two cesium sensors.

The advantage of gradient measurements was recognized to be of key importance considering the targeting situation. Land mines and UXO are near surface objects with magnetic anomaly dimensions proportional to the sensor separation, the sensor height, and the spatial sampling interval. Since the G-858 console allows for the input of two sensors, the upper sensor is connected to port number 1, and the lower to port number 2. The sensor staff is assembled with a 'T' connector for the mounting of each sensor, and the

addition of a heavy counterweight allows for stable maneuverability in the field, despite the overall weight of the instrument and the length of the assembly.

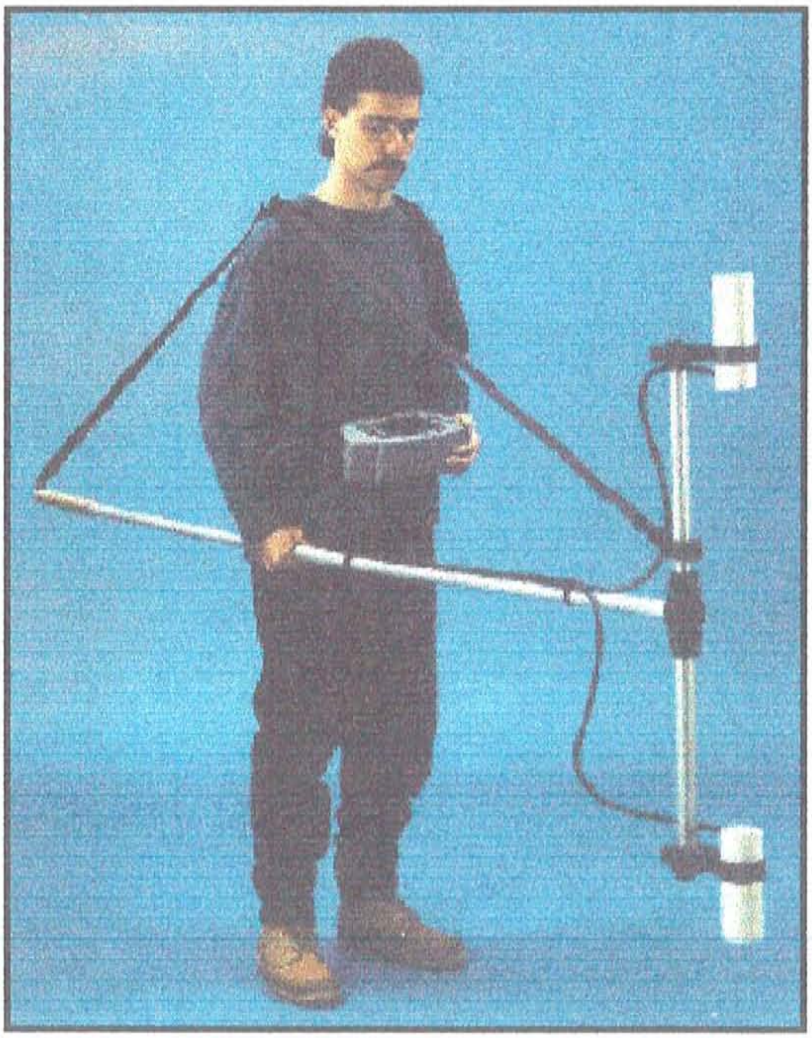

Figure 2.4: The Geometrics G-858 may be used as a vertical or horizontal gradiometer. The addition of a second cesium sensor and staff segments allows the operator to simultaneously sample the total magnetic field strength at two heights and compute the resulting spatial gradient based on the distance separating the sensors. (Geometrics, 1997)

Figure 2.5 presents a diagram of the cesium sensor configuration that became the standard operating design during this project. The vertical gradients computed through the use of this survey technique, as with all derivative filtering, aid in the removal of long period absolute magnetic deviatoric phenomenon such as diurnal (temporal) and regional (spatial) fluctuations. This ability will be discussed further in a following chapter.

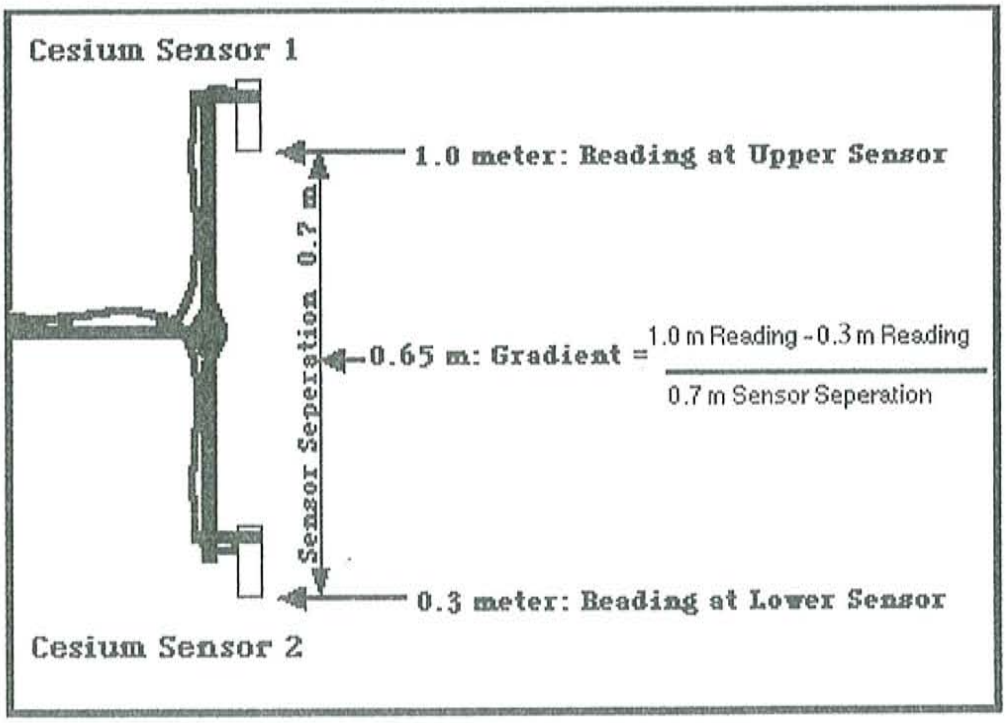

Figure 2.5: Diagram of the G-858 Cesium Sensors in the vertical gradiometer mode. During a measurement sequence, magnetic field strengths are simultaneously recorded by both sensors, the computed gradient is the sensor reading difference (nT) normalized by the separation (m).

2.2.3 Data Format, Transfer, and Manipulation

The data recorded to memory and downloaded for analyses consisted of data strings. Each string has two sensor readings, a calculated gradient, location, and time of observations. For a typical grid survey performed in the MAPPED mode of the magnetometer, in a gradiometer configuration, the data strings would provide the information shown in Table 2.1. MAPPED SURVEY mode provides a position convention based an a rectangular coordinate system. In this system, individual survey lines comprise one axis (usually the x-axis), while the observation points within a line comprise the other axis (usually the y-axis). The scale of the coordinate system, including the distance between lines, the distance between observation points within a line, and its starting and ending positions is at the programmable discretion of the operator.

Table 2.1: G-858 Gradiometer Sample Data Output

X	Y	Sensor 1 (nT)	Sensor 2 (nT)	Gradient (nT/m)	Line	Hour	Julian Day
0	0	50438.1	50648.6	299.944	0	14.1624	240
0	1	50436.9	50642.6	293.906	0	14.1625	240
0	2	50428.2	50464.9	52.349	0	14.1626	240
1	0	50418.9	50344.9	-105.765	1	14.1627	240
1	1	50402.8	50323.7	-113.008	1	14.1629	240
1	2	50400.4	50337.3	-90.246	1	14.163	240

The magnetic data consists of a field intensity measurement from each of the two sensors (nT) and a gradient value (nT/m) based on a 1 meter sensor separation. If the actual separation differs from 1 meter, the gradient will have to be adjusted during the download and conversion phase. The time of each observation recorded includes the Julian day, hour, minute, second, and tenth of second that the measurement was taken (Geometrics, 1995).

Following the survey, the data is transmitted via high-speed RS-232 data link to a PC computer for further analysis and map generation. The magnetometer to PC interface software used is a Geometrics supplied MS-DOS formatted system called MAGMAP (Geometrics, 1995). It allows for the downloading of the magnetometers' binary data and conversion into the ASCII format, and also for significant data review and editing capabilities.

The post-survey procedure used during the course of this project involved downloading the magnetometer binary data and ASCII conversion using MAGMAP v1.20 on an IBM 386 PC, and transferring it to a Macintosh. The Macintosh then became the computing tool of choice where data set manipulation was performed using Microsoft Excel v4.0 and Matlab v4.2. Plotting and mapping designs were facilitated by Spyglass Plot v1.0 for anomaly curves, and Spyglass Transform v3.01 for contour maps. Diagrams were created using ClarisWorks v2.1, and all picture graphics and illustrations were processed with GraphicsConverter v2.2.2. Finally, this report was compiled and published via Microsoft Word v5.1a.

Chapter 3

Data: EMRTC Testing Episodes at Control Test Pad

3.1 Magnetic Surveys at the Control Test Pad

3.1.1 CTP Location And Grid Maps

The most important aspect of this research project included the controlled magnetic investigation of sub-surface objects and the resulting disruption on the soils' magnetic characteristics. This was accomplished at an area of controlled survey grids designed for this research project. This Control Test Pad (CTP) allowed for the systematic investigation of magnetic signatures associated with an array of magnetic and non-magnetic targets. This pad provided a near homogenous half-space layer that lacked large surface rocks and vegetation. The location of the CTP was within an Energetic Materials Research and Testing Center (EMRTC) artillery range known as the 1000 Meter Range, or '1K'.

The CTP was approximately 500 meters down range of the artillery pad, located within the alluvial valley upon which 1K is built. The artillery pad at 1K can be seen in the photograph in Figure 3.1. Although the CTP was placed along an artillery range of considerable testing activity, rigid scheduling provided ample time for magnetic experimentation between range projects. The position of the CTP was selected to minimize the occurrence of artillery related debris landing among the test grids, although some clean-up was eventually required.

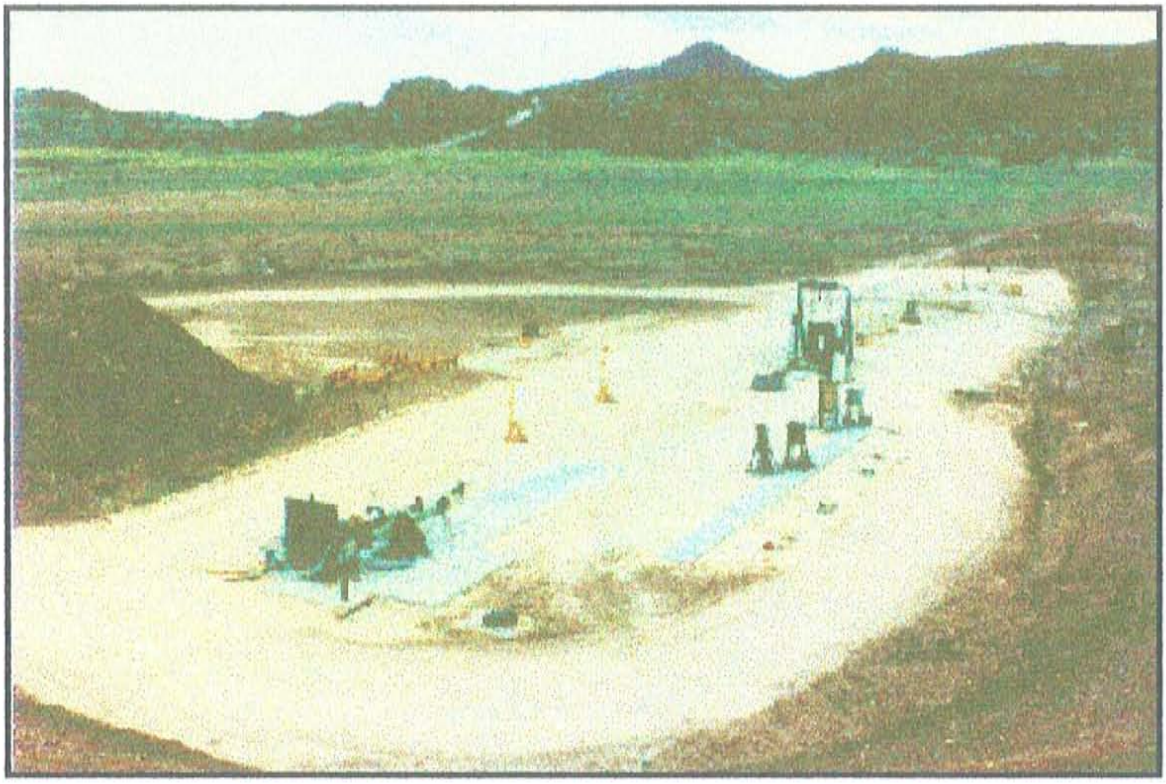

Figure 3.1: The artillery pad at the EMRTC site known as the 1000 Meter Range or 1K. The Control Test Pad (CTP) was approximately 500 meters down range of the artillery pad, 30 meters west of the service road. (EMRTC, 1996)

A diagram presenting a map view of the CTP grids' orientation and dimension is shown in Figure 3.2. The main test grid was a 5 by 5 meter square grid with survey lines delineated at 0.5 m intervals. This grid's purpose was to determine the magnetic signature of an array of buried targets. Auxiliary grids provided additional areas for void detection and threshold experiments. There were four such Auxiliary Grids surrounding the Main Grid. They varied in size and station spacing allowing for rapid data collection at different lateral resolutions. Magnetic surveys were performed with the magnetometer in a discrete MAPPED SURVEY mode of operation. Field strength measurements were then made at discrete observation points along each survey line. These

points were seperated by a distance referred to as the station spacing. This spacing was equal to the distance between each survey line. The station spacing, x-axis length, and y-axis length were entered into the data file of each survey providing a coordinate system for the grid. Coordinates attached to each data point maintained a rectangular positioning scheme within the grid following a Cartesian convention. The 'base station' or origin was consistently placed at the southwest corner of each grid, with survey lines running south to north. The areas of magnetic investigation at the CTP were divided into four categories: soil magnetism, void detection, detection thresholds, and buried target mine signatures.

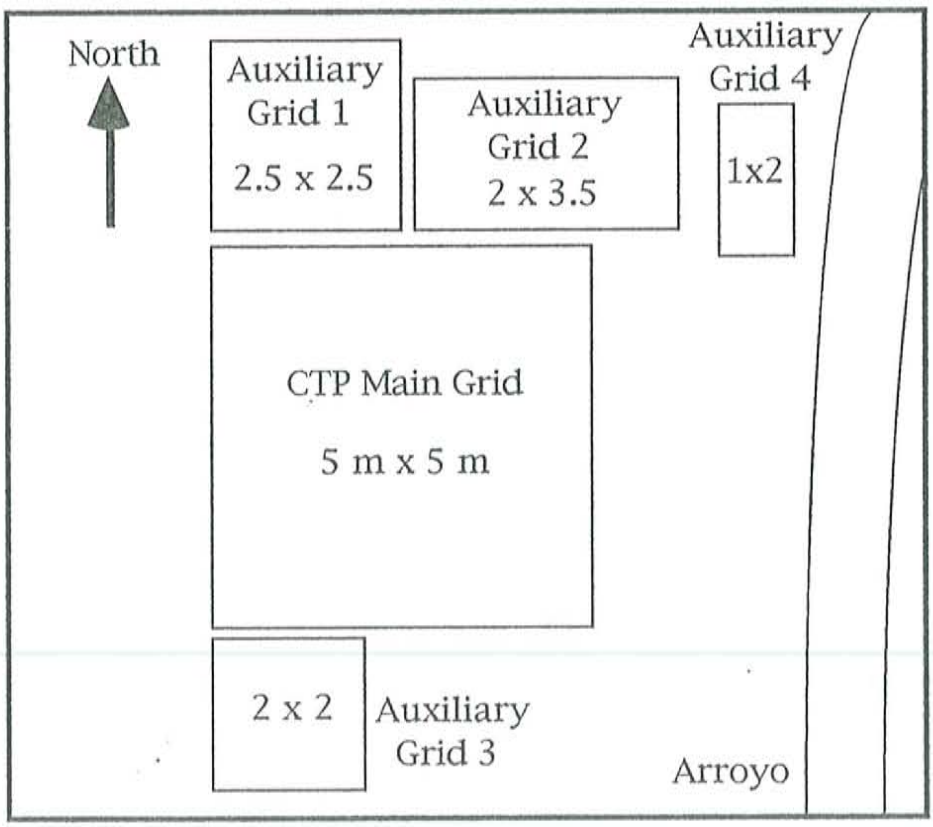

Figure 3.2: Diagram presenting a map view of the CTP grids. The Main Grid was 5 by 5 meters with a 0.5 m station spacing. Auxiliary Grids 1, 2, and 3 provided experimentation areas with 0.25 meter spacing. Auxiliary Grid 4 was used for single line profiles with a 0.1 meter interval.

3.2 CTP Testing Environment

3.2.1 Site Petrology and Soil Characteristics

The main Control Test Pad grid and surrounding Auxiliary grids were located on an alluvial fan on the southwestern slope of Socorro Mountain, northeast of Sedillo Hill. The fan, which consists almost entirely of clays and silts, has sustained erosional gulleying. The gulley exposures provide a stratigraphic picture of the soil horizons beneath the test pad to a 2 meter depth. These natural soil pits expose poorly indurated clay rich silt with no definite horizons or soil boundaries other than a thin crust of volcanic tuft erosional sediment. The soil is essentially a massive homogenous fill with a low distribution of even moderate size sandstone clasts. The lack of induration, limited lithological complexity, and lack of a well developed desert pavement suggests that the valley fill is young. Judging from exposures in adjacent arroyos, the stratigraphy remains unchanged for a considerable distance. The thick, homogenous, and relatively non-magnetic nature of the soil overburden provided a well defined medium with which to conduct magnetic surveys where environmental control was a driving motivation.

3.2.2 Climate and Magnetic Field Variations

The magnetic surveys where performed at the CTP during the spring and summer months providing rapid sensor start up in the warm morning hours. The spring afternoons presented surveying difficulties associated with seasonal strong winds. Surveys during the summer could be interupted by afternoon rain and lightning. However, early surveys were conducted in clear skies at moderate temperatures.

Fluctuations in the magnetic field varied with the season as well. Spring months provided a stable magnetic field with a near linear diurnal drift average of about 14 nT per hour, with the slope of the drift curve dependent on the time of day. Figure 3.3 shows a representative afternoon diurnal drift curve as recorded during the 14th hour MST of a spring month. The summer months possessed slightly greater diurnal drifts and occasional magnetic storms.

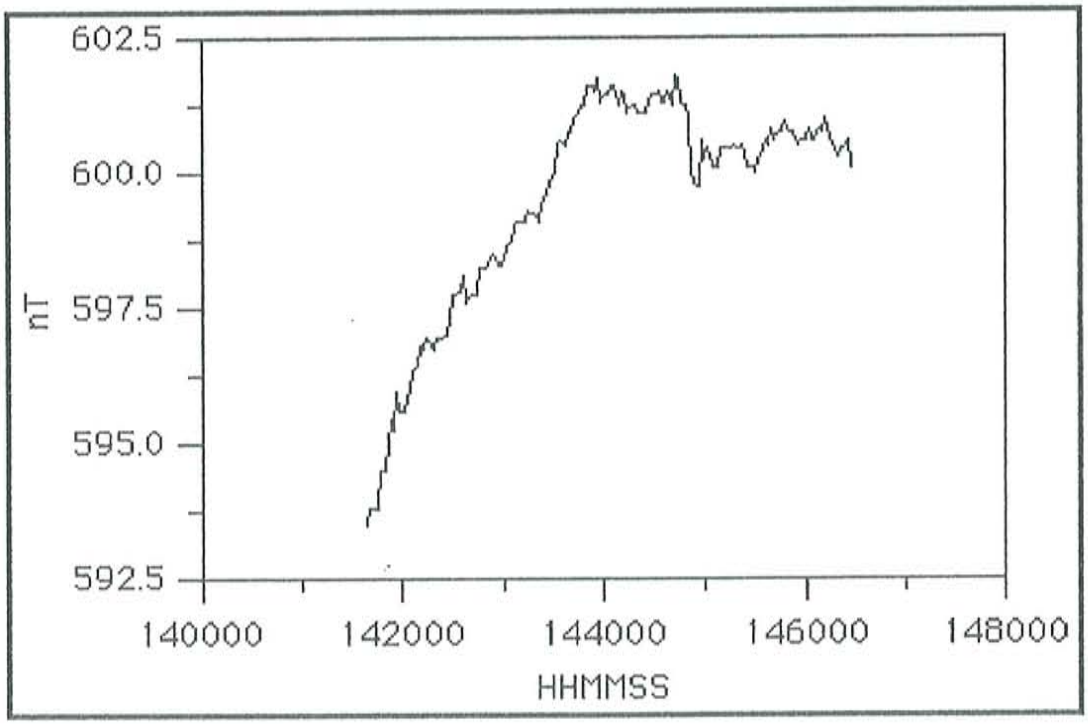

Figure 3.3: Diurnal drift curve recorded between 14:15 and 14:50 MST on May 16, 1996. It shows a steady positive diurnal increase of 14 nT per hour and a slight plateau.

3.3 Control Test Pad Data

3.3.1 Background Soil Magnetism

The first experiments at the CTP involved determining the *Background Soil Magnetism* at the relevant depths of burial for land mines and UXO, between the surface and 0.5 meters. Background magnetism surveys were performed at each of the five grids. Figures 3.4 and 3.5 show background vertical gradients of the Main Test Grid at two different heights. Figures 3.6, 3.7 and 3.8 show the background vertical gradients of the Auxiliary Grids.

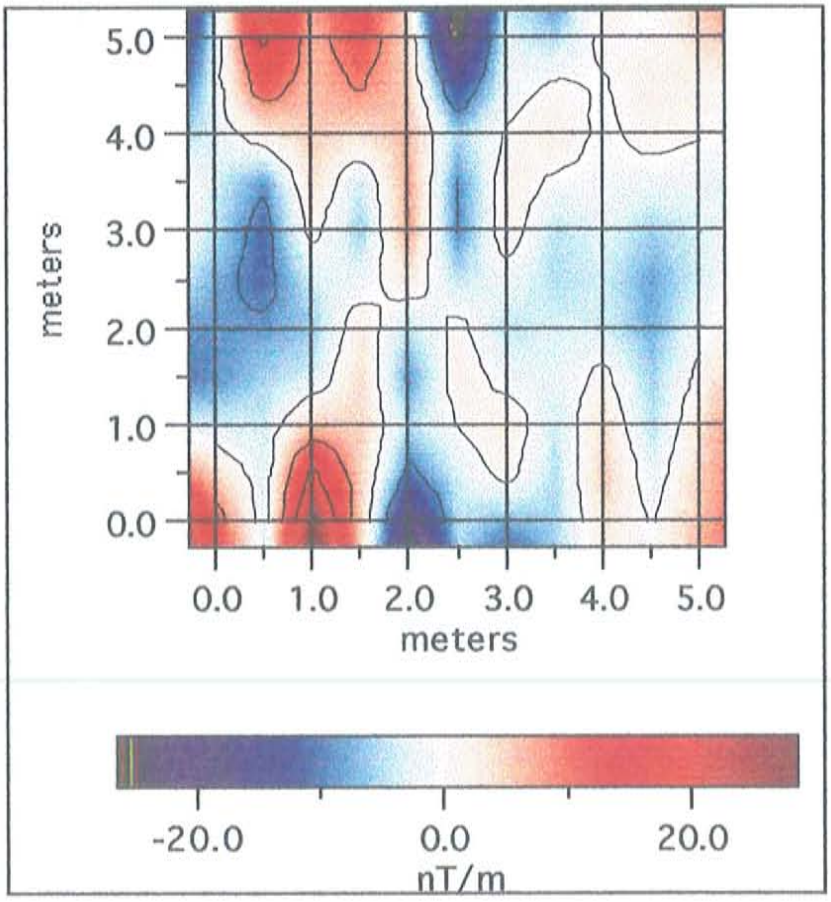

Figure 3.4: Magnetic vertical gradient map of the CTP Main Grid. The magnetic gradients were taken at a 0.5 meter station spacing. Sensor separation was 0.3 meters, and gradient measurements were calculated at a height of 0.7 meters. The data was recorded on 5/9/96.

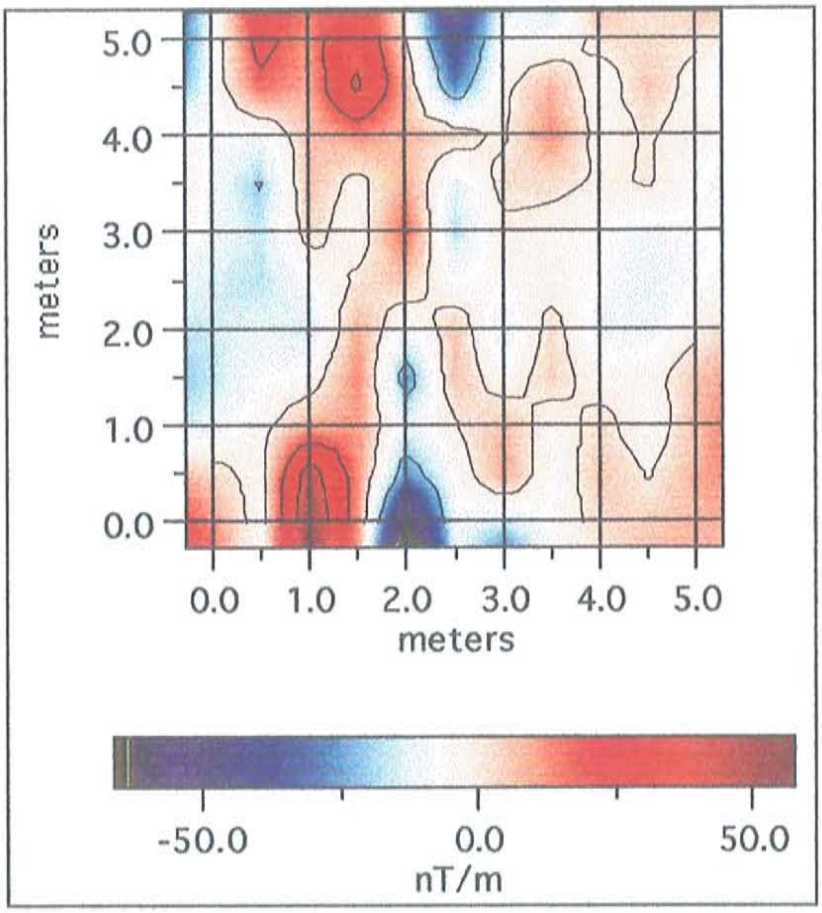

Figure 3.5: Magnetic vertical gradient map of the CTP Main Grid. The magnetic gradients were taken at a 0.5 meter station spacing. Sensor separation was 0.5 meters, and gradient measurements were calculated at a height of 1.1 meters. The data was recorded on 4/30/96.

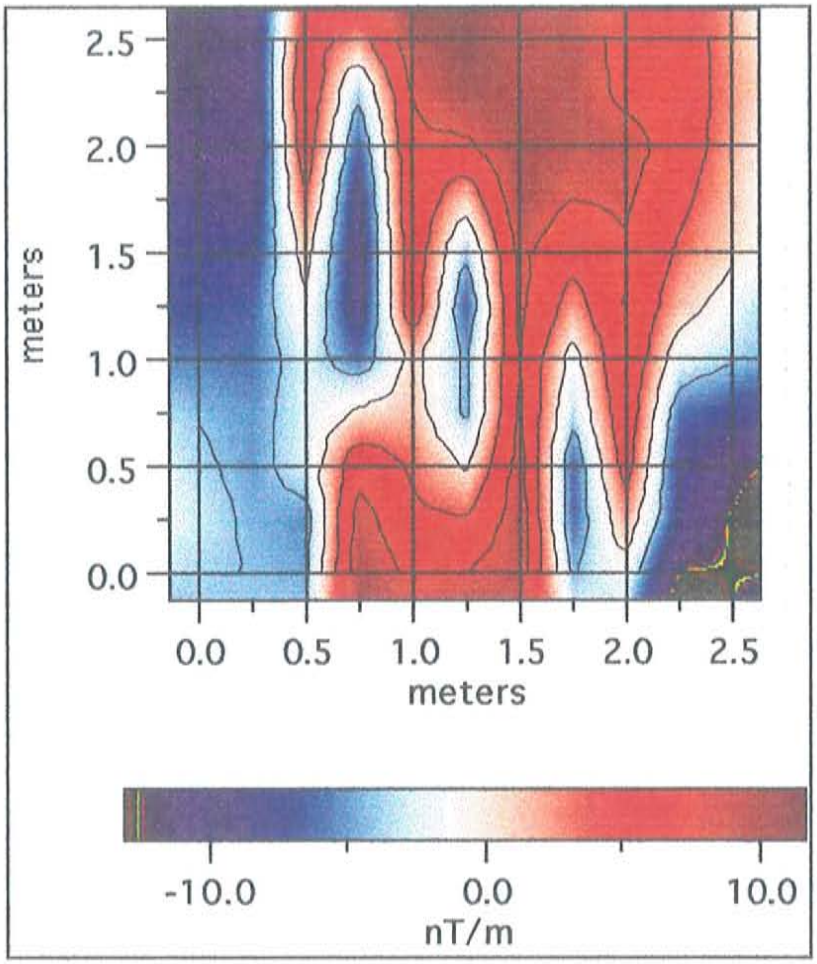

Figure 3.6: Magnetic vertical gradient map of CTP Auxiliary Grid 1. Station spacing was 0.25 meters. Sensor separation was 0.7 meters, and gradient measurements were calculated at a height of 0.7 meters. The data was recorded on 7/18/96.

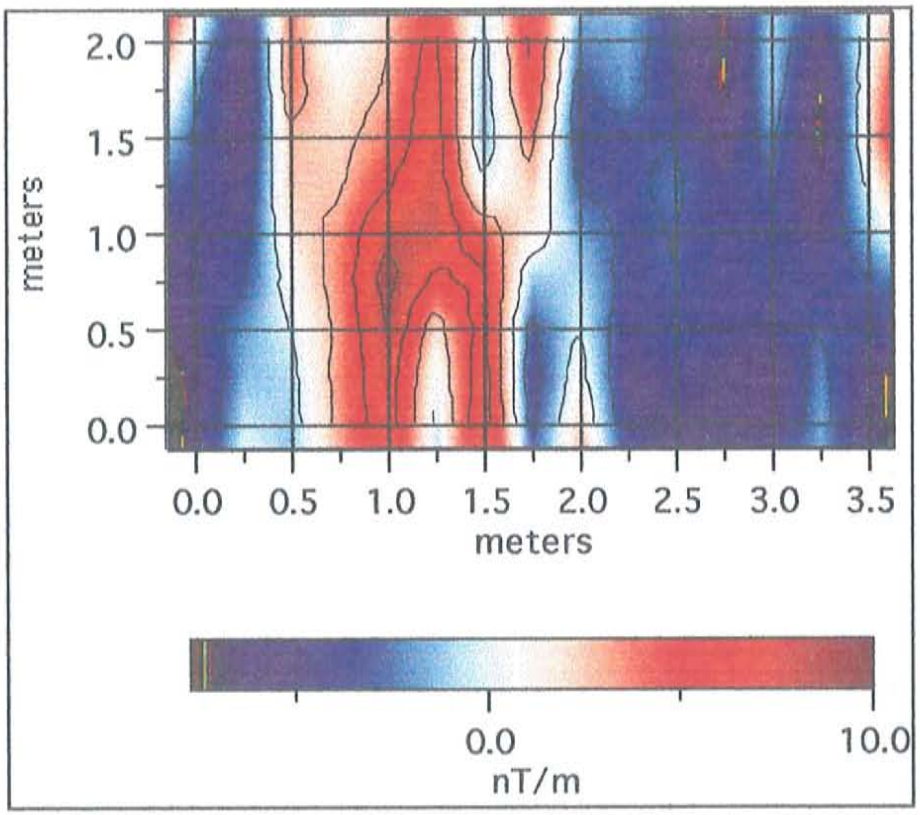

Figure 3.7: Magnetic vertical gradient map of CTP Auxiliary Grid 2. Station spacing was 0.25 meters. Sensor separation was 0.7 meters, and gradient measurements were calculated at a height of 0.7 meters. The data was recorded on 5/20/96.

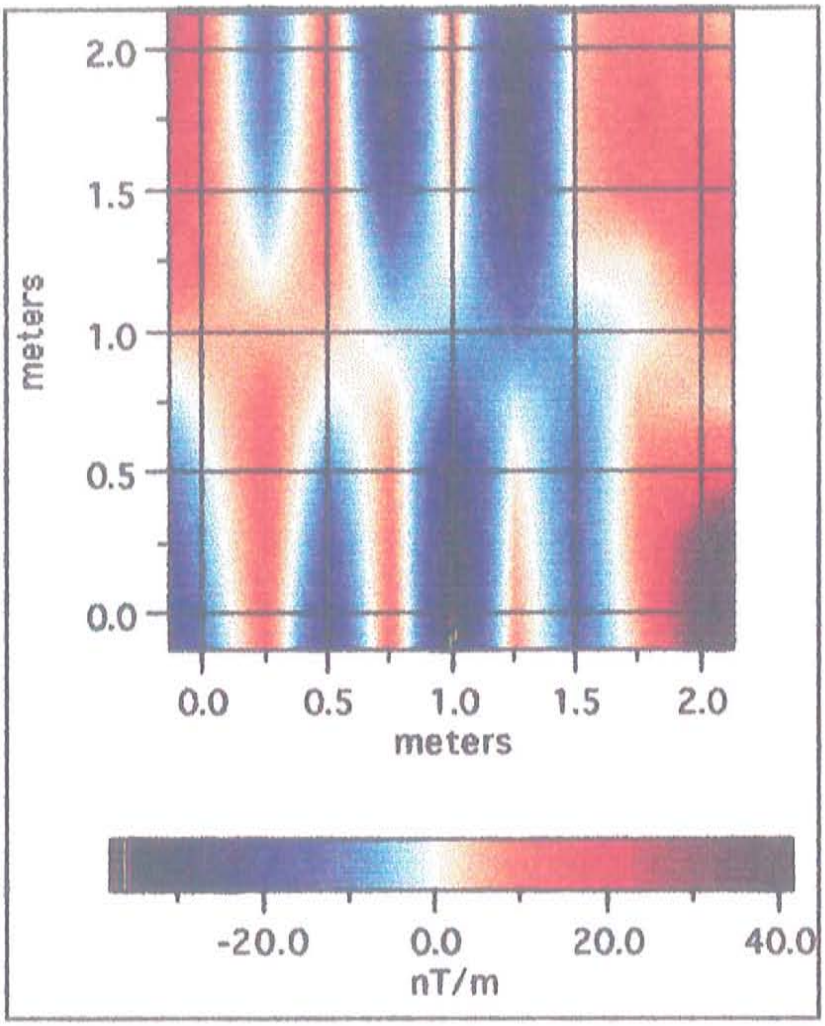

Figure 3.8: Magnetic vertical gradient map of CTP Auxiliary Grid 3. Station spacing was 0.25 meters. Sensor separation was 0.7 meters, and gradient measurements were calculated at a height of 0.7 meters. The data was recorded on 5/22/96.

3.3.2 Void Characterization

The initial investigation of soil magnetism was floowed by the magnetic characterization of buried low to non-magnetically susceptible objects, whether true target land mines or false target lithologics. These *Void Characterization* tests involved determining the magnetic signature of a

region of soil with a moderate void buried at depth. Performed on Auxiliary Grid 1, these surveys incorporated a series of 3.8 liter plastic canisters, sealed and buried at known depths. Figures 3.9 and 3.10 show the resulting vertical gradient anomalies associated with the voids. Depth of burial, sensor height and separation, void volume, and void position are indicated in the figure captions.

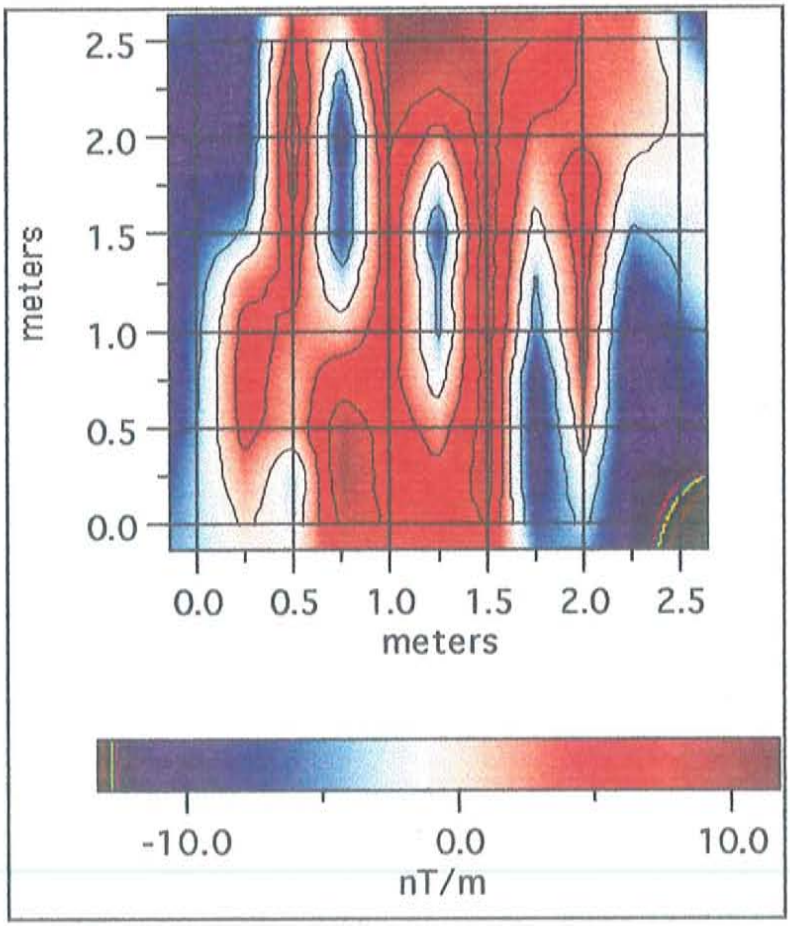

Figure 3.9: Magnetic vertical gradient map of a void survey at CTP Auxiliary Grid 1. A 7.6 liter void was located between 0.15 and 0.35 meters depth at position (1.5m,1.5m). Station spacing was 0.25 meters, sensor separation was 0.7 meters, and gradients were calculated at a height of 0.65 meters. The data was recorded 7/18/96.

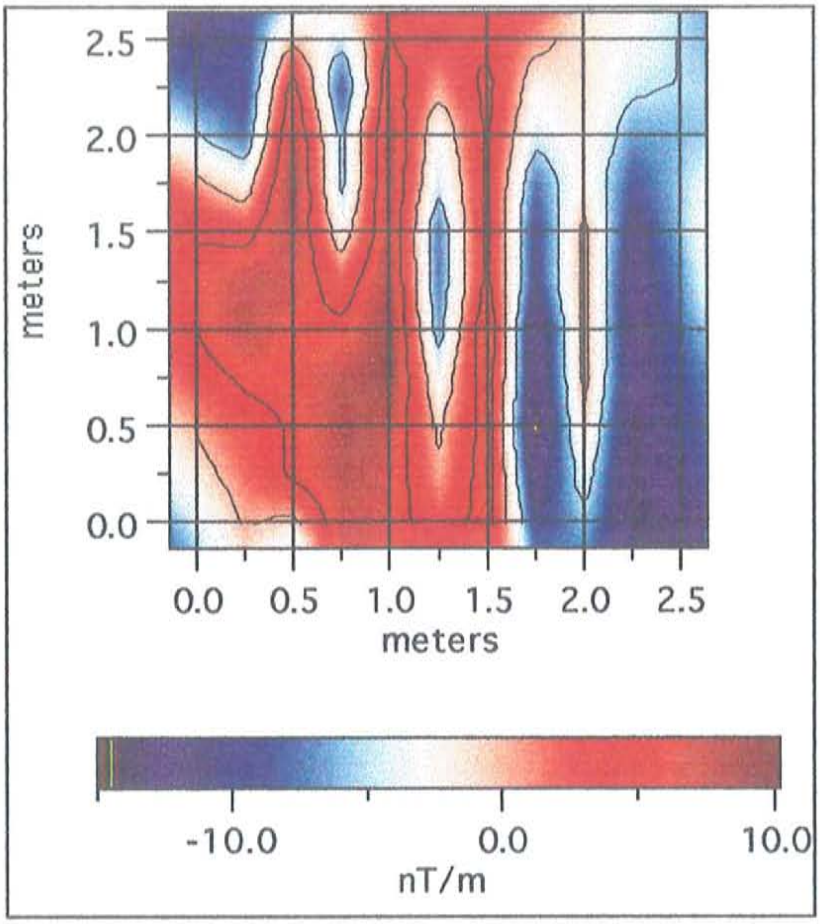

Figure 3.10: Magnetic vertical gradient map of a void survey at CTP Auxiliary Grid 1. An 11.4 liter void was located between 0 and 0.35 meters depth at position (1.5m,1.5m). Station spacing was 0.25 meters, sensor separation was 0.7 meters, and gradients were calculated at a height of 0.65 meters. The data was recorded 7/18/96.

3.3.3 Smallest Buried Object Detectability

These experiments were designed to place resolution limitations on the gradiometer. The sources for these measurements were high magnetic susceptibility targets possessing induced magnetism. The targets used were iron pins of variable size and all surveys maintained the common goal of determining the point at which the gradiometer could no longer resolve a true

magnetic anomaly beyond the background noise. The surveys were conducted at Auxiliary Grid 4 for the smallest iron pin targets, and at Auxiliary Grid 2 for a large iron target. Figures 3.11 and 3.12 show vertical gradient plots for successively increasing masses of iron pins. Figure 3.13 is a contour map of the gradient anomaly produced by a 1.36 kg iron hammer. Sensor heights and station spacing are indicated in the figure captions.

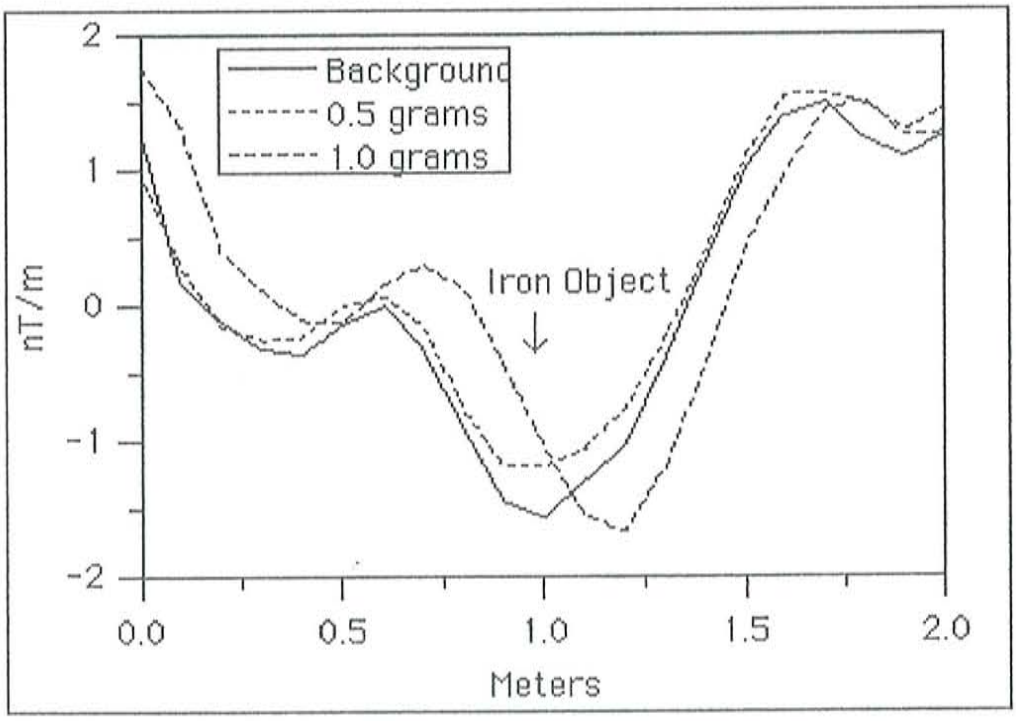

Figure 3.11: Magnetic vertical gradient plots for buried iron pins at Auxiliary Grid 4. Shown are the background magnetic gradient curve and gradient anomalies for 0.5 and 1.0 gram vertical iron pins buried 2 cm at the 1 meter position. Station spacing was 0.1 meters, sensor separation was 0.7 meters, and gradients were calculated at a height of 0.5 meters. The data was recorded on 3/15/96.

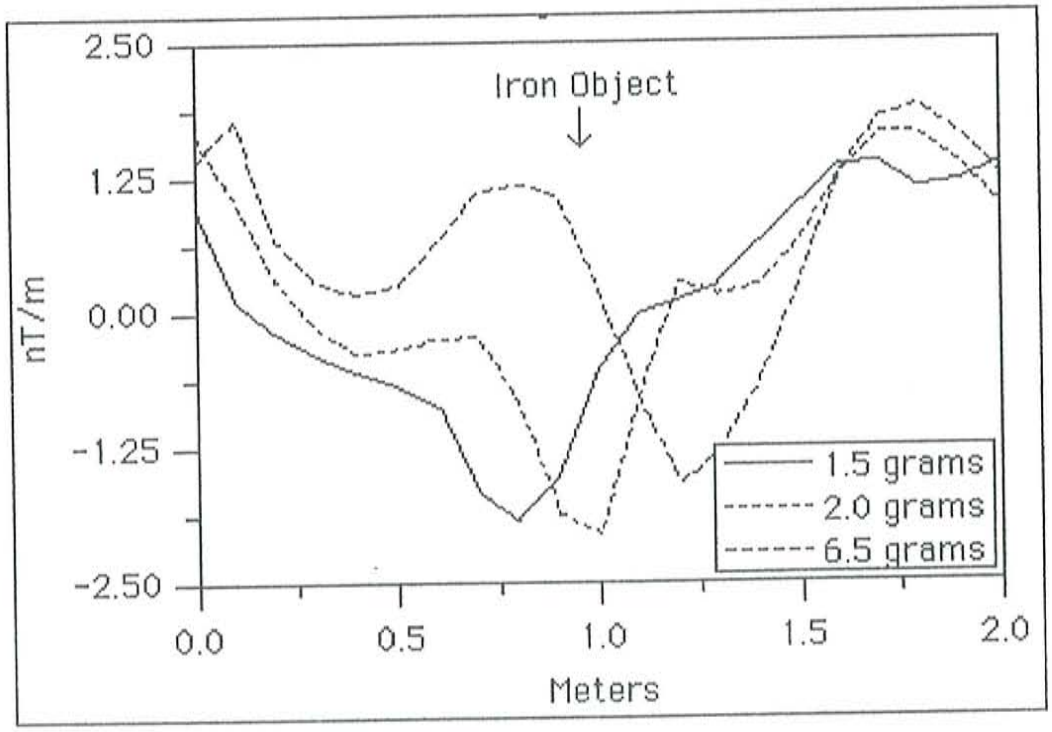

Figure 3.12: Magnetic vertical gradient plots for buried iron pins at Auxiliary Grid 4. Shown are the gradient anomalies for 1.5, 2.0 and 6.5 gram vertical iron pins buried 2 cm at the 1 meter position. Station spacing was 0.1 meters, sensor separation was 0.7 meters, and gradients were calculated at a height of 0.5 meters. The data was recorded on 3/15/96.

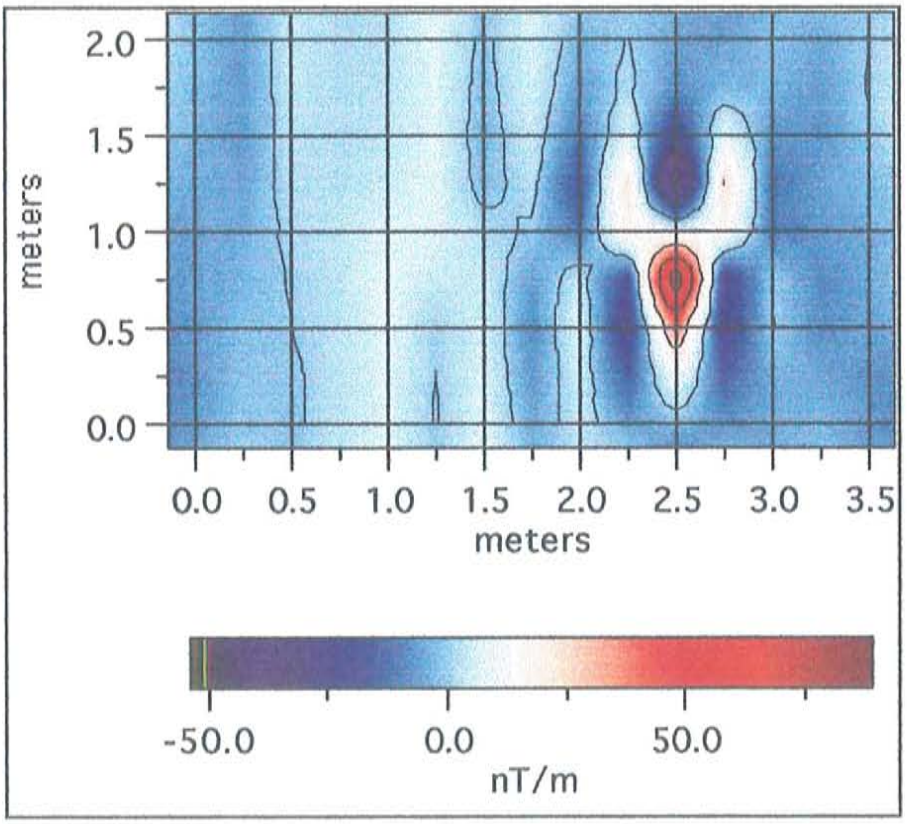

Figure 3.13: Magnetic vertical gradient map for iron hammer Auxiliary Grid 2. A 1.36 kg iron hammer was placed north-south on the surface at location (2.5m, 1m). Station spacing was 0.25 meters, sensor separation was 0.7 meters, and gradients were calculated at a height of 0.5 meters. The data was recorded on 3/15/96.

3.3.4 Inert Mine Experiments

The final field of investigation at the CTP involved the magnetic characterization of land mines and UXO. Termed Inert Mine Experiments, the targets under investigation included metallic and non-metallic dummy mines used in military demining training programs. Although the targets sampled at the CTP were not actual land mines or UXO, they simulate all physical and magnetic characteristics of the mines and UXO except for the presence of explosives and detonators.

The following sections present the magnetic survey maps of dummy mines divided into metallic and non-metallic composition. Pertinent physical parameters of the targets used are listed in Table 3.1.

Table 3.1: Dummy Mine Parameters

Target	Mine Type	Sensor Class	Diameter	Thickness	Casing
A	Anti-Personnel	Electomagnetic (EM)	15 cm	6 cm	Plastic
G	Anti-Tank	Electomagnetic (EM)	30.5 cm	8.5 cm	Plastic
B	Anti-Personnel	Nuclear (NUC)	15 cm	6 cm	Metallic
J	Anti-Personnel	Nuclear (NUC)	7.5 cm	3 cm	Metallic

Non-metallic Mine Data

The non-metallic dummy mines were surveyed within the CTP Main Test Grid. The two targets chosen simulated both an anti-personnel mine, type A, and an anti-tank mine, type G. These dummy targets had plastic casings with styrofoam filler. Magnetic gradient maps for the Type A and G dummy mines are shown in Figures 3.14 and 3.15. The depth of burial, sensor height and separation, station spacing, and mine position are indicated in the figure captions.

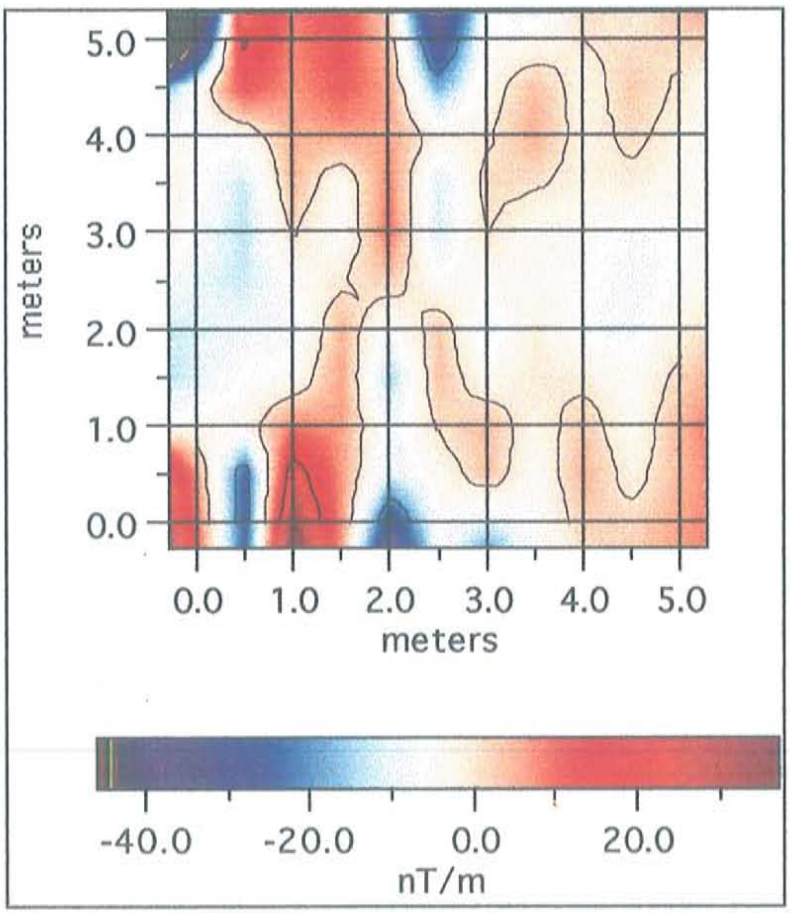

Figure 3.14: Magnetic vertical gradient map of a non-metallic dummy anti-personnel mine at CTP Main Grid. Mine type A was buried 6 cm at location (2.5m,2.5m). Station spacing was 0.5 meters, sensor separation was 0.5 meters, and gradients were calculated at a height of 0.85 meters. The data was recorded on 4/30/96.

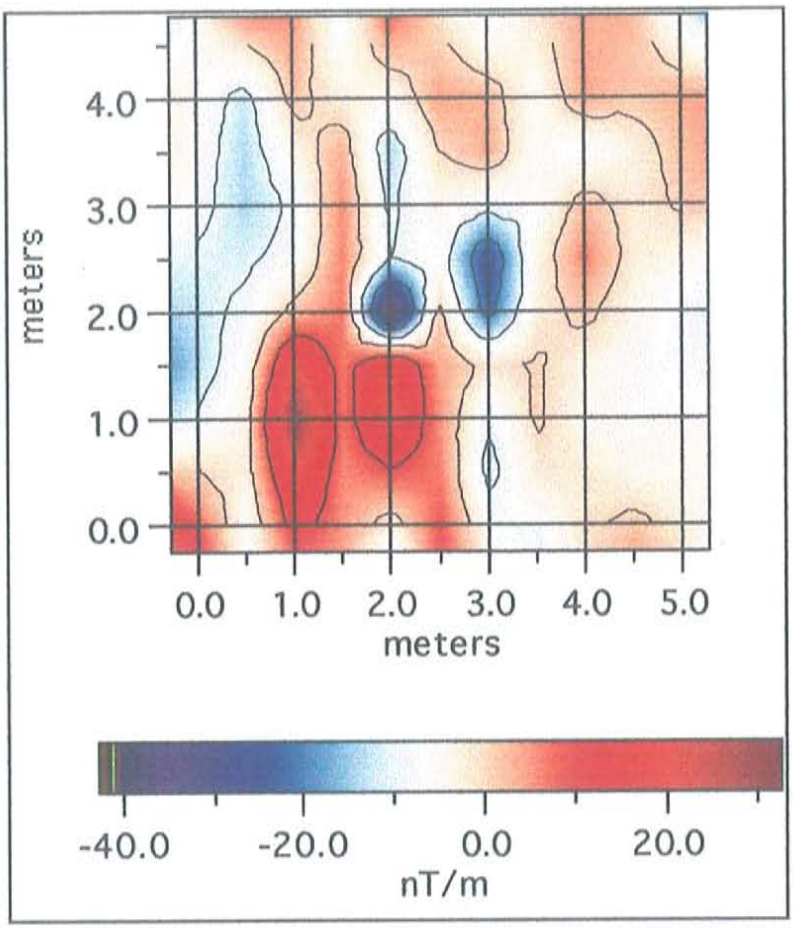

Figure 3.15: Magnetic vertical gradient map of a non-metallic dummy anti-tank mine at CTP Main Grid. Mine type G was buried 10 cm at location (2.5m,2.5m). Station spacing was 0.5 meters, sensor separation was 0.7 meters, and gradients were calculated at a height of 0.45 meters. The data was recorded on 5/14/96.

Metallic Mine Data

The metallic dummy mines were surveyed within the CTP Main Test Grid and in Auxiliary Grid 3. The two targets chosen simulated two types of anti-personnel mines. Type B is a large anti-personnel dummy mine similiar in metallic content to bounding fragmentation mines. Type J is a smaller dummy

mine comparable to blasting land mines. Type B was used for vertical and horizontal gradient surveys of variable sensor seperation and height. The horizontal gradient for the Type B mine is shown for two sensor heights in Figures 3.16 and 3.17. The depth of burial, sensor height and separation, station spacing, and mine position are indicated in the figure captions.

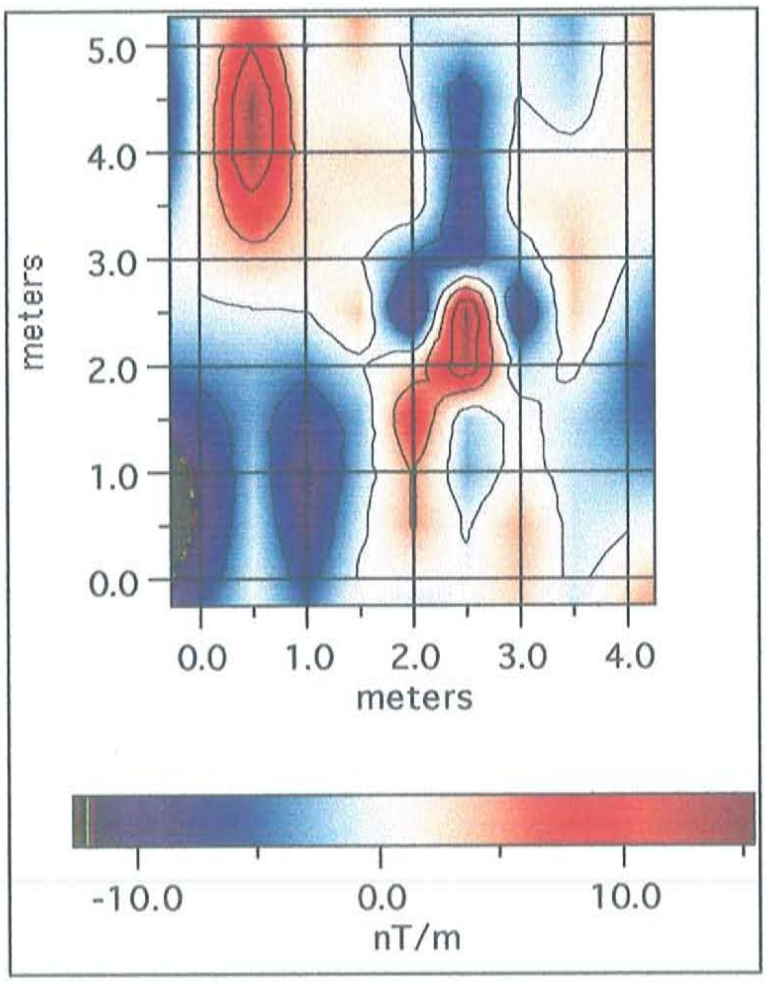

Figure 3.16: Horizontal north-south gradient map of a metallic dummy anti-personnel mine at the CTP Main Grid. Mine type B was buried 6 cm at location (2.5m,2.5m). Station spacing was 0.5 meters, sensor separation was 0.7 meters, and gradients were calculated at a height of 0.8 meter. The data were recorded on 5/14/96.

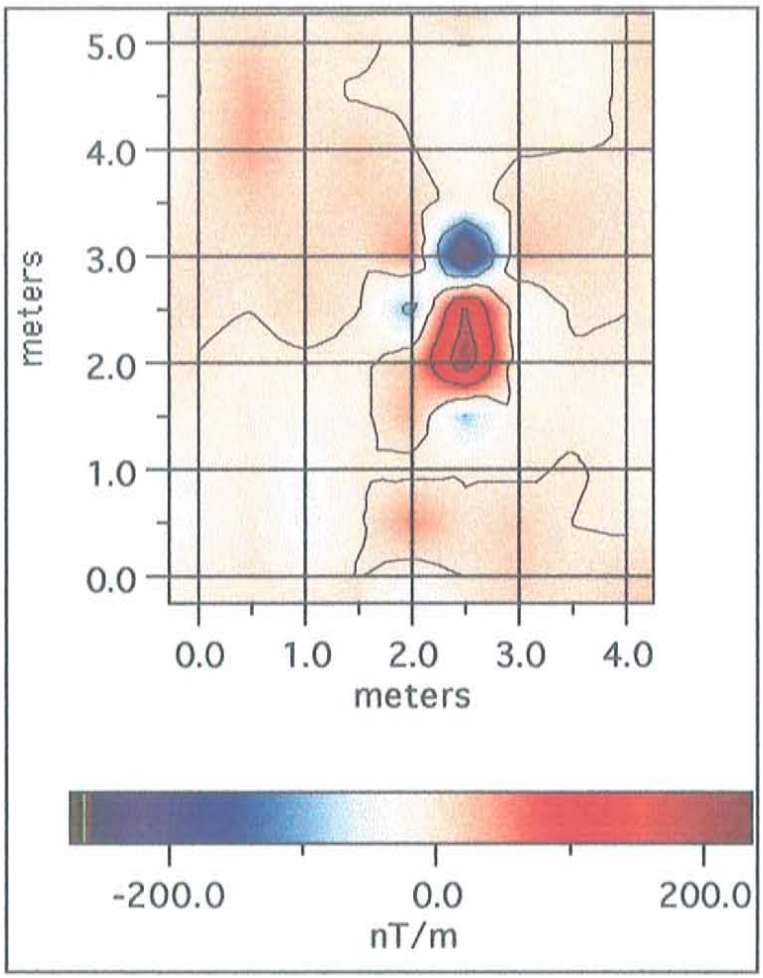

Figure 3.17: Horizontal north-south gradient map of a metallic dummy anti-personnel mine at the CTP Main Grid. Mine type B was buried 6 cm at location (2.5m,2.5m). Station spacing was 0.5 meters, sensor separation was 0.7 meters, and gradients were calculated at a height of 0.1 meter. The data were recorded on 5/14/96.

Vertical gradient surveys of the Type B mine were performed for two burial depths and station spacing. Figure 3.18 shows the vertical gradient of the mine on the Main Grid. Figure 3.19 shows a surface mine on Auxiliary Grid 3. Both surveys used a 0.7 meter seperation and 0.7 meter gradient height. Only the station spacing and the position of the mine were changed.

The Type J mine was surveyed at Auxiliary Grid 3 and the resulting vertical gradient map is shown in Figure 3.20

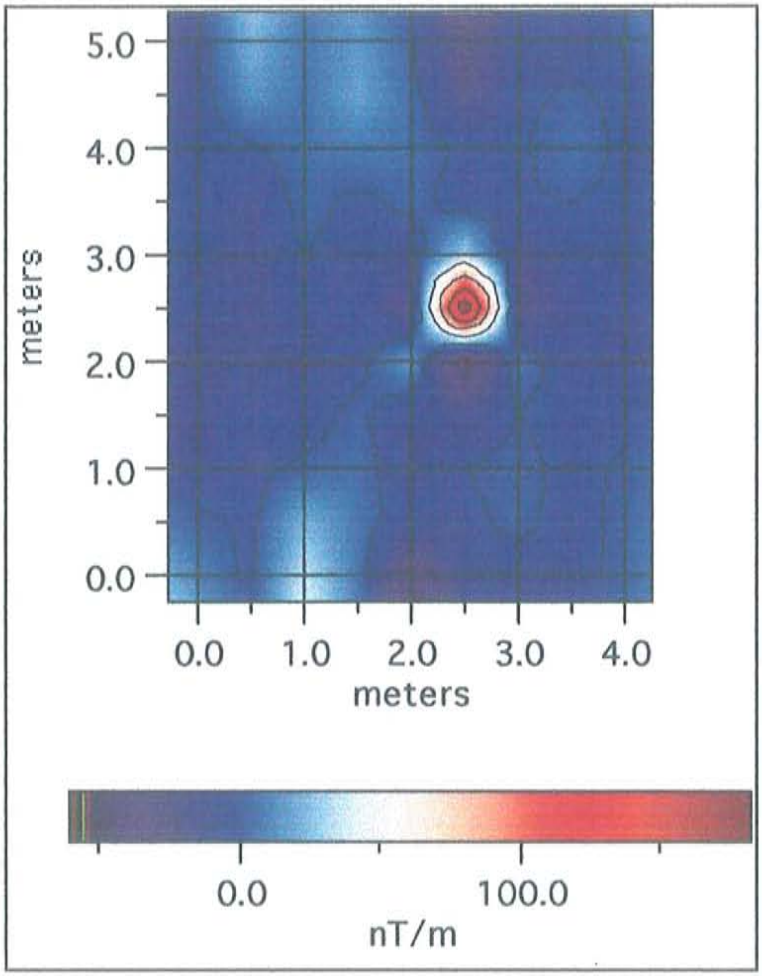

Figure 3.18: Magnetic vertical gradient map of a metallic dummy anti-personnel mine at the CTP Main Grid. Mine type B was buried 6 cm at location (2.5m,2.5m). Station spacing was 0.5 meters, sensor separation was 0.7 meters, and gradients were calculated at a height of 0.7 meter. The data were recorded on 5/14/96.

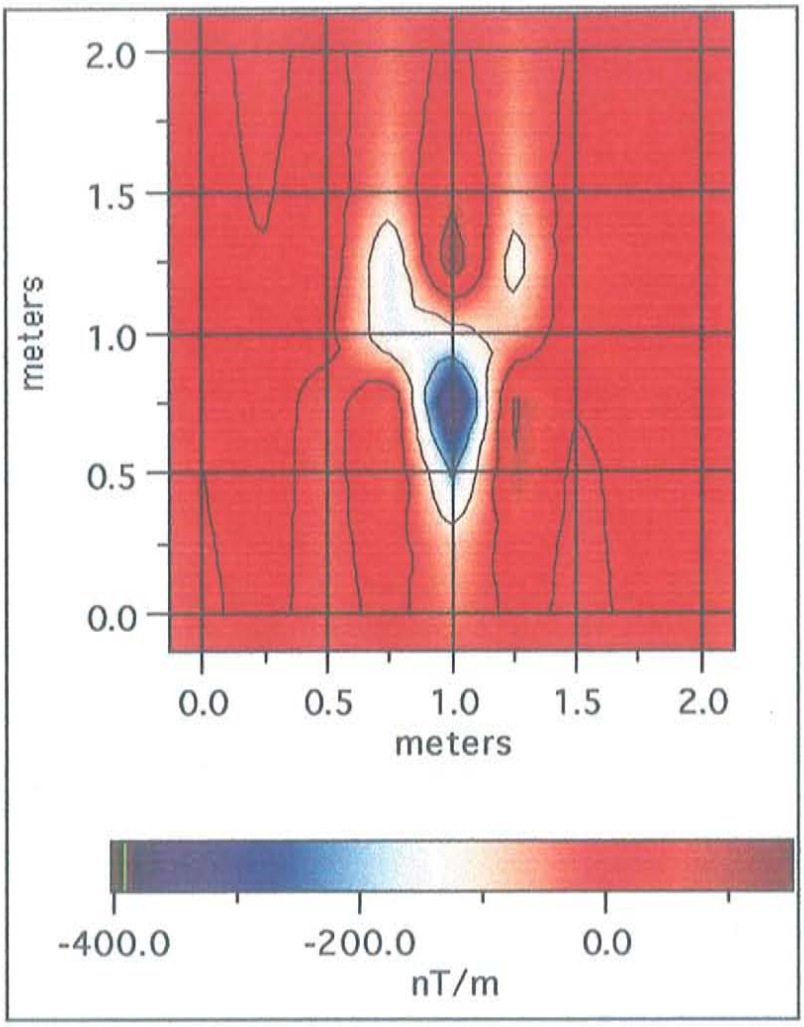

Figure 3.19: Magnetic vertical gradient map of a metallic dummy anti-personnel mine at Auxiliary Grid 3. Mine type B was placed on the surface at location (1m, 1m). Station spacing was 0.25 meters, sensor separation was 0.7 meters, and gradients were calculated at a height of 0.7 meter. The data were recorded on 5/22/96.

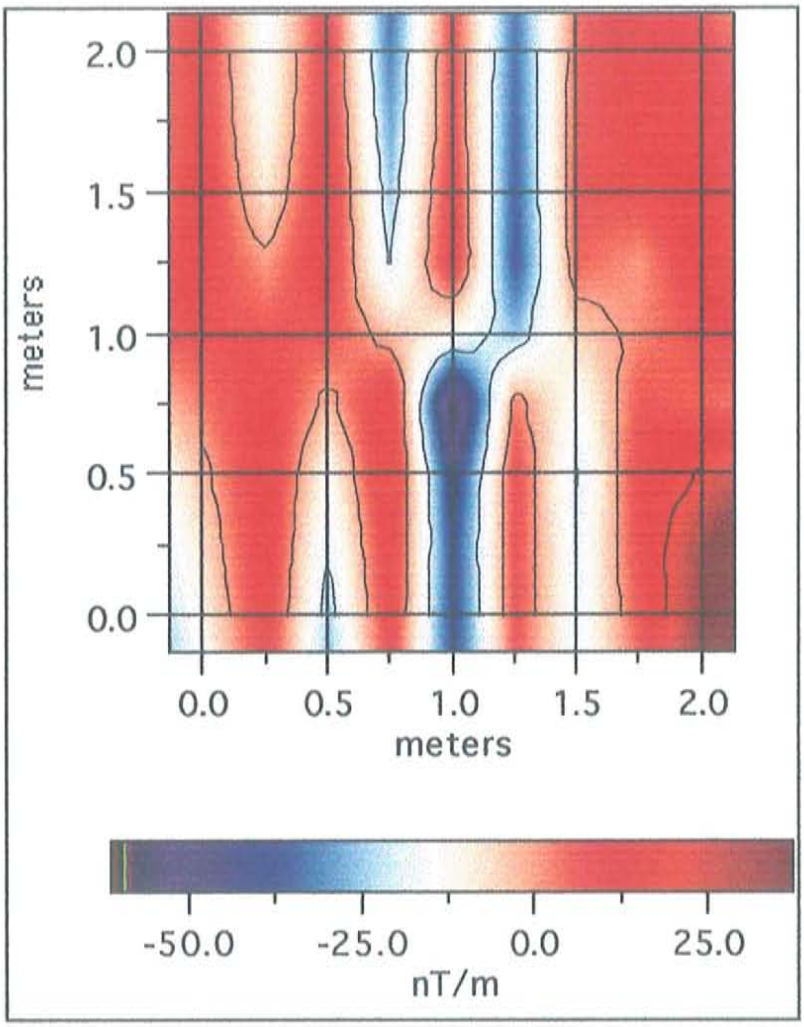

Figure 3.20: Magnetic vertical gradient map of a small metallic dummy anti-personnel mine at Auxiliary Grid 3. Mine type J was placed on the surface at location (1m, 1m). Station spacing was 0.25 meters, sensor separation was 0.7 meters, and gradients were calculated at a height of 0.7 meter. The data were recorded on 5/22/96.

The data presented in this chapter are some of the Control Test Pad experiments conducted during this research project. The next chapter deals with land mine and UXO test lanes constructed at the EMRTC Counter-Mine Test Site. The data generated from the Control Test Pad and the Counter-Mine Test Site will be evaluated in Chapter 5, Magnetic Data Analyses.

Chapter 4

Data: EMRTC Testing Episodes at Counter-Mine Test Site

4.1 Magnetic Surveys at the Counter-Mine Test Site

4.1.1 CTS Location And Track Maps

The majority of magnetometer data was gathered at a dedicated counter-mine testing facility coordinated by the Energetic Materials Research and Testing Center (EMRTC). It was during research and development projects organized by EMRTC, and several major defense contractors, that the field sites where prepared for data gathering. These preparations included the deployment and burial of a number of foreign and domestic anti-personnel mines, anti-tank mines, and sources of unexploded ordnance. The deployment areas were GPS surveyed and carefully monitored to ensure a safe and controlled testing environment.

The Counter-Mine Test Site (CTS) was developed specifically to test and evaluate technologies for the detection and neutralization of anti-tank and anti-personnel mines, as well as sources of unexploded ordnance and bombs. The site consists of four oval flat tracks, ranging from 100 to 255 meters in length, and support facilities. Figure 4.1 shows an aerial photograph of the main security and storage buildings, instrumentation trailers, and two of the four test track ovals.

Figure 4.1: Oblique aerial photograph of the EMRTC Counter-Mine Test Site (CTS). The viewed is from the east and shows instrumentation shelters, the Off-Road Track (foreground), and On-Road Track 1 (background). The CTS was developed to test and evaluate technologies for the detection and neutralization of anti-tank mines, anti-personnel mines, and UXO. (EMRTC, 1996)

A diagram of the CTS facility is shown in Figure 4.2. This diagram presents a map view of the test tracks' orientations and dimensions. For the purpose of this project the On-Road tracks have been labeled numerically 1 to 3 moving west to east. Each track consisted of a two to three meter wide road upon which smaller test lanes were delineated. These test lanes were generally one to two meters wide and ran along the straight legs of the oval track. Several testing episodes had mines deployed along the track's entire circumference, however, only 50 or 100 meter sections were surveyed by the magnetometer on any particular track.

The resulting test lane surveys generated data sets of two types. The first type was a single line survey of magnetic measurements taken down the center line of a test lane. These survey data generated one-dimensional anomaly curves of vertical gradients versus horizontal distance. The second type was a series of line surveys beginning at the left most lane boundary and spaced at 0.5 meter intervals until the right boundary was reached. This type generated parallel anomaly curves that could be contoured together into two-dimensional maps. The type of survey used depended on the purpose of the test lane including sensor calibration, controlled data collection, or blind detection examinations.

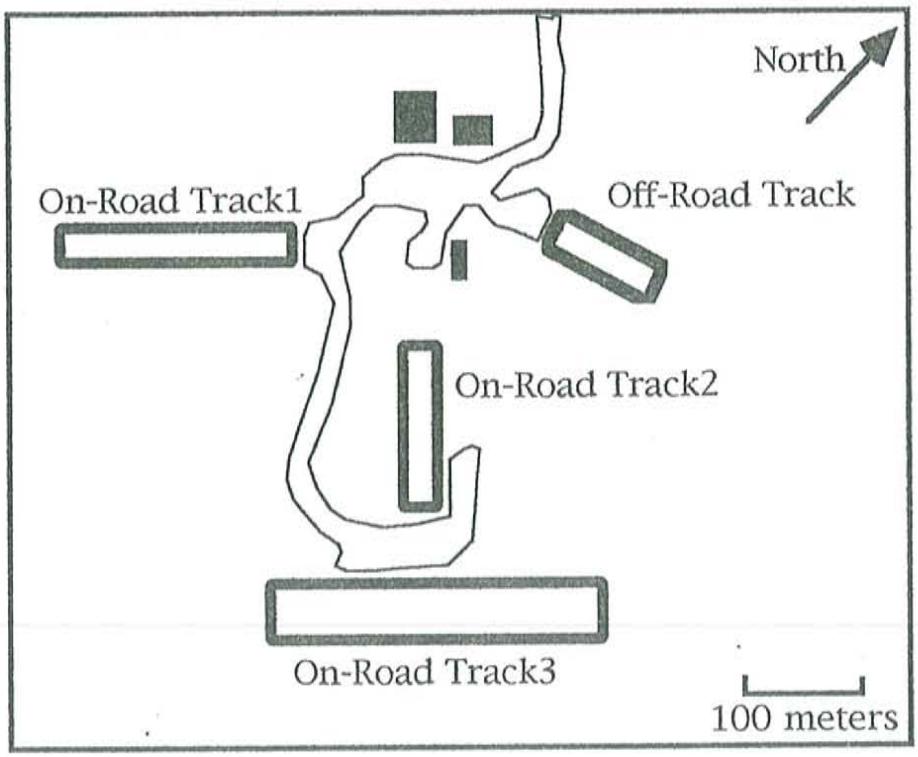

Figure 4.2: Map view of the CTS Test Tracks. The site consists of four oval flat tracks, ranging from 100 to 255 meters in length, and support facilities.

4.1.2 Test Lane Survey Procedure

Magnetic data were recorded during scheduled testing visits from leading scientific laboratories including GDE, SAIC, GeoCenters, and Jaycor. Once the target land mines, or unexploded ordnance, had been defused, planted, and the overburden significantly settled, the data were recorded. Lanes were delineated by rope or chalk boundaries that were paced with the magnetometer while recording. Figure 4.3 shows the operation of the G-858 within a test lane on Track 1.

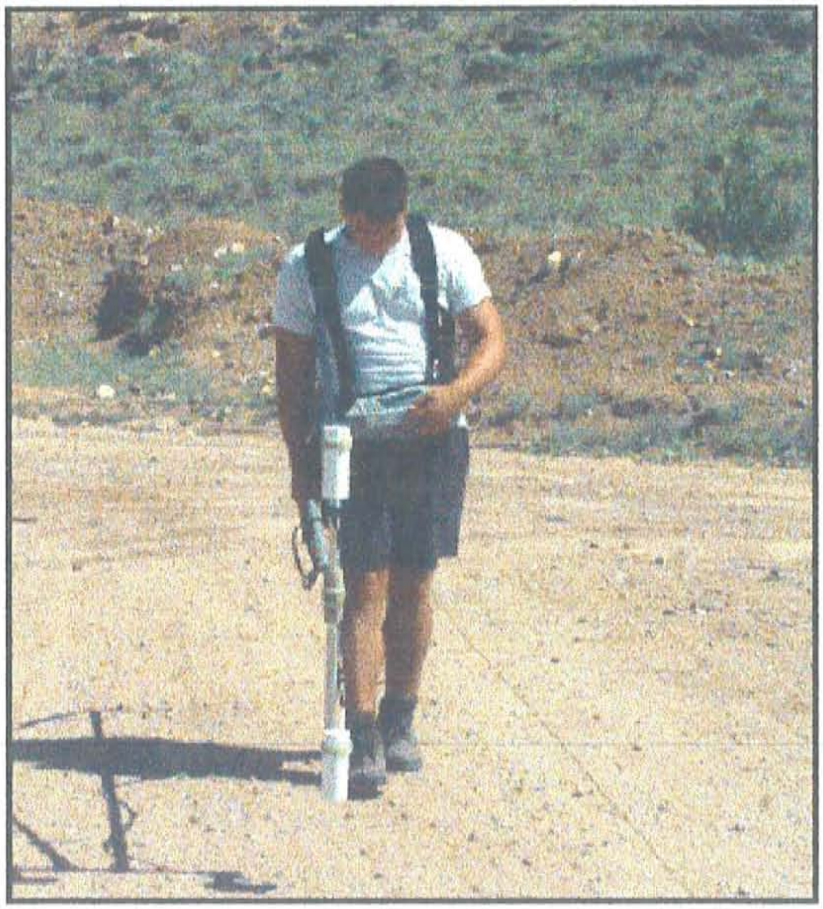

Figure 4.3: Magnetic data acquisition with the Geometrics G-858 Portable Magnetometer. The compact mobility and extended memory and power reserves of the G-858 allowed for lengthy magnetic exploration of the CTS land mine and UXO tracks.

The G-858 CPU was preset to sample the magnetic field at a continuous rate of time. The audio cadence emitted from the magnetometer allowed the lane to be paced in consistent time intervals creating a similar number of data points within each line, as well as correlation between the lateral position of data points in neighboring survey lines. As seen in Figure 4.4, the automated sampling provided the ability to monitor the steady position of the sensors and the magnetic readings on the display.

Figure 4.4: Cesium sensors and body-mounted CPU/Battery pack in operation at the CTS On-Road Track 1. The sensors were in a vertical gradiometer configuration which allows for gradients to be calculated at a point between the sensors. For this survey, sensor separation was 0.7 meters, lower sensor height was 0.25 meters, yielding gradient values at 0.6 meters (0.25 + 0.7/2).

The cesium sensors were maintained at a constant separation, height, and directional orientation throughout each survey line. The CPU recorded the vertical field strength at each sensor, position coordinates depending on operating mode, a general gradient value based on a default sensor separation, and the time and date.

After a survey, the magnetometer was taken to an instrumentation trailer on the CTS facility, downloaded to a PC, and the data taken off-site for post-acquisition processing. This processing included spatial filtering, mapping and graphical machinations, and determination of possible target location and characteristics. The results of processing are presented in the next chapter. The following sections within this chapter address the testing environment at the CTS and the initial magnetic data recorded at individual segments of mined test lanes.

4.2 Testing Environment

4.2.1 Site Petrology and Soil Characteristics

The testing environment at the CTS consisted of road-like tracks within which an assortment of mines and ordnance was buried. The tracks where created upon natural mesas within the volcanic outcrops and sedimentary fans of the southwest side of Socorro Peak. The test tracks were created to mimic unpaved roads that might possess a land mine threat. The degree of compaction, thickness of artificial overburden, and distribution of vegetation and native rock clasts varied between tracks. All the tracks were well maintained and allowed for ease of field measurements and mapping via differential GPS survey.

The petrology of the area is dominantly volcanic. The top soil consisted of weathered tuft sediments and thin accumulations of silts and clays derived from adjacent alluvial fans. Forming berms between the test tracks are ridges of basaltic tephra, boulders, and thick tuft layers. The ridges, both naturally and artificially shaped, are similar in scale to the tracks themselves, often skirting the lanes by only meters. They pose some risk of lithology-based lateral magnetic noise.

The soil is relatively free of magnetic grain minerals such as magnetite. As these tracks have been constructed within the last year, there are no significant accumulations of magnetite baring erosional sediment. After the emplacement of a land mine or UXO, the soil is raked, saturated, and dried repeatedly to ensure the targets anonymity. Thus the only sources of magnetic anomalies expected in the testing lanes other than the buried ordnance are some volcanic clasts, survey stakes, and metallic debris resulting from previous inhabitation or testing programs in the area.

4.2.2 Climate and Magnetic Field Variations

The magnetic surveys where performed at the CTS during the spring and summer months providing rapid sensor start up in the warm morning hours. The spring afternoons presented surveying difficulties associated with seasonal strong winds. Surveys during the summer could be interrupted by afternoon rain and lightning.

Fluctuations in the magnetic field varied with the season as well. Spring months provided a stable magnetic field with a near linear diurnal drift average of about 14 nT per hour, with the slope of the drift curve dependent on the time of day. The summer months possessed slightly greater diurnal drifts and occasional magnetic storms.

4.2.3 Magnetic Noise

The local geology was the greatest source of magnetic noise as large volcanic clasts were abundant within the surface layer of some test tracks. Another possible source of noise were outcrops several meters in height paralleling portions of the track. Also present was the magnetic noise of metallic objects associated with surveying equipment and position markers. Only data sets with low magnetic noise were passed through to analyses unless the noise sources themselves were the focus of the test. The following section presents a representative sample of magnetic data acquired during counter-mine testing at the CTS.

4.3 Counter-Mine Test Site Data

4.3.1 GeoCenters Land Mine Tracks (April 1)

The data collected during the GeoCenters deployment consisted of land mine lanes on two of the test tracks. The tracks surveyed with the magnetometer were the On-Road Track 1 (1 m x 358 m), and On-Road Track 2 (1 m x 352 m). The land mines deployed during this period were the VAL69, M15, M16, M19, M21, and VS2.2. Table 4.1 gives the major physical parameters of the land mines deployed during all the CTS land mine testing episodes in this study.

Table 4.1: Counter-Mine Test Site Land Mine Parameters

Mine	M15	M16	M19	M21	VS2.2	VAL69
Origen	US	US	Korea/US	US	Italy	Italy
Type	Anti-Tank	Anti-Pers.	Anti-Tank	Anti-Tk.	Anti-Tank	Anti-Pers.
Casing	Metallic	Metallic	Non-Metal	Metallic	Non-Metal	Non-Metal
Weight	14.27 kg	3.74 kg	12.56 kg	NA	3.6 kg	3.2 kg
Length	cylindrical	cylindrical	332 mm	NA	cylindrical	cylindrical
Width	337 mm	103 mm	332 mm	NA	246 mm	130 mm
Height	125 mm	199 mm	94 mm	NA	117 mm	205 mm
Charge	Comp B	TNT	Comp B	NA	RDX	Comp B
Chrg. Wt.	10.33 kg	521 g	9.53 kg	NA	NA	420 g
Booster	RDX	Tetryl	RDX	NA	NA	RDX
Bstr. Wt.	11 g	54 / 70 g	52 g	NA	NA	13 g
Op. Force	159-340 kg	1.6-20 kg	136-227 kg	NA	200 kg	6-10.8 kg

The GeoCenters land mine tracks were delineated with rope boundaries on both sides of a 1 meter lane and a rope down the center line. Measurements were recorded while pacing down the track with sensors positioned over the ropes. Thus each track generated three data streams, the left, center, and right lines each 0.5 meters apart running parallel with the long axis of the track.

The magnetometer was operated in a dual sensor gradiometer mode with two different configurations, a 0.5 meter sensor separation/ 0.5 meter lower sensor height for Track 1, and a 0.7 meter sensor separation/ 0.3 meter lower sensor height for Track 2. The magnetometer was operated in SIMPLE SURVEY mode with location points recorded within the data set indicating horizontal distances down track. The magnetic field was sampled in Continuous mode at a 0.3 second interval. The following sections present magnetic gradient profiles for portions of the GeoCenters land mine tracks.

On-Road Track 1

Figure 4.5 is a map showing track length and buried land mine types, depths of burial, and approximate locations for Track 1. Also shown is the division of Track 1 into the two recorded portions termed Segments A and B. Figures 4.6 and 4.7 show the magnetic gradient profiles of the Segment's center lines.

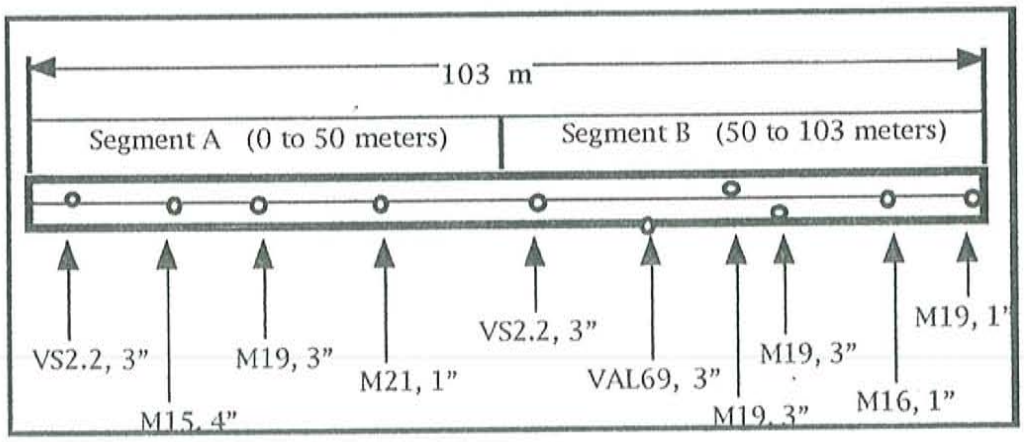

Figure 4.5: Diagram map of Test Track 1 during a land mine deployment for GeoCenters. The portions of this track surveyed with the magnetometer are labeled as Segments A and B. The map shows the land mine types, depths of burial, and approximate location within the track. This mine deployment occurred in April 1996.

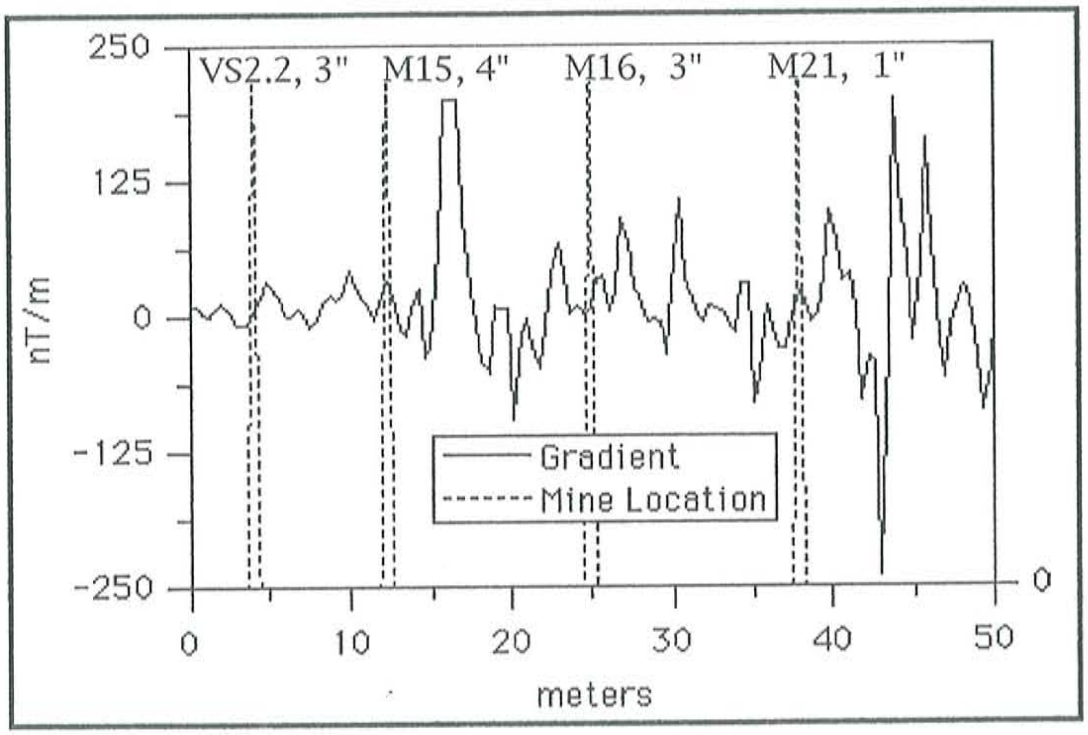

Figure 4.6: Magnetic vertical gradient curve (solid line) of Track 1 centerline, segment A (0 to 50 meters). Sensor separation was 0.5 meters and gradients were calculated at a height of 0.75 meters. Continuous sampling rate was at 0.3 seconds. Plot shows approximate location of buried land-mines (dashed line), their type, and depth of burial. The data were recorded on 4/3/96.

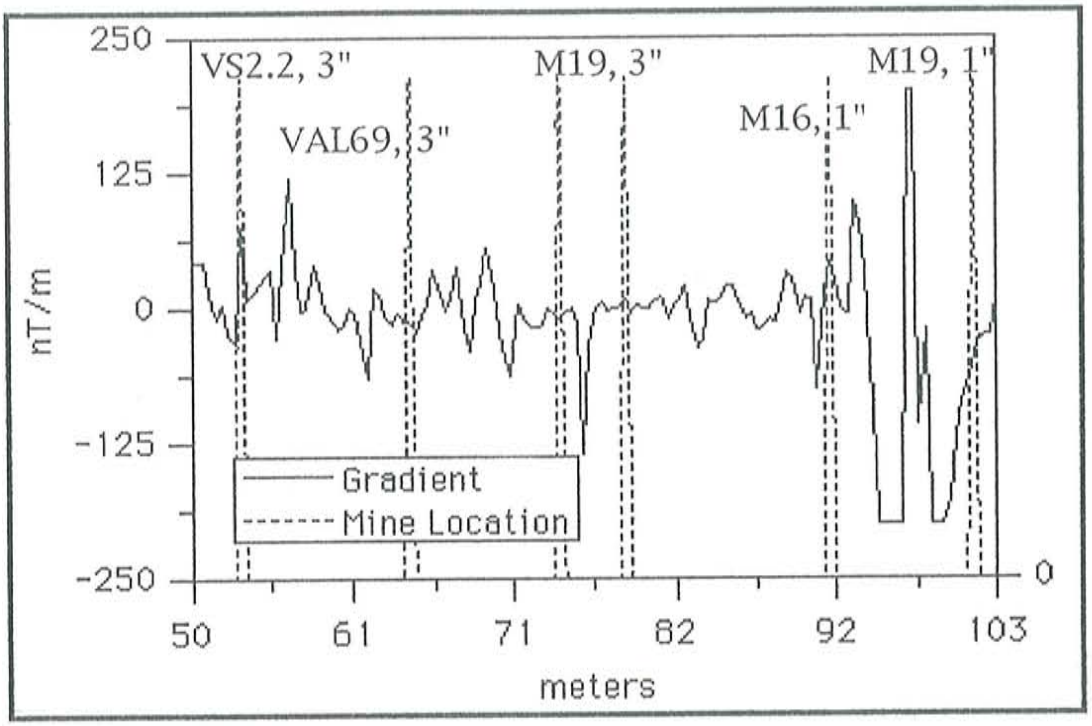

Figure 4.7: Magnetic vertical gradient curve (solid line) of Track 1 centerline, segment B (50 to 103 meters). Sensor separation was 0.5 meters and gradients were calculated at a height of 0.75 meters. Continuous sampling rate was at 0.3 seconds. Plot shows approximate location of buried land-mines (dashed line), their type, and depth of burial. The data were recorded on 4/3/96.

On-Road Track 2

Figure 4.8 is a map showing track length and buried land mine types, depths of burial, and approximate locations for GeoCenters On-Road Track 2. Also shown is the division of Track 2 into the two recorded portions termed Segments A and B. Figures 4.9 and 4.10 show the magnetic gradient profiles of the Segment's center lines.

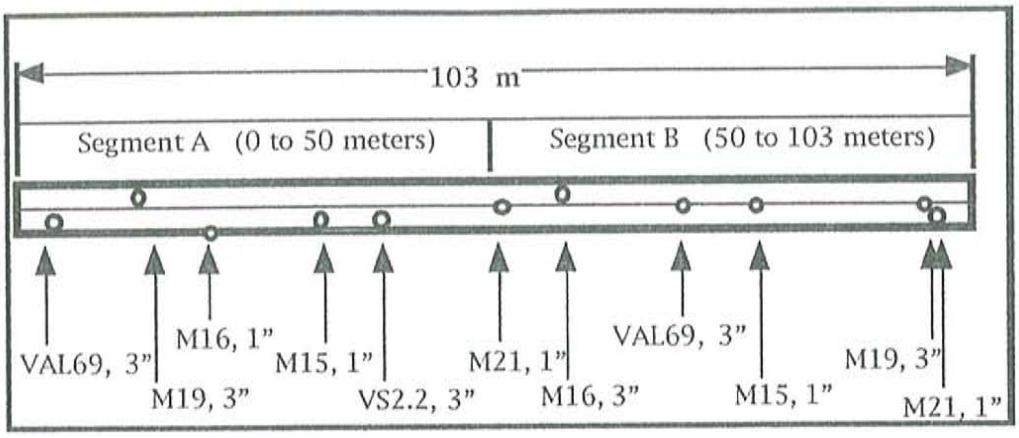

Figure 4.8: Diagram map of Test Track 2 during a land mine deployment for GeoCenters. The portions of this track surveyed with the magnetometer are labeled as Segments A and B. The map shows the land mine types, depths of burial, and approximate location within the track. This mine deployment occurred in April 1996.

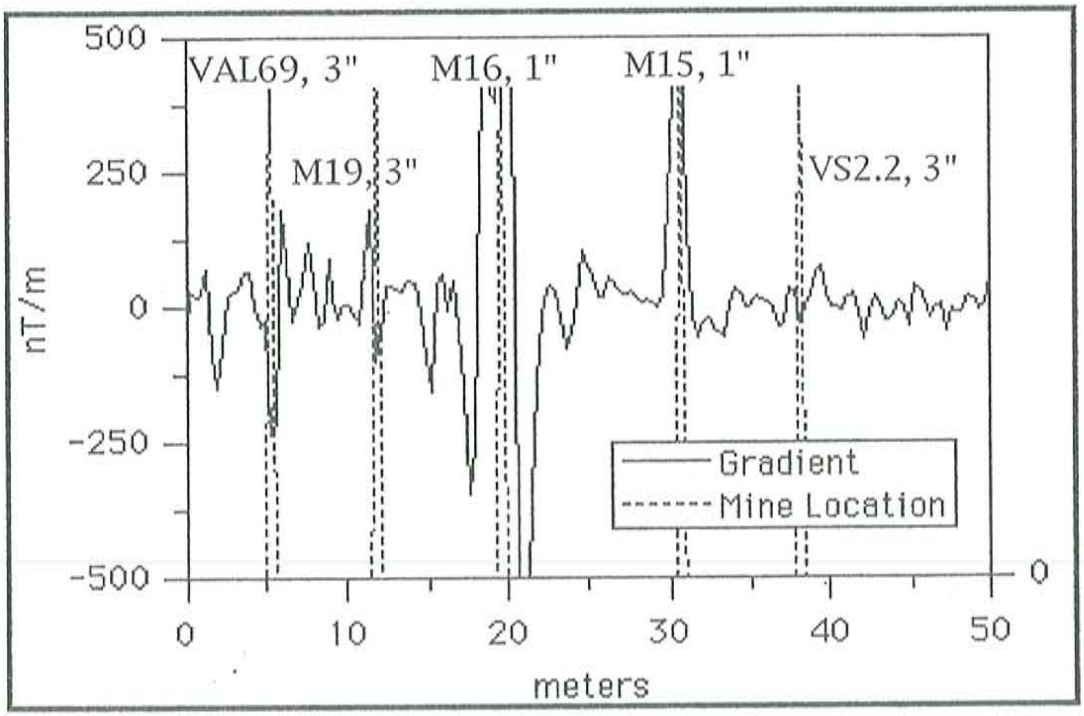

Figure 4.9: Magnetic vertical gradient curve (solid line) of Track 2 centerline, segment A (0 to 50 meters). Sensor separation was 0.7 meters, gradients were at 0.65 meters, and continuous sampling rate was 0.3 seconds. Plot shows approximate location of buried land-mines (dashed line), their type, and depth of burial. Data recorded 4/3/96.

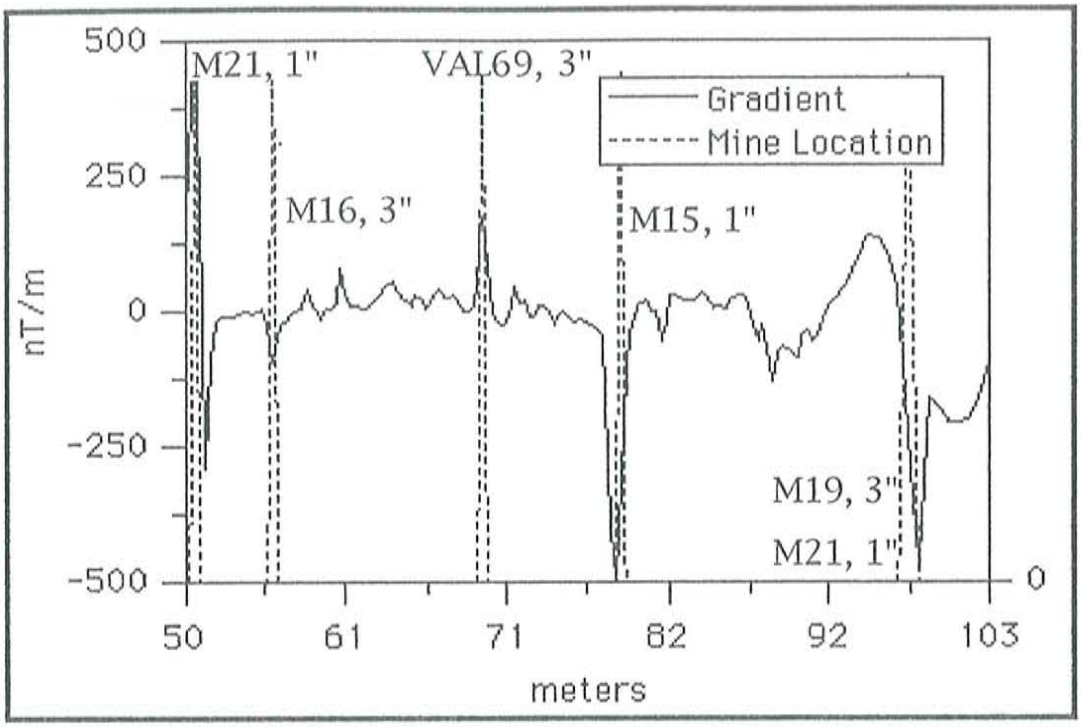

Figure 4.10: Magnetic vertical gradient curve (solid line) of Track 2 centerline, segment B (50 to 103 meters). Sensor separation was 0.7 meters and gradients were calculated at a height of 0.65 meters. Continuous sampling rate was at 0.3 seconds. Plot shows approximate location of buried land-mines (dashed line), their type, and depth of burial. The data were recorded on 4/3/96.

4.3.2 SAIC UXO Track (June 30)

The data collected during the SAIC deployment were from a survey of unexploded ordnance in a test lane on the On-Road Track 3. The lane surveyed with the magnetometer was 2 meters wide and 103 meters long. The UXO sources deployed were the 20mm HE round, 30mm HEDP round, 60mm mortar, 100 and 200 g shells, small arm surface clutter, and 105mm HEP-T projectile.

Target UXO contained significant metallic and explosive content. Table 4.2 presents major physical parameters of each UXO type encountered during this survey.

Table 4.2: Counter-Mine Test Site UXO Parameters

UXO Source	20mm HE	30mm HEDP	60mm	105mm HEPT	100g	200g
Type	Art. Round	Art. Round	Mortor	Projectile	Art. Shells	Art. Shells
Casing	Metallic	Metallic	Metallic	Metallic	Metallic	Metallic
Weight	NA	NA	NA	NA	NA	NA
Length	~200 mm	~400 mm	~300 mm	NA	NA	NA
Width	20 mm	30 mm	60 mm	105 mm	NA	NA
Height	cylindrical	cylindrical	cylindrical	cylindrical	cylindrical	cylindrical
Charge	H761	PBXN-5	Comp B	Comp A3	NA	NA
Charge Wt.	10.7 g	22 g	0.79 lb	6.6 lb	NA	NA

The lane was delineated with a single rope indicator down the long axis of the lane's center. Measurements were recorded while pacing down the lane with the sensors positioned over the rope. The lateral distance of the buried UXO from the center line was not known thus their detectability was dependent on proximity to the center line, as well as the magnetic parameters of the target. Testing schedules did not permit more than a single line survey for this lane.

The magnetometer was operated in a dual sensor gradiometer mode with a 0.7 meter sensor separation and a 0.3 meter lower sensor height. The magnetometer was operated in SIMPLE SURVEY mode with location points recorded within the data set indicating horizontal distances down track. The magnetic field was sampled in Continuous mode at a 0.1 second interval.

Figure 4.11 is a map showing track length and buried UXO types, depths of burial, and approximate locations for Lane 1 on the SAIC On-Road Track 3. Figure 4.12 shows the magnetic gradient profile of the lane's center line.

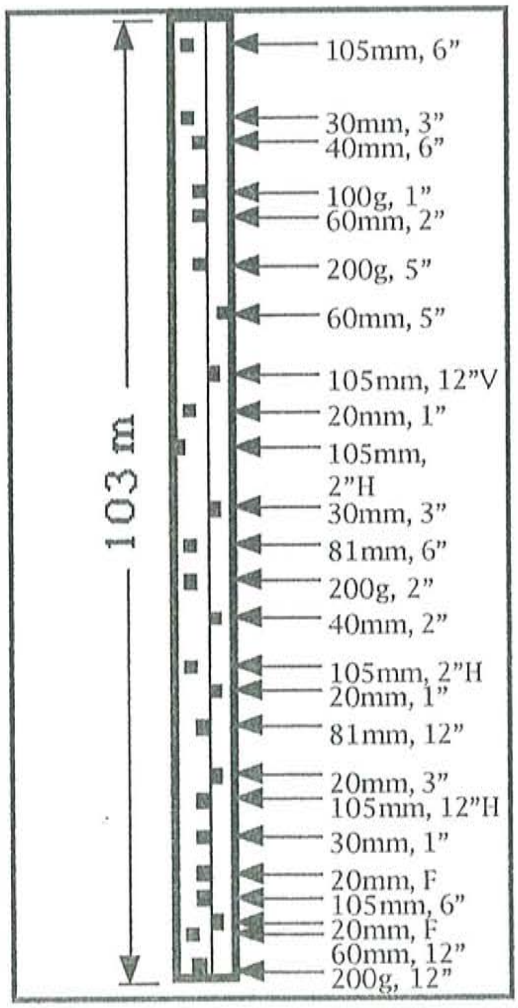

Figure 4.11: Diagram map of Test Track 3, Lane 1 during a UXO deployment for SAIC and ESTPC. The map shows the approximate location, type, and depth of burial of each ordnance target within the track. This UXO deployment occurred in June 1996.

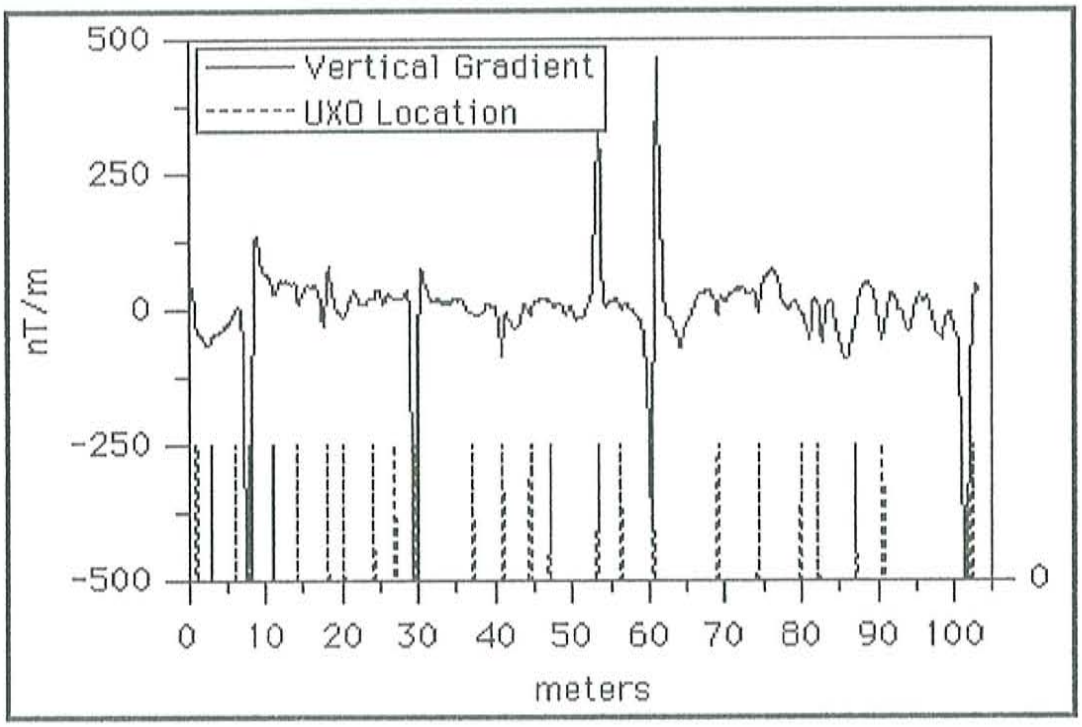

Figure 4.12: Magnetic vertical gradient curve (solid line) of Track 3, Lane 1 centerline (0 to 103 meters). Sensor separation was 0.7 meters and gradients were calculated at a height of 0.65 meters. Continuous sampling rate was at 0.1 seconds. Plot shows approximate location of buried UXO (dashed line). The data were recorded on 6/30/96.

4.3.3 Jaycor Land Mine Tracks (July 18)

The data collected during the Jaycor deployment were from surveys of land mines in lanes on two of the test tracks. The tracks surveyed with the magnetometer were the On-Road Track 2, Lane 2 (2 m x 198 m) and On-Road Track 3, Data Collection Lane (2 m x 255 m). The land mines deployed during this episode were the M15, M21, and VS2.2. Pertinent physical parameters of each land mine type have been shown in Table 4.1.

The boundaries of each test lane were delineated with chalk lines. Located within the lanes were five long axis lines evenly positioned laterally. Measurements were recorded while pacing down the track with sensors positioned over the lines. Thus each track generated five data streams. Track 3 also had position points every 10 meters, indicated in the data stream. This Data Collection Lane was known to have one or more land mine sources every 30 meters.

The magnetometer was operated in a dual sensor gradiometer mode with a 0.7 meter sensor separation and a 0.3 meter lower sensor height. The magnetometer was operated in SIMPLE SURVEY mode with location points recorded within the data set indicating horizontal distances down track. The magnetic field was sampled in Continuous mode at a 0.3 second interval. The following sections present contour maps of the vertical magnetic gradients recorded during this episode.

On-Road Track 2

Figure 4.13 is a map showing track length and buried land mine types, depths of burial, and approximate locations for Jaycor On-Road Track 2, Lane 2. Figure 4.14 shows the magnetic gradient contour map of the Lane 2 survey.

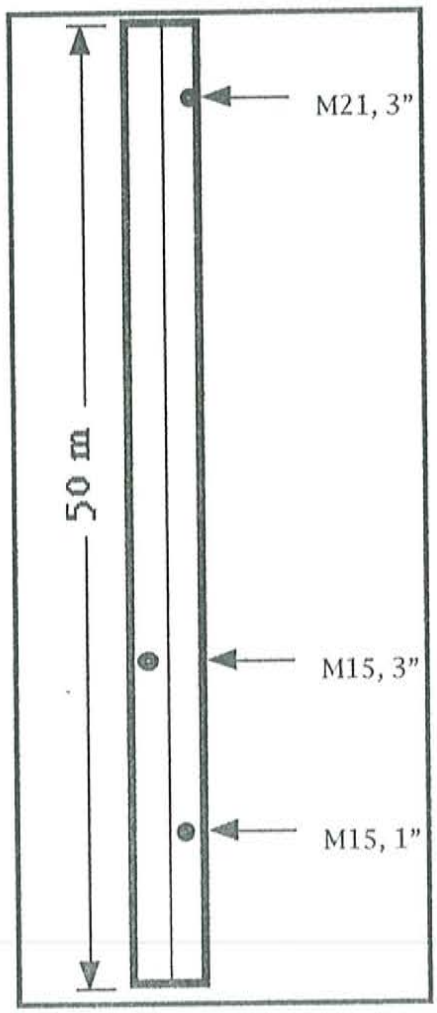

Figure 4.13: Diagram map of Test Track 2, Lane 2 (0 to 50 meters) during a land mine deployment for Jaycor. The map shows the land mine types, depths of burial, and approximate location within the lane. This mine deployment occurred in July 1996.

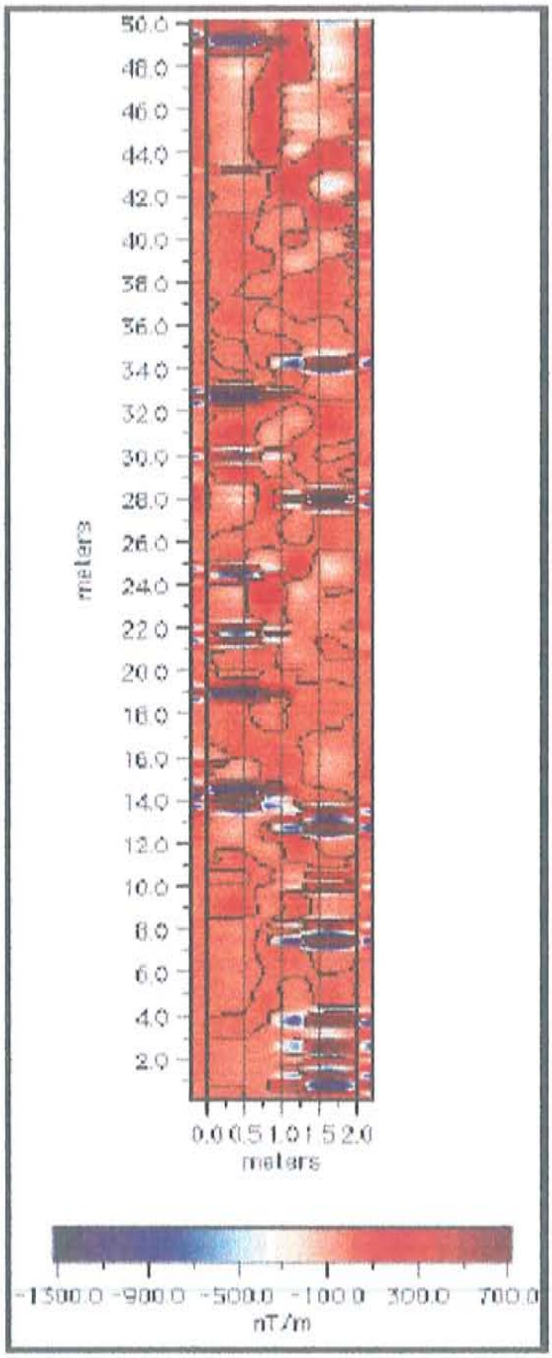

Figure 4.14: Magnetic vertical gradient contour map of Track 2, Lane 2 (0 to 50 meters). Sensor separation was 0.7 meters and gradients were calculated at a height of 0.65 meters. Continuous sampling rate was at 0.3 seconds along five lines equally spaced within the 2 meter width of Lane 2. The data were recorded on 7/18/96.

On-Road Track 3

Figure 4.15 is a map showing track length and buried land mine types, depths of burial, and approximate locations for Jaycor On-Road Track 3, Data Collection Lane. Figure 4.16 shows the magnetic gradient contour map of the Data Collection Lane survey.

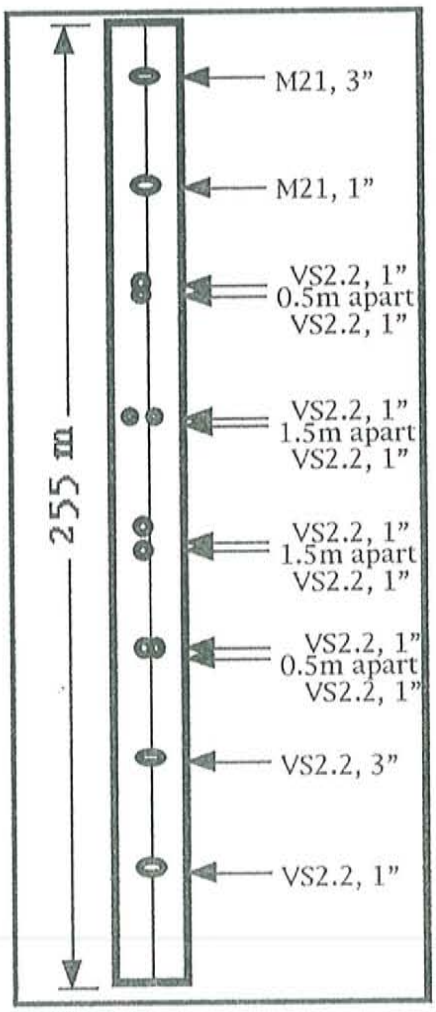

Figure 4.15: Diagram map of Test Track 3, Data Collection Lane (0 to 255 meters) during a land mine deployment for Jaycor. The map shows the land mine types, depths of burial, and approximate location within the lane. This mine deployment occurred in July 1996.

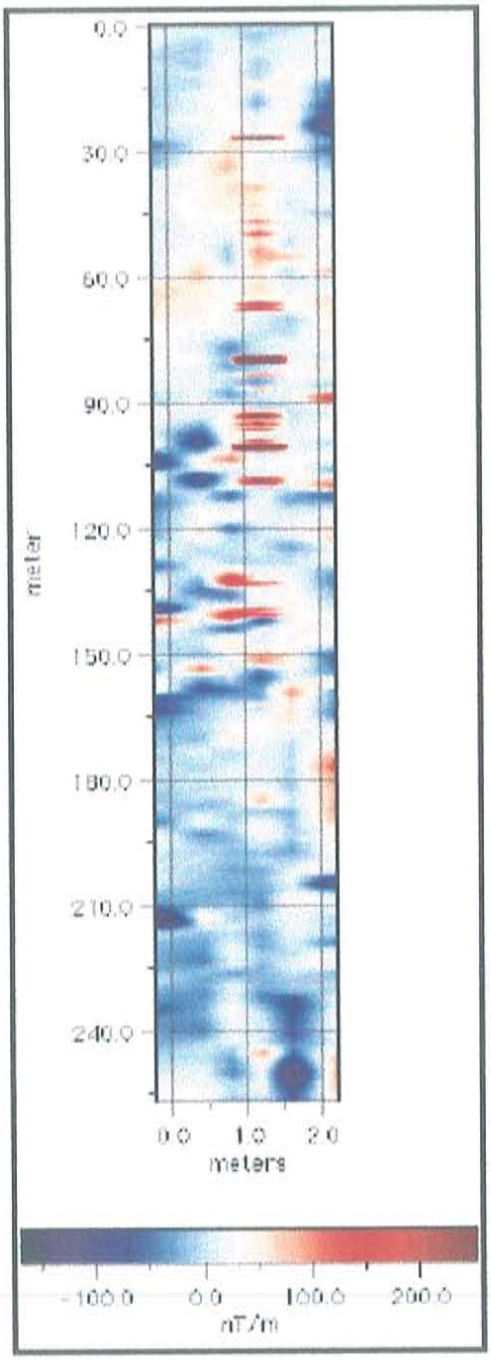

Figure 4.16: Magnetic vertical gradient contour map of Track 3, Data Collection Lane (0 to 255 meters). Sensor separation was 0.7 meters and gradients were calculated at a height of 0.65 meters. Continuous sampling rate was at 0.3 seconds along five lines equally spaced within the 2 meter width of the lane. The data were recorded on 7/18/96.

4.3.4 GDE Land Mine Track Blind Test (August 28)

The data collected during the GDE deployment were from surveys of buried land mines on a lane of the On-Road Track 1 (1.6 m x 101.96 m). The mines deployed during this period were the M15, M19, M21, and VS2.2. Pertinent physical parameters of each land mine type are found in Table 4.1.

The tracks were delineated with rope boundaries on both sides of the 1.6 meter wide lane. Magnetic gradient values were obtained first while pacing down the track using a sweeping sensor technique for the blind test portion of the survey. The magnetometer was in SEARCH mode. Then a survey using the SIMPLE SURVEY recording provided data for post-processing analyses to compare detection results with the sweeping sensor infield blind test.

The magnetometer was operated in a dual sensor gradiometer mode with a 0.7 meter sensor separation and a 0.3 meter lower sensor height for the continuous sampling. The magnetometer was operated in SIMPLE SURVEY mode with location points recorded within the data set indicating horizontal distances down track. The magnetic field was sampled in Continuous mode at a 0.5 second interval.

Figure 4.17 is a map showing track length and buried land mine types, depths of burial, and approximate locations for GDE On-Road Track 1, Blind Test Lane. Figure 4.18 shows the magnetic gradient contour map of the Blind Test Lane survey.

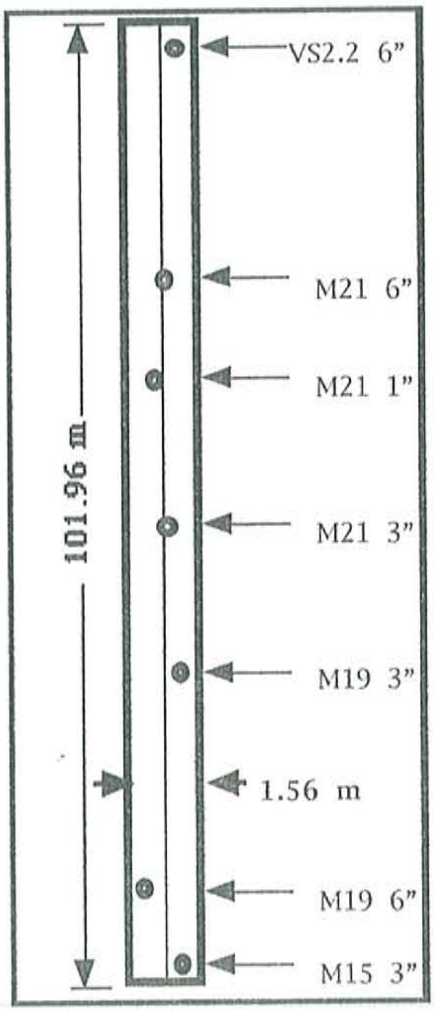

Figure 4.17: Diagram map of Test Track 1, Blind Test Lane (0 to 101.96 meters) during a land mine deployment for GDE. The map shows the land mine types, depths of burial, and approximate location within the lane. This mine deployment occurred in August 1996.

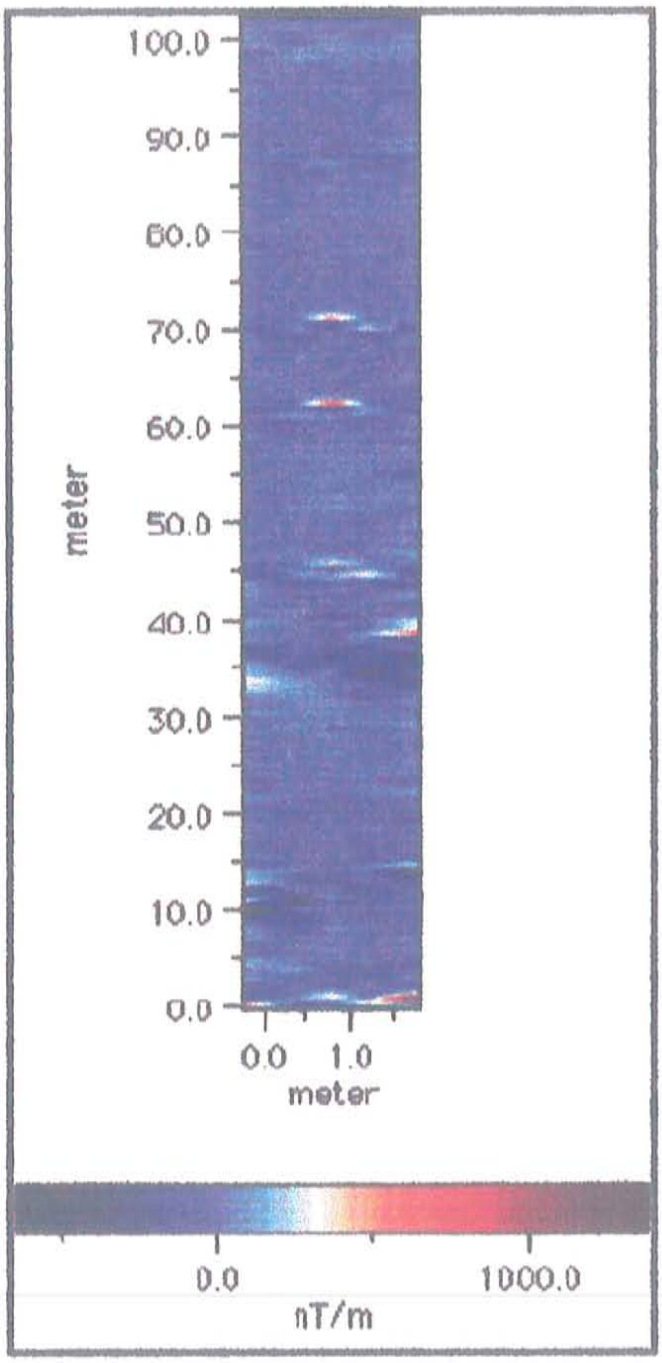

Figure 4.18: Magnetic vertical gradient contour map of Track 1, Blind Test Lane (0 to 101.96 meters). Sensor separation was 0.7 meters and gradients were calculated at a height of 0.65 meters. Continuous sampling rate was at 0.5 seconds along five lines equally spaced within the 1.6 meter width of the lane. The data were recorded on 8/28/96.

This chapter presented the magnetic data recorded during surveys of ordnance buried in test lanes at the Counter-Mine Test Site. All the data presented are without filtering or correction. Computer processing was only for mapping, plotting, or scaling purposes. The next chapter, Magnetic Data Analyses, deals with filtering schemes, location efforts, and analyses of target parameters.

Chapter 5
Results: Magnetic Data Analyses

5.1 Gradiometric Data Realizations

5.1.1 Analyzing the Gradiometric Data

The experiments described in Chapters 3 and 4 generated significant amounts of gradiometric measurements encompassing several magnetic prospecting techniques. An understanding of how magnetic gradiometry may be useful in counter-mine operations must now come from properly analyzing the data and the significance of their results. Generally, magnetic data are transformed to plotted images whereby structures and shapes in the field strength lines help determine the location of magnetic targets.

The magnetic anomaly plots and contour maps themselves are easily generated and provide quick identification of most subsurface magnetic objects and their respective position and depth. However to effectively detect some targets it is often necessary to apply reduction and filtering procedures to the data. During a survey for land mines and UXO, a recording of the magnetic gradients along only a 100 meter trail may produce several thousand data strings like those shown in Table 2.1. These data must first be reduced and mapped with accurate positioning and with attention paid to spurious variations. Only then can specific images be declared as either positive targets or false positive targets.

In understanding the significance of the magnetic maps obtained from surveys at the CTP and CTS, this chapter will attempt to provide specific results as determined from those maps. These results will include non-unique gradiometric signatures of target objects, detectability limits on magnetic and

non-magnetic targets, and detection results of staged mine surveys. This chapter will also provide explanations of the data-processing used in the analyses, including spatial and amplitude filtering.

5.1.2 Avoiding Diurnal and Regional Corrections

The magnetic gradient of the Earth's field was chosen as an investigation tool for several reasons. Primarily, the discrimination between adjacent targets is generally enhanced using the gradiometer method, rather than a single sensor methods. This results from the fact that a gradiometer is essentially a first derivative operator that can resolve composite or complex anomalies into individual components (Steiner, 1977). This allows a gradiometer to have greater sensitivity to subsurface objects and it becomes an effective automated filter. This filtering occurs during the gradient calculation itself, when a normalized differentiation is determined, i.e. the sensor reading difference normalized by the separation distance. This differentiation ignores the amplitude or trend of all single sensor readings, and provides a measurement based on the spatial rate of change between the sensors. This effectively removes long period variations in the data. A long period variation is one who's lateral extent is several times greater than the gradiometer sensor separation. These variations result from several sources, both spatially and temporally.

Temporal, or transient, variations are time dependent and vary in amplitude. Variations in the ambient magnetic field occurring over the course of hours or days are termed diurnal variations. They are the result of sun-spot activity, variations in solar ionization, and daily and monthly atmospheric tides. These diurnal variations affect magnetic intensity as recorded throughout the day as field intensity decreases rapidly during the

early morning sunrise, reaching a minimum at noon, and increases during the afternoon and night (Aitken, 1974). This affect was described in Chapter 3 and is illustrated in the diurnal drift curve of Figure 3.4.

Spatial variations result from lateral changes in the magnetic properties of the surface and subsurface within a survey area. These changes may occur within the subsurface as abrupt sedimentary facies changes or as faults. These variations are common in areas of buried ultra basic rocks, magnetic ore bodies, or metallic structures (Steiner, 1977). Their effect on gradiometer data is to produce high magnetic gradients that can exceed anomaly strengths produced by the target objects. These variations often have a long wavelength relative to that produced by the targets and are corrected by filtering out long period trends in the data.

Generally, field surveys must be corrected for these variations. However, the data sets used in this study have not been diurnally or regionally corrected. This was considered acceptable for two reasons. The first is again based on the fact that magnetic gradients are 'first derivative' operators that effectively ignore components of diurnal or regional drift present in the ambient field. The second motivation is the small scale of the surveys in both space and time, which limited the the possible variations.

5.1.3 Filtering Schemes Applied

In an attempt to increase the effectiveness of the gradiometer, some filtering schemes were applied to specific data sets. These filtering schemes were useful in pinpointing target locations, increasing the magnetometers detection rate, and reducing the number of false positives. Staying as mathematically simple as possible, two main data filters were applied, one for frequency and one for amplitude.

The frequency filter performs high pass filtering of the data during which only high frequency, or short wavelength, anomalies survive. Based on a discrete Laplacian weighting convention, the data matrix is transformed into a matrix of the same size, but possessing elements equal to the difference between the element and its neighboring average. The Laplacian filter may then be considered a first derivative operation in the horizontal plane. Thus the resulting filtered data sets are second derivative maps of the vertical field strength, the first occurring in the vertical direction and the second in the horizontal. For two-dimensional contour maps, this five-point Laplacian filter accentuated the small scale anomaly images of land mines and UXO, and reduced long-wavelength geologic anomalies contributing to the magnetic noise in the data. The filter was also applied to one-dimensional anomaly plots with similar effect but the loss of weighting elements decreased its effectiveness.

The second major data-processing technique involved gradient magnitude reduction. This amplitude filter essentially placed limits on the data magnitudes themselves. This was performed to allow identification of several scales of anomaly strengths within a single survey. A magnetic map containing objects of vastly different signal strengths may only allow imaging of the higher signal targets. During this amplitude scaling, excessively high magnetic gradient values are either normalized by a fraction of their amplitude or cut off at a specific fraction. For example, this allows for identification of a 50 nT/m anomaly within a contour map containing a 1000 nT/m anomaly. Normally the lesser image would be lost in the contouring interval required by the greater image. The filtering code limits the larger anomaly to a fraction of its amplitude or scales it by a regional average. The details of this scaling method varied with site conditions and target type.

The following section provides detailed results on the magnetic testing done during the course of this research project at the EMRTC field laboratories. The results presented are based on survey data in the last two chapters.

5.2 Control Test Pad Survey Results

5.2.1 CTP Background Magnetism

Consistent with the assumptions mentioned in section 3.2 concerning the CTP testing environment, the background magnetism of the site was low level. The background contour maps shown in Figures 3.5 through 3.9 indicate that the test grids contained vertical gradients in the ± 10 nT/m range near the grid boundaries, while the center portions were near zero nT/m. A gradient of zero indicates that the field strength is constant within a meter above the surface and thus the soil has no lateral changes in magnetic susceptibility.

Again it should be pointed out that the gradients calculated are based on the upper sensor minus the lower sensor, thus negative gradients indicated that the reading nearest the ground is larger. Extremely large negative gradients imply high field strength near the lower sensor which drops rapidly approaching the upper sensor, a phenomenon indicating a localized and very shallow source such as that produced by magnetic mines and UXO. On the other hand a positive gradient implys a lower field strength at the lower sensor than at the upper, a situation that occurs because of shallow voids or pockets of low susceptibility material. High positive readings are nearly always associated with corresponding negative peaks, and vise versa, as this is characteristic of the dipole nature of induced magnetization at magnetic mid-latitudes, i.e. inclinations such as the local 60.8 degrees.

5.2.2 Void Characterization

The magnetic contour maps of the Void Characterization Experiments reflect very small changes in the ambient field with introduced voids. The voids used were 7.6 and 11.4 liter plastic containers buried beneath the surface to a depth of 15 and 35 cm, respectively. The resulting gradient maps from Chapter 3 are shown as a composite anomaly curve in Figure 5.1. This figure contains the gradient background and the anomalies produced by the voids.

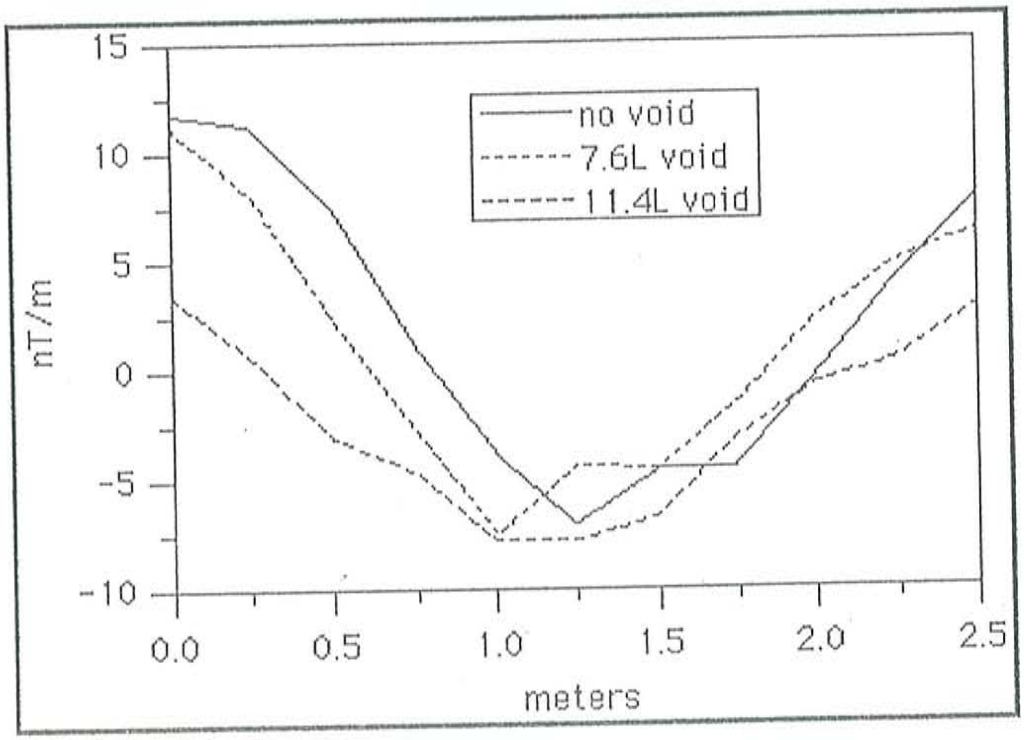

Figure 5.1: Magnetic vertical gradient curves of a void survey at the CTP Auxiliary Grid 1. The surveys were for the background, a 7.6 L void located between 0.15 and 0.35 meters depth, and a 11.4 L void located between the surface and 0.35 meters depth. The voids were at the 1.25 meter position. Station spacing was 0.25 meters, sensor separation was 0.7 meters, and lower sensor was 0.3 meters. The data presented are unfiltered and were recorded on 7/18/96.

The gradient data from Figure 5.1 were extracted from three contour maps by using only the north-south survey line that passed directly over the center of the buried voids. The curves themselves possess similar shapes which broaden with void volume but maintained the same absolute gradient of about -7 nT/m directly over the void. Thus the lack of soil magnetism yielded an insufficient susceptibility contrast for void detection based on gradient values alone. Figure 5.2 shows the same void anomaly survey but with the background magnetism subtracted out. This was done in an attempt to isolate the gradient signature of the voids themselves. The resulting curves maintain similar features and show a small positive peak above the void location. While this positive peak is low amplitude (less than 5 nT/m) its small width can be distinguished from the background.

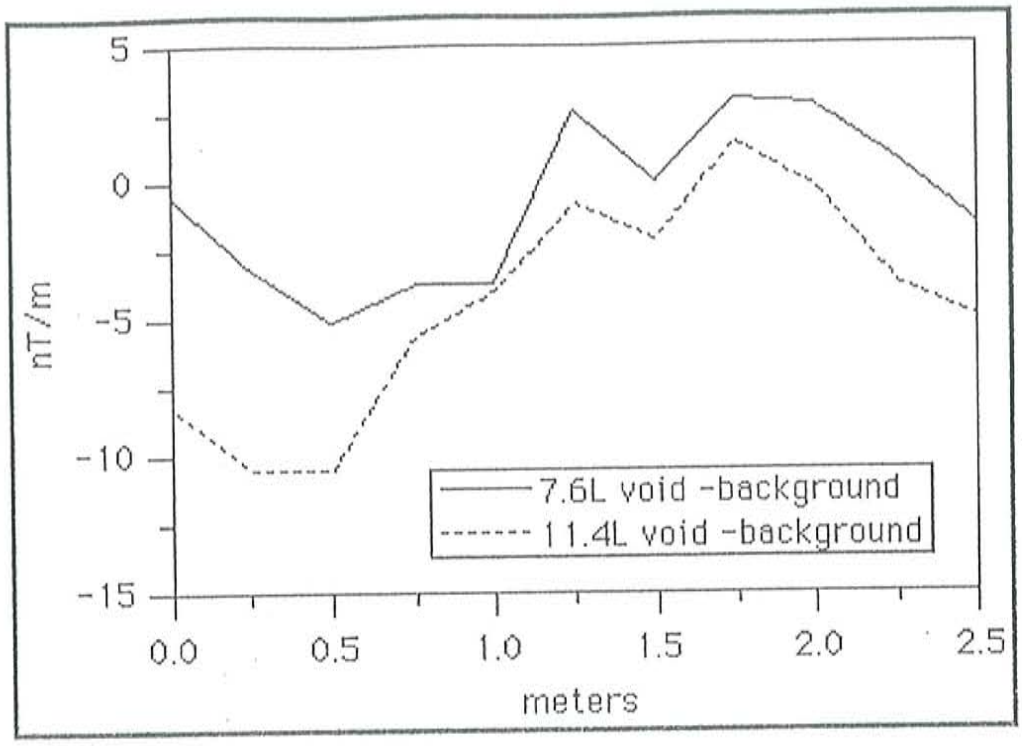

Figure 5.2: Magnetic vertical gradient signatures of voids surveyed at the CTP Auxiliary Grid 1. The two signatures shown are of a 7.6 L void and a 11.4 L void located at the 1.25 meter position. Station spacing was 0.25 meters, sensor separation was 0.7 meters, and gradient measurements were calculated at a height of 0.65 meters. The data presented have had the background magnetism removed but are unfiltered.

Using the Laplacian filter, the small peak of the 7.6 L void is accentuated further (Figure 5.3). The dashed line of the filtered data shows that the absolute value of the horizontal gradient is greatest directly over the buried void. Although this may be an artifact of the soil noise it is interesting considering its consistency. Regardless of this second derivative peak, the amplitude of the void anomaly from the initial data is too faint to provide credence to reliable low volume/low susceptibility void detection just yet. This result was expected considering the local geologic conditions.

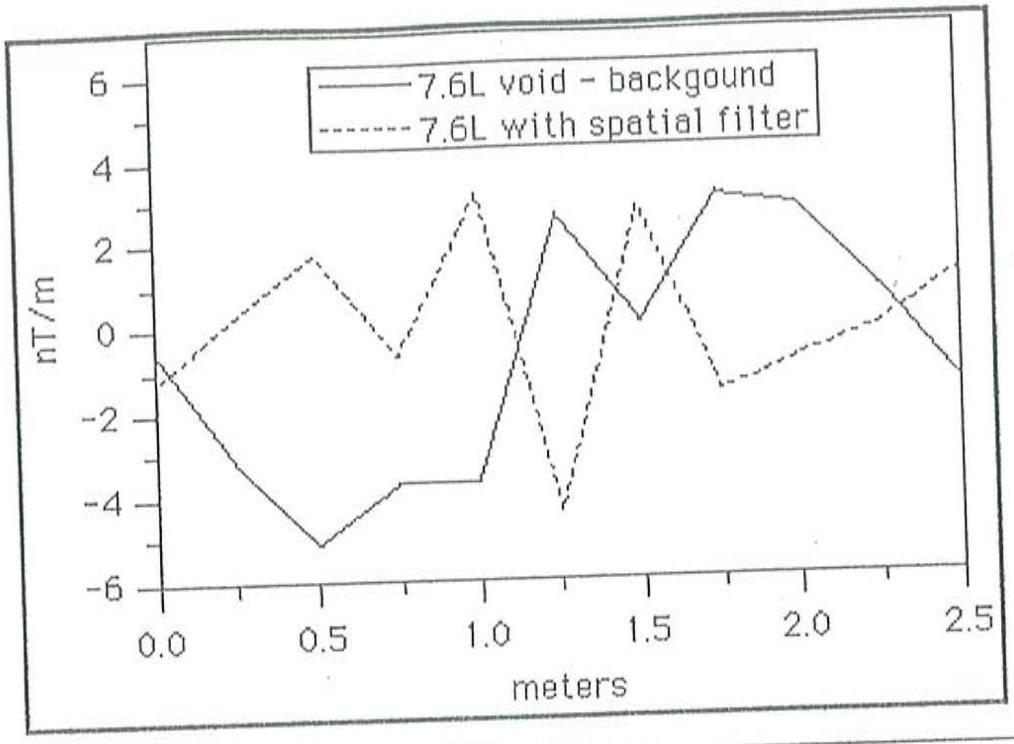

Figure 5.3: Magnetic vertical gradient signatures of a void surveyed at the CTP Auxiliary Grid 1. The two signatures shown are for a 7.6 L void with and without Laplacian filtering. The void is located at the 1.25 meter position, and both curves have had the background magnetism removed.

5.2.3 Detectability Thresholds

During the Smallest Buried Object Detectability Experiments completed at the CTP, a series of magnetic targets were surveyed in an attempt to place a limitation on the mass of metallic debris that may be detected by the gradiometer. For the purpose of relative comparison, a large 1.36 kg iron hammer was surveyed to represent the gradiometric signature of large, shallow metallic targets such as land mines or UXO; a valid comparison considering the hammer is less than half the weight of the metallic anti-personnel mines described in Table 4.1. During the survey, the hammer was placed on the surface, parallel to a North-South line, with its head to the south.

The results of this survey are shown as a contour map in Figure 3.17, and again in Figure 5.4 as an anomaly curve on the line directly over the hammer's long axis. The curve possesses both positive and negative gradient peaks of equal amplitude with their connecting maximum slope centered over the hammer. The negative peak lies directly over the head of the hammer wherein the majority if its metallic mass is found. The peak to peak amplitude of the curve is 140 nT/m at a 0.65 meter height.

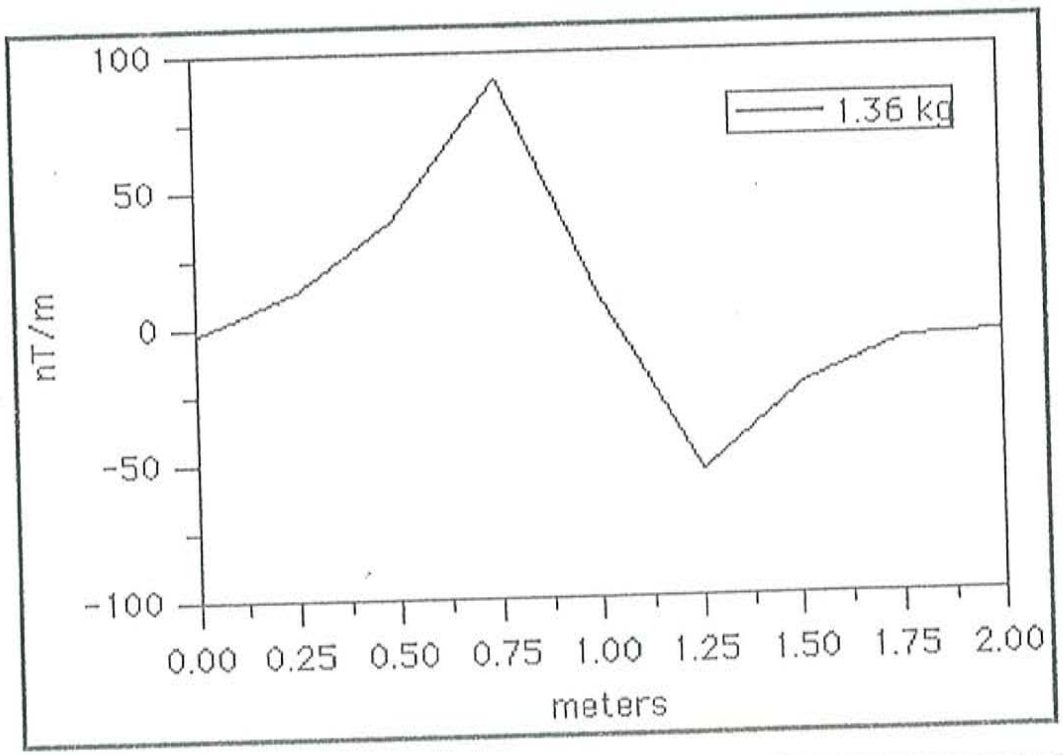

Figure 5.4: Magnetic vertical gradient plot for an iron hammer at Auxiliary Grid 2. Shown is the anomaly curve of the line containing a 1.36 kg iron hammer positioned at 1 meter on the surface. Station spacing was 0.25 meters, sensor separation was 0.7 meters, and gradient measurements were calculated at a height of 0.65 meters (lower sensor at 0.3 meters). The data are unfiltered and were recorded on 5/20/96.

The detectability experiment continued with the surveying of small iron pins. The resulting anomaly curves are shown in Figures 5.5 and 5.6, with the background gradient (less than 2 nT/m) subtracted to accentuate the iron pin signatures. With the 3 cm long pins buried vertically at a depth of 2 cm, the 0.5 gram iron pin is undetectable at nearly zero nT/m but the 1.0 gram pin begins to show the same peaked structure as the hammer target but at a 2 nT/m amplitude. The corrected anomaly curves for the 1.5, 2.0, and 6.5 gram pins maintain the same maximum slopes over the target pins, vary in the negative peak locations, and increasing in amplitude.

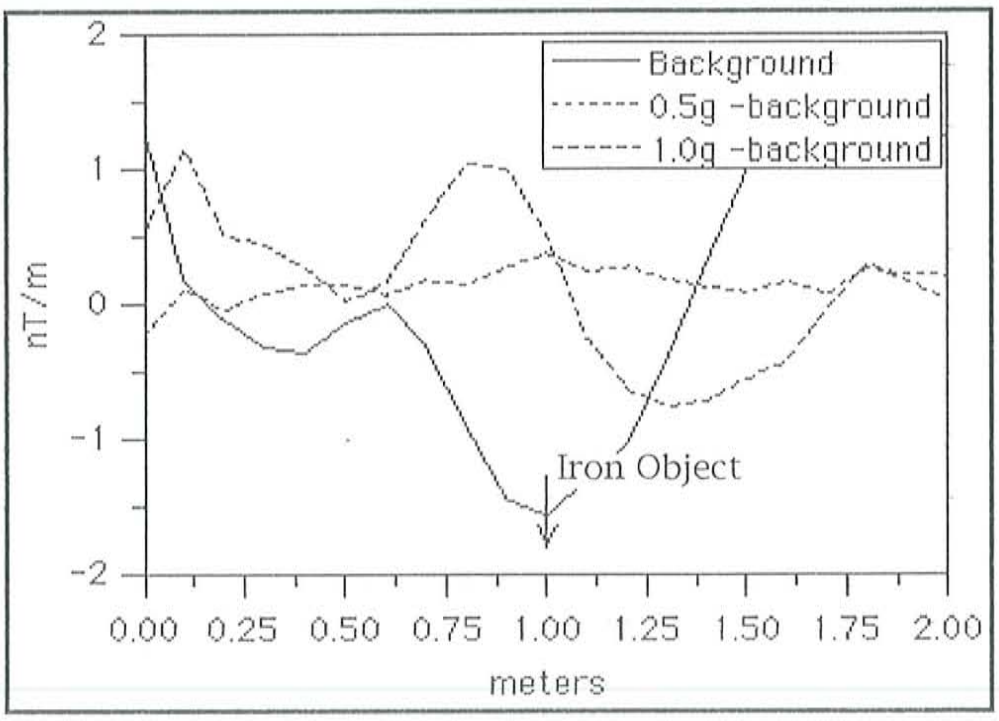

Figure 5.5: Magnetic vertical gradient plots for buried iron pins at Auxiliary Grid 4. Shown are the background curve and anomaly curves for 0.5, and 1.0 gram vertical iron pins buried 2 cm at the 1 meter position. Station spacing is 0.1 meters, sensor separation is 0.7 meters, and gradient measurements were calculated at a height of 0.5 meters (lower sensor at 0.15 meters). The pin data have had the background removed and were recorded on 3/15/96.

Thus the detectability limits for a vertical iron pin at this sensor configuration and background magnetism is 1.0 gram. This was also apparent in the initial uncorrected data of Figure 3.15, where the 0.5 gram pin mirrors the background curve, while the 1.0 gram curve is indicative of a magnetic metal target. The 1.0 gram iron pin has a mass and dimensions similar to the fuse mechanisms of both metallic and non-metallic mines.

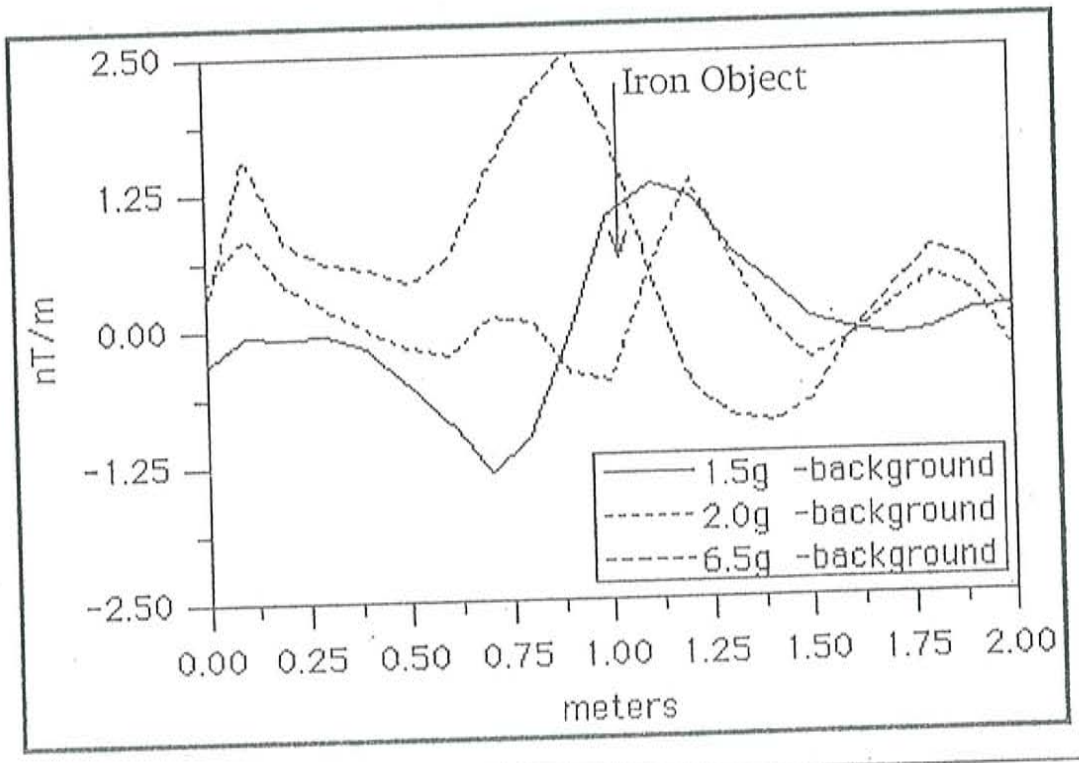

Figure 5.6: Magnetic vertical gradient plots for buried iron pins at Auxiliary Grid 4. Shown are the anomaly curves for 1.5, 2.0, and 6.5 gram vertical iron pins buried 2 cm at the 1 meter position. Station spacing is 0.1 meters, sensor separation is 0.7 meters, and gradient measurements were calculated at a height of 0.5 meters (lower sensor at 0.15 meters). The pin data have had the background removed and were recorded on 3/15/96.

5.2.4 Inert Dummy Mine Signatures

The dummy target mines listed in Table 3.1 were intended to provide information on the expected magnitude and form of land mine magnetic signatures. Both metallic and non-metallic dummy mines were surveyed and the results are displayed in Figure 3.18 through 3.25 as contour maps from CTP Grids. To further analyze their magnetic signatures, curves have again been extracted from map survey lines containing the mine anomaly. The first non-metallic mine, Type A, is shown sampled at three different sensor configurations in Figure 5.7.

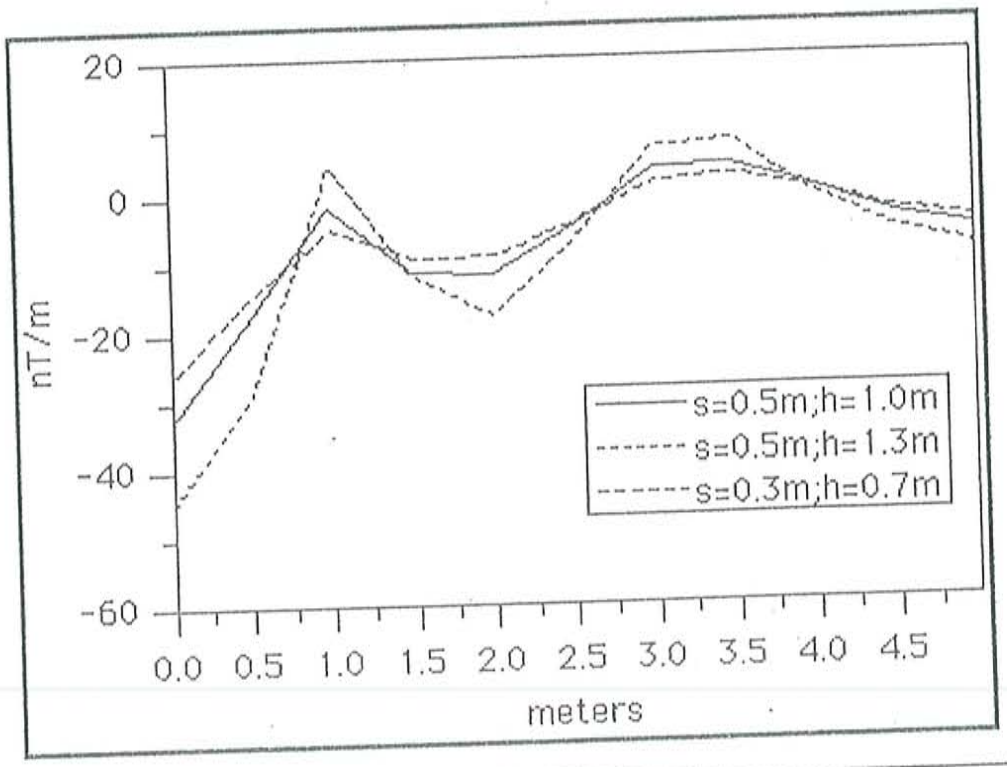

Figure 5.7: Magnetic vertical gradient plots of a non-metallic anti-personnel dummy mine at the CTP Main Grid. Shown are gradient curves of the Type A dummy mine at three sensor configurations. The sensor separation/height combinations were 0.5/1.0 meters, 0.5/1.3 meters, and 0.3/0.7 meters. Mine A was buried at a 6 cm depth at the 2.5 meter position, and station spacing was 0.5 meters. The data presented are unfiltered and were recorded on 4/30/96.

It was apparent in this Figure that the anomaly curves for a 0.3 and 0.5 meter sensor separation failed to reveal the mines location, as the gradient sensitivity is insufficient for a non-metallic mine of this size (see Table 3.1). It was at this point (actually the earliest testing done) that a standard 0.7 meter sensor separation and 0.65 to 0.7 meter sensor midpoint height, was adopted for land mine detection. Sensitivity increased with sensor separation and the 0.3 meter separation curve was nearly a flat response at zero nT/m. The decision to exclusively use the 0.7 meter separation was based on several factors. Gradient sensitivity increases with sensor separation, however this effect is mathematically linear, while the sensor's measurement is affected by the cube of the distance to the object. Considering the magnetic noise levels, expected depth of targets, and the limitations of the sensor staff assembly, the lower sensor was needed to be close to the ground while preserving maximum separation with the upper sensor.

The second, and last non-metallic dummy mine surveyed was mine Type G. Maintaining the 0.7 meter separation but lowering the sensors midpoint to 0.45 meters aided in detecting this anti-tank mine of appreciable size. While the mine casing is non-metallic, it contains a small metallic dummy fuse assembly that contributed to a -40 nT/m gradient signature as shown in Figure 5.8. Mine G was buried to 10 cm on the CTP Main Pad, and while 30.5 cm in diameter, the mine's fuse assembly is located within a 5 cm radius of the center.

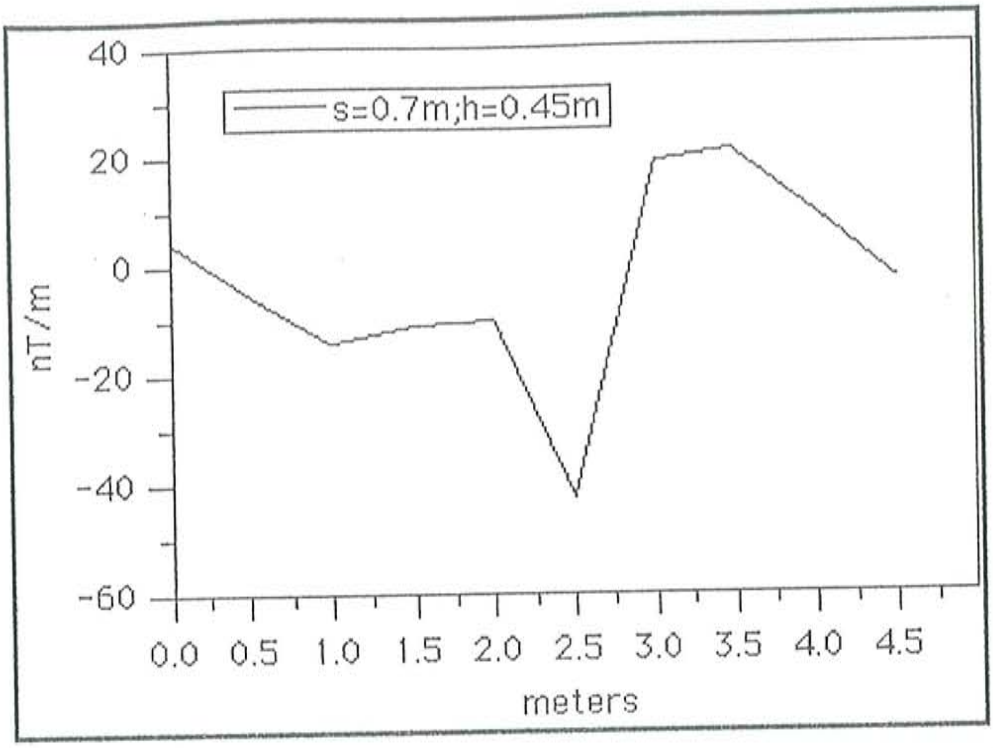

Figure 5.8: Magnetic vertical gradient plot of a non-metallic anti-tank dummy mine at the CTP Main Grid. Shown is a gradient curve of the type G dummy mine for a 0.7 meter sensor separation and a 0.45 meter gradient height (lower sensor at 0.1 meter). Mine G was buried at a 10 cm depth at the 2.5 meter position, and station spacing was 0.5 meters. The data presented are unfiltered and were recorded on 5/14/96.

Of the metallic dummy mines surveyed, both Types B and J (Table 3.1) were readily detectable with the adapted survey configurations. Type B mine was sampled in both a vertical and horizontal gradient mode. During the horizontal mode the number 1 sensor (upper) was placed in the northern position, while the number 2 sensor (lower) was to the south. The sensors were horizontal and separated by 0.7 meters. The resulting anomaly curves for this horizontal gradient survey of the Type B mine are shown in Figure 5.9 for the two sensor heights of 0.1 and 0.8 meters.

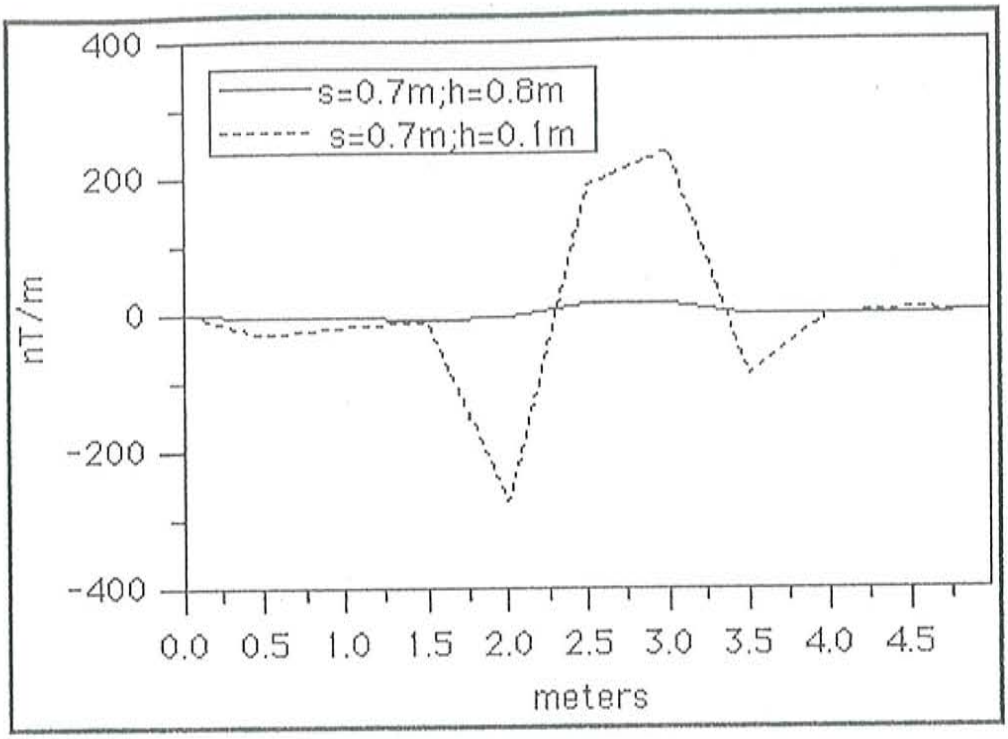

Figure 5.9: Magnetic horizontal gradient plots (N-S) of a metallic anti-personnel dummy mine at the CTP Main Grid. Shown are gradient curves for the Type B dummy mine at a 0.7 meter sensor separation and at gradient heights of 0.1 meters and 0.8 meters. Mine B was buried at a 6 cm depth at the 2.5 meter position, and station spacing was 0.5 meters. The data presented are unfiltered and were recorded on 5/14/96.

The mine's gradient anomaly signature for the 0.8 meter height has a peak to peak amplitude of 20 nT/m, but pales in comparison to the 511 nT/m peak to peak amplitude of the 0.1 meter height curve. The positive and negative peaks result from sensor proximity, and not from the dipole nature of the magnetism as previously seen. With the sensors at the same height, one sensor passes directly over the mine before the other, thus during subtraction of sensor 1 from sensor 2, the differential value is either positive or negative, depending on which sensor is closest. This leads to the anomaly curve possessing peaks of equal amplitude and a zero gradient directly above the mine. From the contour map in Figure 3.20 it is also apparent that horizontal

gradient surveys produce peaks on the east and west sides of the target as well, resulting from the same sensor proximity relationship.

Vertical gradient surveys were also made of the Type B mine at the 6 cm burial depth. Figure 5.10 shows the 244 nT/m peak to peak signature anomaly of the B mine using sensor heights of 0.35 and 1.05 meters. As with the previously surveyed iron objects, this anomaly curve has both positive and negative peaks who's amplitude is dependent on the mines orientation and depth of burial.

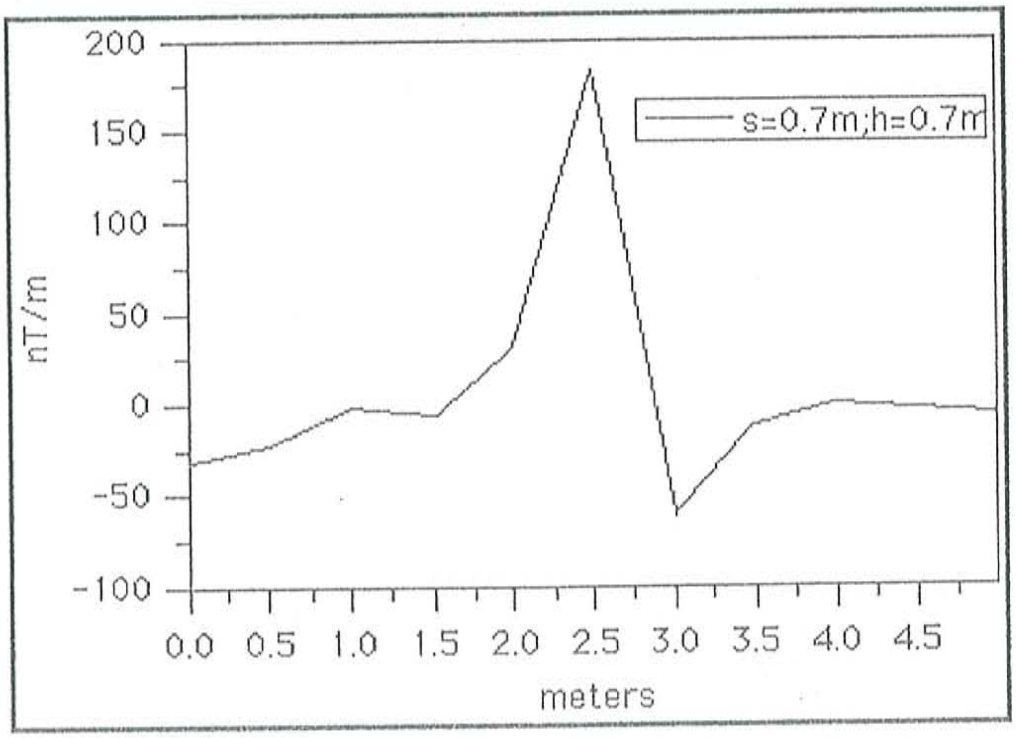

Figure 5.10: Magnetic vertical gradient plot of a metallic anti-personnel dummy mine at the CTP Main Grid. Shown is a gradient curve of the Type B dummy mine for a 0.7 meter sensor separation and a 0.7 meter gradient height. Mine B was buried at a 6 cm depth at the 2.5 meter position, and station spacing was 0.5 meters. The data presented are unfiltered and were recorded on 5/14/96.

During additional metallic dummy mine experiments on Auxiliary Grid 3, Types B and J mines were placed on the surface and vertical gradient surveys were made with sensor heights of 0.35 and 1.05 meters (Figures 3.23 and 3.25). The resulting extracted anomaly curves in Figures 5.11 and 5.12 are similar in shape for the two mines and have the signatures expected for metallic targets. However, they have vastly different amplitudes; Type B and Type J have corrected peak to peak amplitudes of about 500 nT/m and 50 nT/m, respectively. As the mine dimensions in Table 3.1 indicate, Type B mine is 8 times larger in volume than Type J, thus the expected signature amplitude is greater.

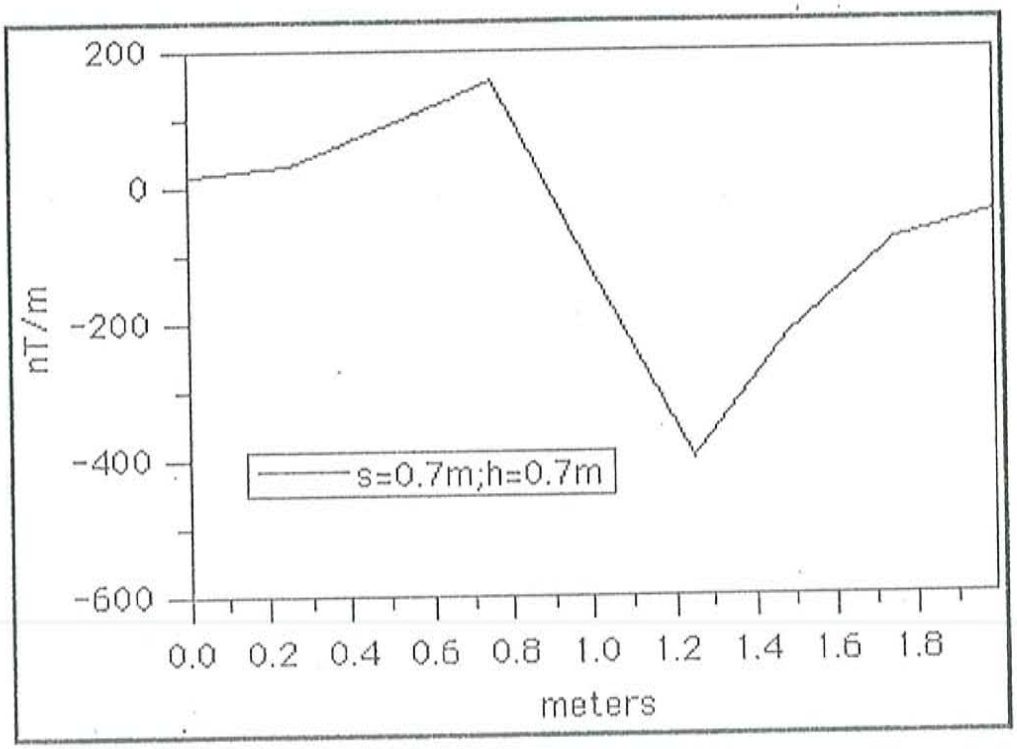

Figure 5.11: Magnetic vertical gradient plot of a metallic anti-personnel dummy mine at the CTP Auxiliary Grid 3. Shown is a gradient curve of the Type B dummy mine for a 0.7 meter sensor separation and a 0.7 meter gradient height. Mine B was placed on the surface, unburied, at the 1.0 meter position, and the station spacing was 0.25 meters. The data presented are unfiltered and were recorded on 5/22/96.

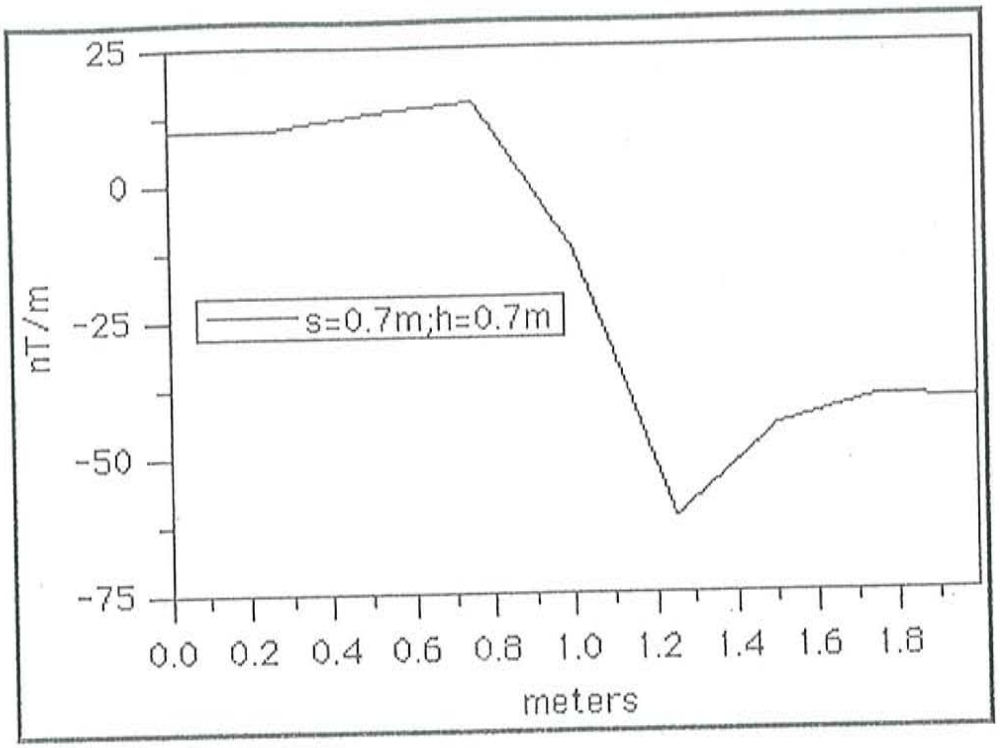

Figure 5.12: Magnetic vertical gradient plot of a metallic anti-personnel dummy mine at the CTP Auxiliary Grid 3. Shown is a gradient curve of the Type J dummy mine for a 0.7 meter sensor separation and a 0.7 meter gradient height. Mine J was placed on the surface, unburied, at the 1.0 meter position, and the station spacing was 0.25 meters. The data presented are unfiltered and were recorded on 5/22/96.

The CTP experiments provided magnetic anomaly signatures for metallic and non-metallic targets that aid in the understanding of gradiometric detection technique. The anomaly signatures of test targets are based on average gradient peaks as measured from the initial survey plots. The amplitudes and anomaly curves shown for each target are one of many possible non-unique signatures depending on soil conditions, target orientation and depth, sensor configuration, and target construction. However, the clues provided in the experiments lend much needed boundary conditions to the problem of mine and UXO detection.

5.3 Counter-Mine Test Site Survey Results

5.3.1 CTS Background Magnetism

The CTS testing environment, the background magnetism of the sites was of a moderate to high level, depending on the test track used. The maps shown in Chapter 4 indicate that the test tracks possessed vertical gradient noise of a ± 70 nT/m range. The greatest noise sources came from metal survey stakes, metal culverts, and magnetic volcanic rocks in the upper soil horizons. The soil, of variable magnetic susceptibility, created local field strength variations within a meter of the surface. Thus it is assumed that the data generated during the surveys were representative of actual land mine and UXO contaminated areas.

The data recorded during land mine and UXO deployments created two types of results. The first is a catalog of vertical gradient signatures based on the test track maps generated. The targets catalogued are described in Tables 4.1 and 4.2, and the survey results are presented as anomaly curves for individual land mine sources in this chapter. The second type of results deals with the detection and location abilities of both initial and processed gradiometer data. The detected mines and UXO are identified on contour maps and gradient curves with the sources' position, type, and depth of burial indicated within the figure.

5.3.2 Land Mine Signatures

The land mine test tracks described in Sections 4.3.1 and 4.3.3 involved detection of six basic land mine types, four of U.S. Army design, and two of foreign manufacture. Pertinent physical descriptions of all the land mines are found in Table 4.1. To obtain representative gradiometric signatures of these six mines, the entire Jaycor and GeoCenters survey data base was used. Definite in-field mine detections were matched against master location maps, and signatures were compiled for each mine type. Individual signatures were selected for display based on low noise levels and high signal strengths. The signatures shown are based on unfiltered data and are representative of expected in-field anomalies. Peak to peak anomaly magnitudes are given for each mine as well as the detection radii based on the average horizontal distances from the target's center of magnetization where the gradients are measurably higher than the background noise level and thus detectable. Filtering was only performed for detection and location maps.

The M15 was the first of the U.S. mines analyzed. The M15 anti-tank mine possesses a 3.9 kg circular metallic casing 0.34 meters in diameter. Its high degree of metal components makes it a relatively simple mine to detect using the gradiometer. The signature of the M15, for this mine track scenario, is shown in Figure 5.13. The mine's anomaly signature has a peak negative gradient of -490 nT/m and a detection radius of 0.85 meters at a burial depth of 2.54 cm. Anti-tank mines may often be buried significantly deeper, however this particular mine would probably generate a detectable anomaly to depths beyond a meter.

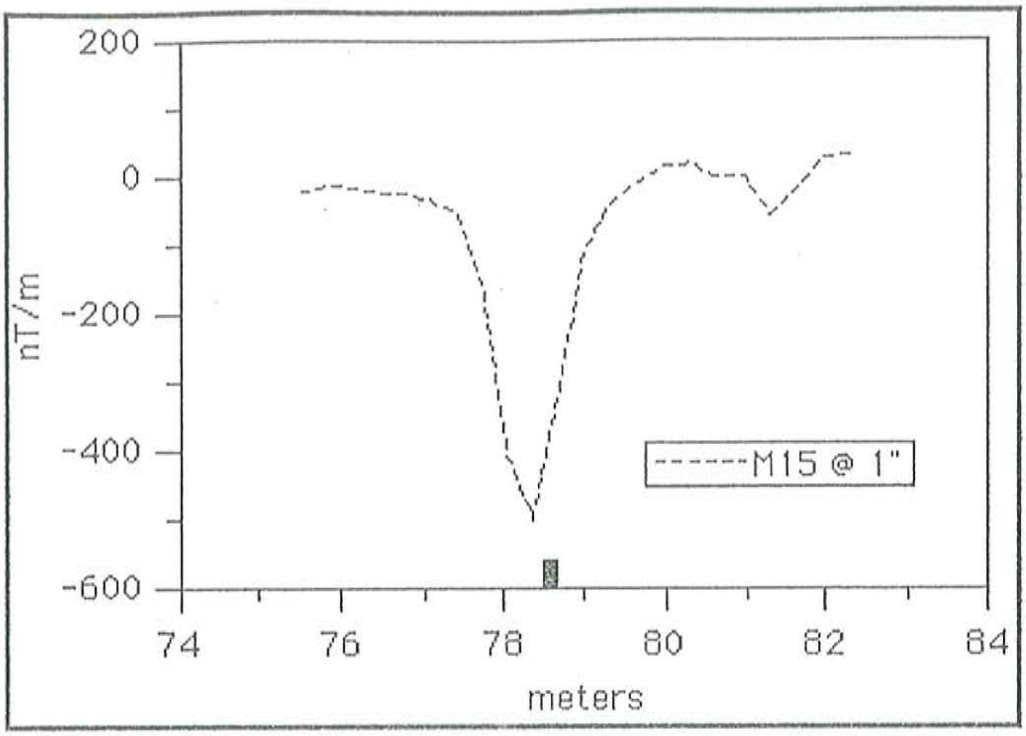

Figure 5.13: Magnetic vertical gradient plot of the M15 metallic anti-tank mine at a CTS land mine track. Shown is the gradient curve at a sensor separation of 0.7 meters and a gradient height of 0.7 meters. The M15 mine was buried 2.54 cm at the 78.6 meter position (black square). The data are unfiltered.

The M16 anti-personnel mine possesses a 3.1 kg cylindrical metallic casing 10.3 cm in diameter and 19.9 cm in height. Although it is volumetrically smaller than the M15, it contains nearly the same metallic components. As shown in Figure 5.14, the anomaly signature of the M16 has a peak negative gradient of -90 nT/m and a detection radius of 0.70 meters at a burial depth of 7.62 cm.

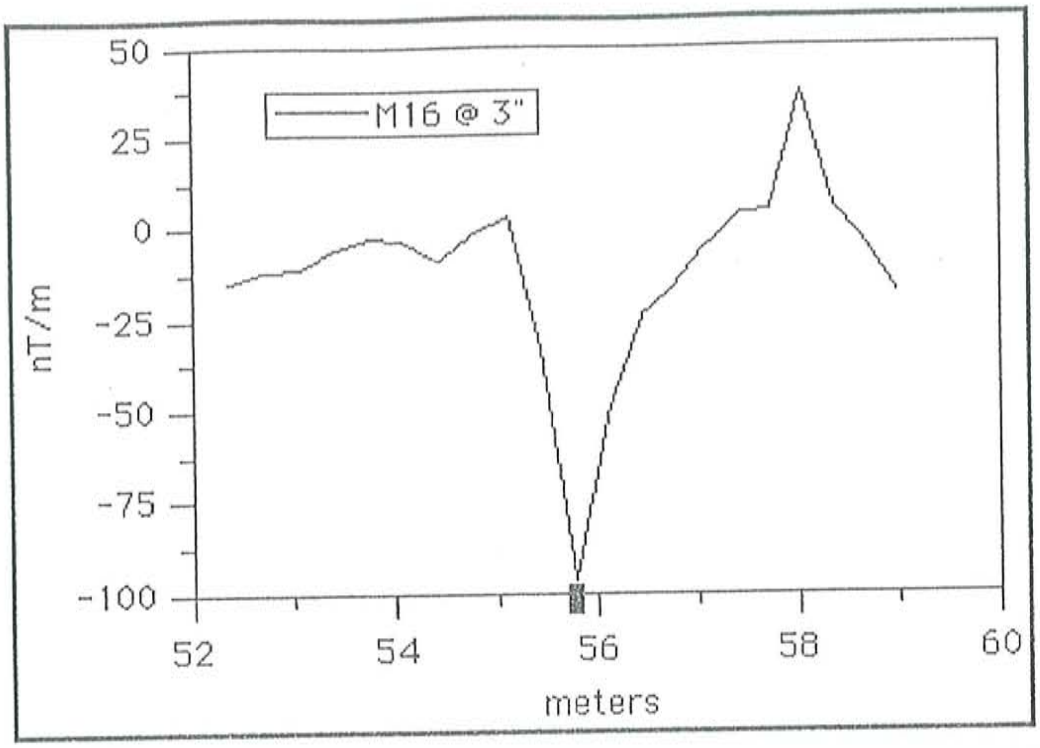

Figure 5.14: Magnetic vertical gradient plot of the M16 metallic anti-personnel mine at a CTS land mine track. Shown is the gradient curve at a sensor separation of 0.7 meters and a gradient height of 0.7 meters. The M16 mine was buried 7.62 cm at the 55.8 meter position (black square). The data are unfiltered.

The M19 anti-tank mine is encased in a 3.2 kg square non-metallic container 0.33 meters in width. The fuse mechanism possesses some small metal components which may aid in the detection of this mine if the background magnetic noise is not too great. The signature of the M19, for this mine track scenario, is shown in Figure 5.15. The anomaly has a negative gradient of -60 nT/m and a detection radius of 0.50 meters at a burial depth of 7.62 cm. Compared to a metallic anti-tank mine, the M19 is much more difficult to detect.

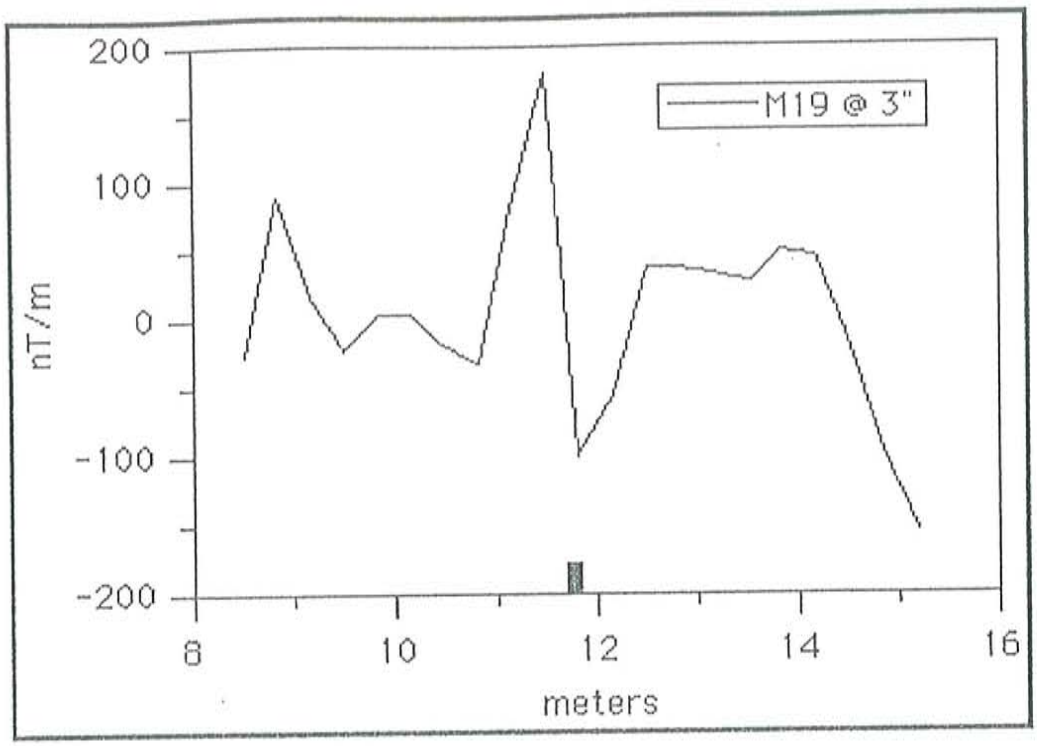

Figure 5.15: Magnetic vertical gradient plot of the M19 non-metallic anti-tank mine at a CTS land mine track. Shown is the gradient curve at a sensor separation of 0.7 meters and a gradient height of 0.7 meters. The M19 mine was buried 7.62 cm at the 11.8 meter position (black square). The data are unfiltered.

The M21 was the final U.S. mine analyzed at the CTS. The M21 anti-tank mine has a metallic casing but detailed physical characteristics were not available. The M21 signature (Figure 5.16) has a dipole structure with a peak to peak gradient amplitude of ± 250 nT/m, and a detection radius of 0.95 meters at a burial depth of 2.54 cm.

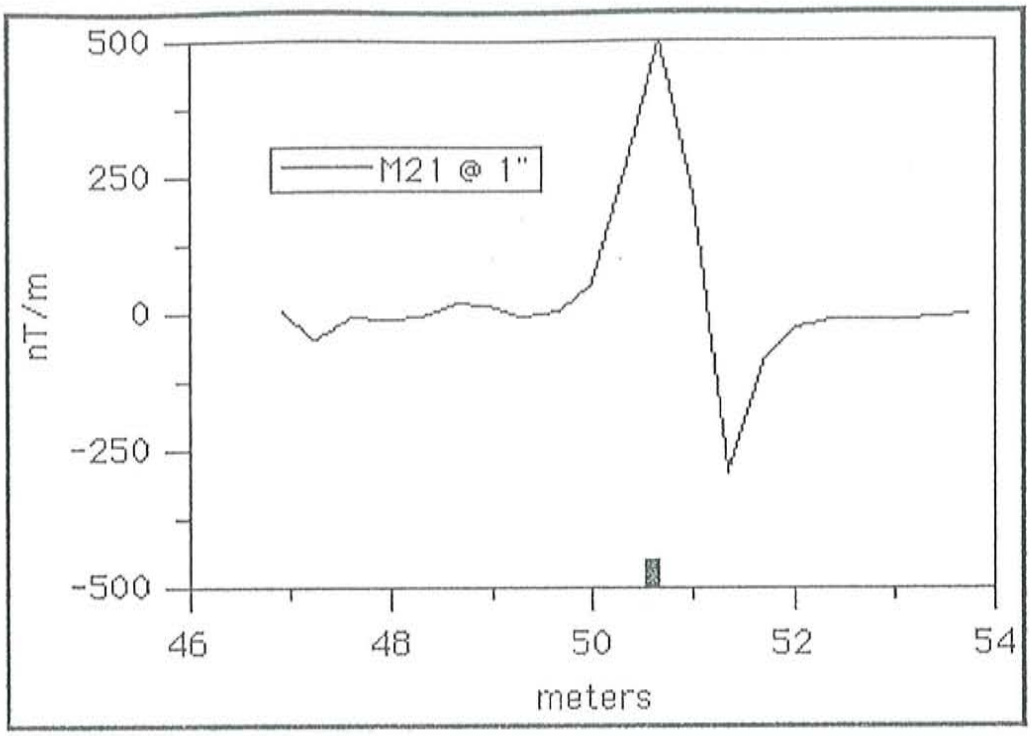

Figure 5.16: Magnetic vertical gradient plot of the M21 metallic anti-tank mine at a CTS land mine track. Shown is the gradient curve of a M21 land mine at a sensor separation of 0.7 meters and a gradient height of 0.7 meters. The M21 mine was buried 2.54 cm at the 50.6 meter position (black square). The data are unfiltered.

The two foreign land mines analyzed were the Italian made Valmara 69 and VS2.2. The Valmara 69 (VAL69) anti-personnel mine has a 2.7 kg cylindrical non-metallic casing 13.0 cm in diameter and 20.5 cm in height. Although it has a plastic casing and fuse cover, the VAL69 has multiple iron trip prongs and internal metallic shrapnel, both of which aid in its detection. As shown in Figure 5.17, the gradiometric signature of the VAL69 has a peak negative gradient of -220 nT/m and a detection radius of 0.35 meters at a burial depth of 7.62 cm.

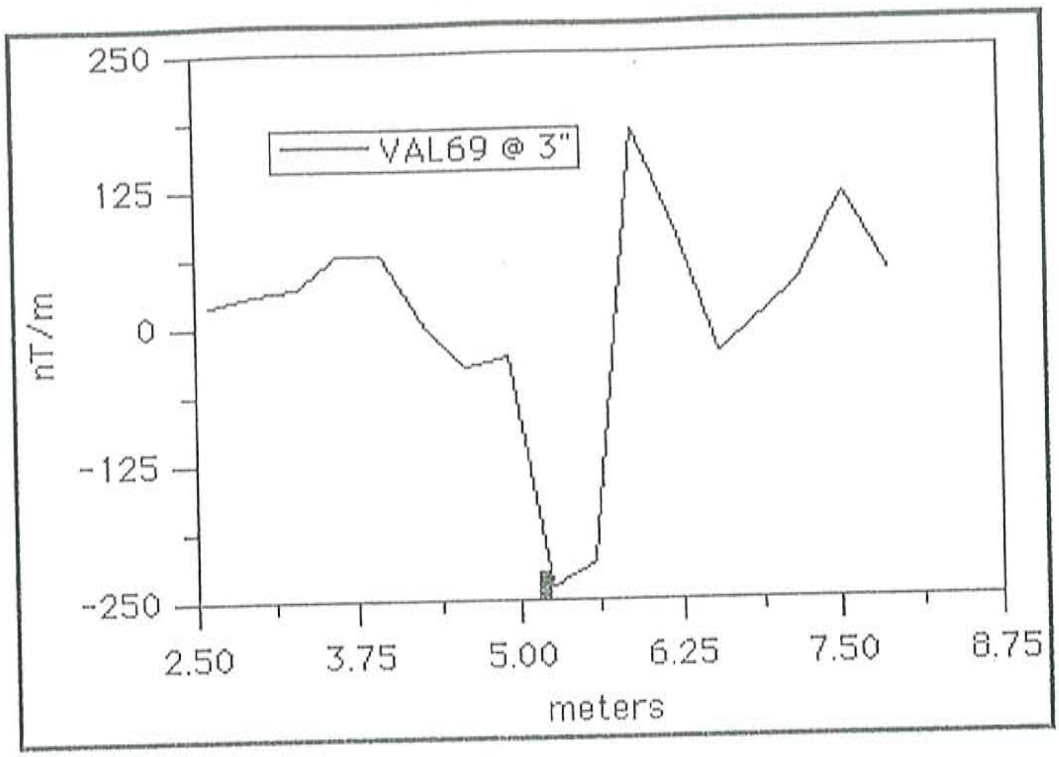

Figure 5.17: Magnetic vertical gradient plot of the Italian VAL69 non-metallic anti-personnel mine at a CTS land mine track. Shown is the gradient curve at a sensor separation of 0.7 meters and a gradient height of 0.7 meters. The VAL69 mine was buried 7.62 cm at the 5.2 meter position (black square). The data are unfiltered.

The VS2.2 anti-tank mine has a circular non-metallic casing but the physical characteristics for this mine were not available, but photographs revealed it to be of similar size to the M15. Its anti-personnel version, the VS50, contains no metallic components and it is assumed that the VS2.2 possesses the same basic fuse mechanism, with only increased RDX main charge mass. Thus it was assumed that it would be difficult to find as a void structure. The best detection signature of the VS2.2, for this mine track scenario, is shown in Figure 5.18. Although of low magnitude, the signature

was consistent during several lane surveys. The anomaly has a gradient of -25 nT/m and a detection radius of 0.35 meters at a burial depth of 2.54 cm

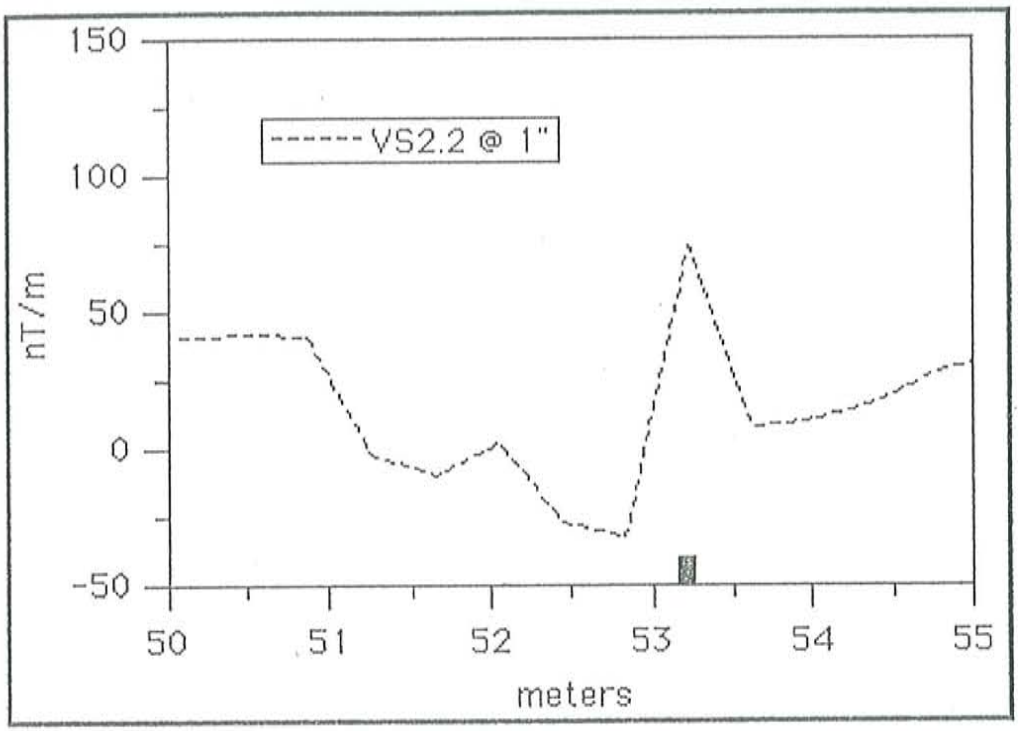

Figure 5.18: Magnetic vertical gradient plot of the Italian VS2.2 non-metallic anti-tank mine at a CTS land mine track. Shown is the gradient curve at a sensor separation of 0.7 meters and a gradient height of 0.7 meters. The VS2.2 mine was buried 2.54 cm at the 53.2 meter position (black square). The data are unfiltered.

For the land mine signatures, several qualifying remarks should be made. The mass of the mines are given in the previous discussions considering only the casing. The land mines are often 3 to 4 times heavier, as seen in Table 4.1, because of the mass of the main and booster charges. Also, it should be noted that the land mines used at the CTS test tracks had been made inert for safety reasons. Thus any fuse modification that involved removal of metallic components resulted in lower signature strengths.

The anomaly signatures for each mine have amplitude and shape, but the curves are not unique. The signatures' characteristics, although based partly on sensor orientation and direction, are dependent on the position of the mine itself. All objects exhibiting induced magnetism have vector components of magnetization. Thus the orientation of the mine, i.e. radial position and angle of inclination, within the Earth's field effects the measured gradiometric signature. However, a range of peak gradients and detection radii are intrinsic properties for each mine. Anomaly characteristics are based on average negative gradient peaks as measured from the initial survey plots. The detection radii are average horizontal distances from the mine's center of magnetization where the gradients are measurably higher than the background noise level.

5.3.3 UXO Detection

During the UXO deployments only one test lane was surveyed. Thus the UXO data set is biased to the geologic noise conditions at Test Track 3. The test lane was 2 meters in width but gradiometric readings were only taken along the centerline of the lane. The detectability of the UXO was therefore highly dependent on the UXO proximity to the lane centerline. The original centerline gradient plot is shown in Figure 4.13. The original gradient plot contained 10 UXO detections out of 25 possible sources, and 7 false positives. Figures 5.19 and 5.20 show the centerline plot after Laplacian filtering, and after filtering and amplitude correction, respectively.

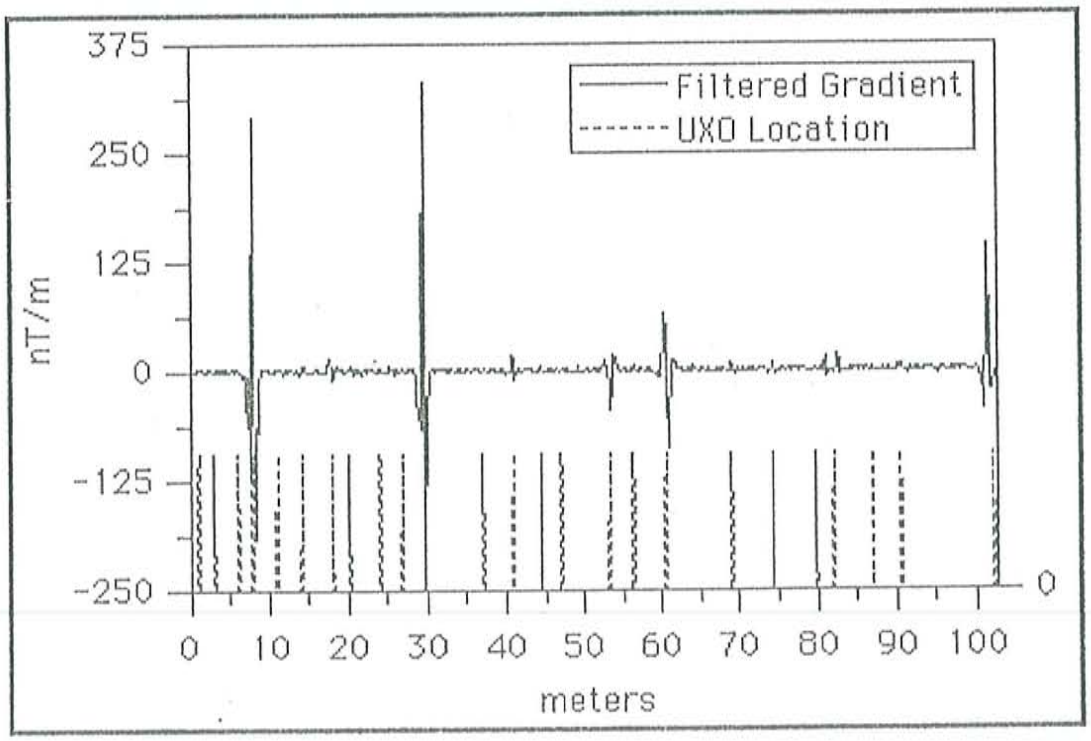

Figure 5.19: Magnetic vertical gradient curve of a UXO survey on the Track 3, Lane 1 centerline. The sensor separation was 0.7 meters and the gradient height 0.85 meters. Recording was continuous at a sampling rate of 0.1 seconds. The plot also shows the approximate location of buried UXO (dashed lines). With the data spatially filtered, the detection ratio was 16 targets found out of 25 UXO sources and 5 false positives.

The dashed peaks at the bottom of the plots show the approximate position of UXO sources within the full width of the test lane, thus a low amplitude peak may indicate a high gradient source far from the centerline. The positive detection of UXO in the figures is evident when the solid line peaks correlate with source position indicator beneath it.

The filtered plot in Figure 5.19 reveals 16 detections out of 25 sources with 5 false positives. By additionally scaling the amplitude (Figure 5.20), the detected sources increases to 20 detections out of 25 sources but the number of false positives increases to 7.

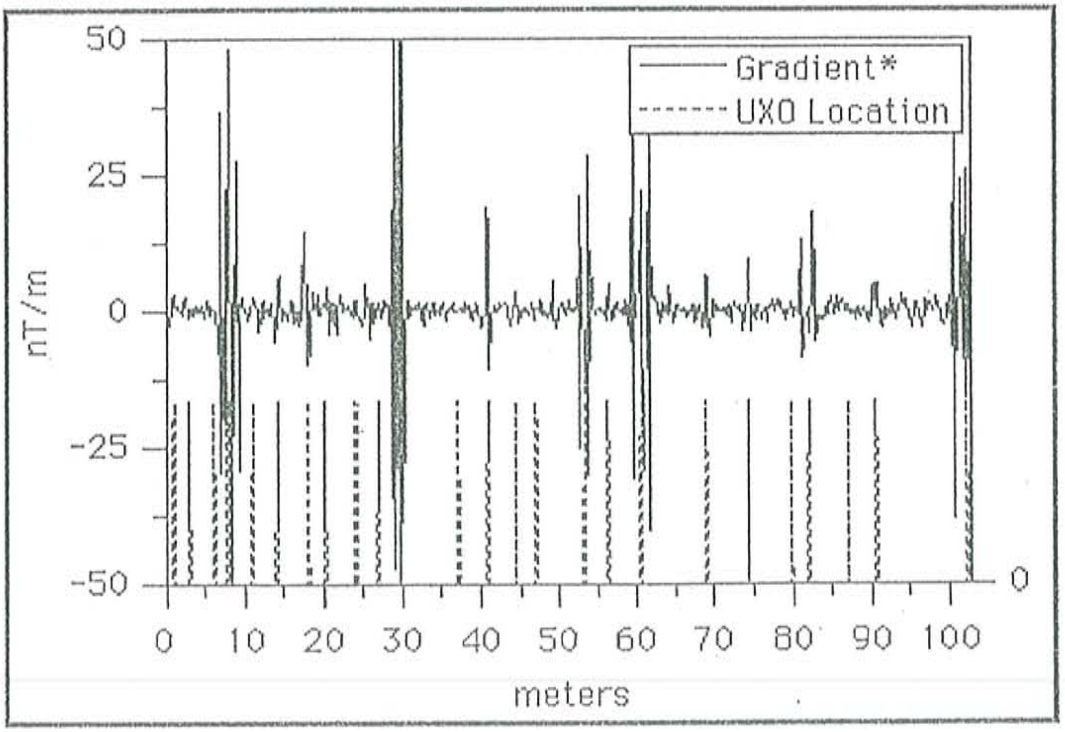

Figure 5.20: Magnetic vertical gradient curve of a UXO survey on the Track 3, Lane 1 centerline. The sensor separation was 0.7 meters and the gradient height 0.85 meters. Recording was continuous at a sampling rate of 0.1 seconds. The plot shows the approximate location of buried UXO (dashed lines). With the data spatially filtered and amplitude scaled, the detection ratio was 20 targets found out of 25 UXO sources and 7 false positives.

5.3.4 Land Mine Detection Blind Test

The ability of the gradiometer to detect land mines, both instantly and after processing, was put to the test during a blind detection survey on Track 1. The initial survey consisted of operating the gradiometer in SEARCH MODE while roaming the test lane in search of anomalous gradient readings. Once I was convinced that an anomaly observed on the console display resulted from a buried land mine, its surface position was marked. At this point I also attempted to note the type of mine and relative depth of burial I expected based on the characteristics of the gradient anomaly. The initial survey was a non-recording search and thus the results consisted of the flagged positions and comments shown on the map in Figure 5.21.

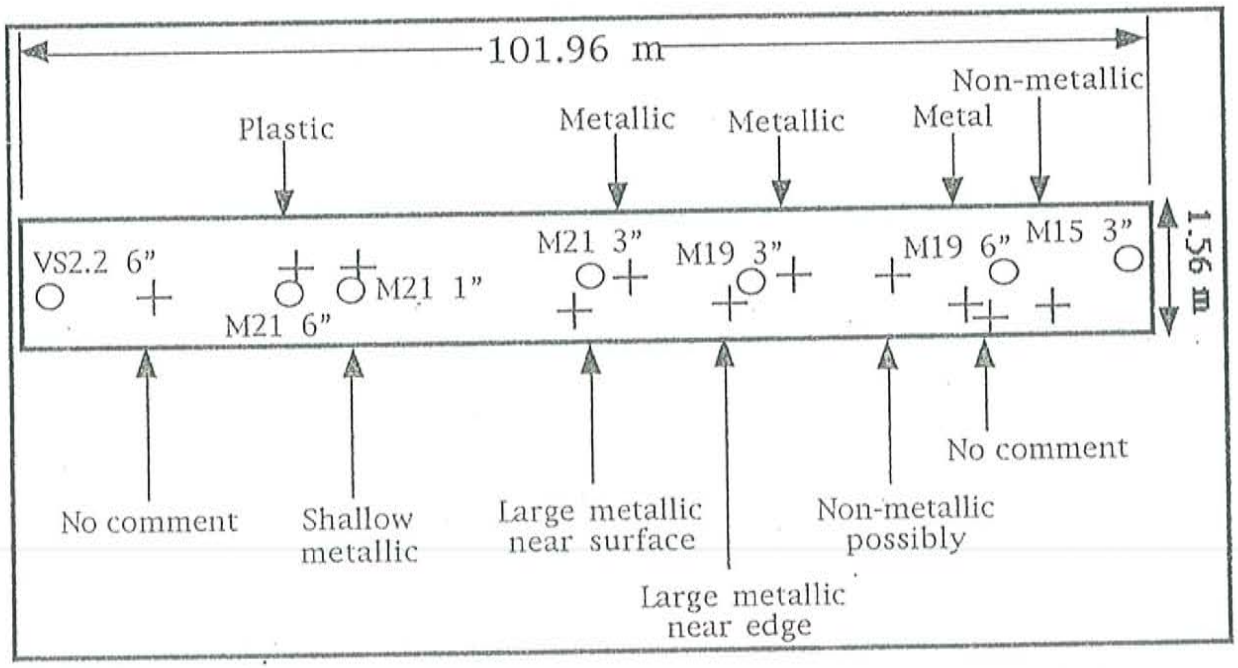

Figure 5.21: Map diagram of the GDE Blind Test Lane. The markings within the lane indicate the search results of a in-field mine detection test. Cross-hairs are the suspected mine locations and circular marks are actual buried mines. These detections were made using the G-858 in the SEARCH MODE while slowly passing the sensors, at a 0.7 meter separation, over the lane's area and scanning for anomalies.

The cross-hair marks within the test lane indicate suspected mine locations. The circles indicate the actual location of buried mines, their type and depth of burial. This initial in-field search yielded a detection rate of 3 targets found out of 7 possible mines and 8 false positives.

Immediately following the SEARCH MODE portion of the blind test, a standard recorded MAPPED SURVEY was performed that generated the gradient contour map seen in Figure 4.19. Processing was performed on the test lane data to increase the signal to noise ratio and enhance the detection rate. This processing included spatial Laplacian filtering and amplitude scaling. The resulting composite detection map is shown in Figure 5.22. The mine type and depth of burial is indicated beside the mapped anomalies for each of the 7 mines. This processed data map yielded a detection ratio of 6 targets found out of 7 possible mines and 3 false positives.

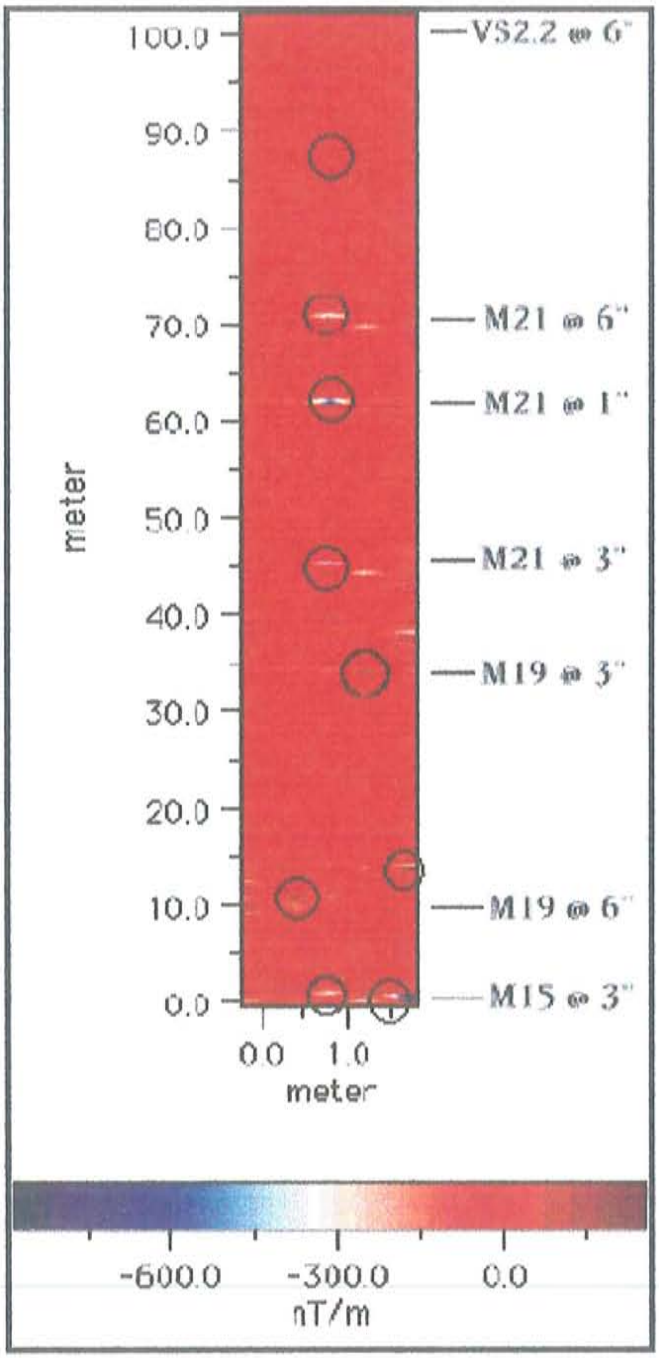

Figure 5.22: Magnetic vertical gradient contour map of GDE Blind Test Lane. The map shows the suspected location of buried land mines (circle within map) and the approximate location of the actual mines (name on side of map). The sensor separation was 0.7 meters, the gradient height was 0.7 meters, and the continuous sampling rate was 0.5 seconds. The data were processed and yielded a detection ratio of 6 targets found out of 7 possible mines and 3 false positives.

The GDE Blind Tests provided detection results based on two different applications of the gradiometer, a search mode operation similar to metal detector techniques, and a magnetic mapping survey similar with geophysical exploration methods. The detection results are listed for comparison in Table 5.1.

Table 5.1: Gradiometric Detection Results for GDE Blind Test

Target Type	Target Description *	Burial Depth (cm)	Detected In-field	Detected on Survey Map
M15	M-AT	7.62	0 for1	1 for 1
M19	M-AT	2.54	0 for1	1 for 1
M19	NM-AT	15.24	0 for 1	1 for 1
M21	M-AT	2.54	1 for 1	1 for 1
M21	M-AT	7.62	1 for 1	1 for 1
M21	M-AT	15.24	1 for 1	1 for 1
VS2.2	NM-AT	15.24	0 for 1	0 for 1
			11 total flags	9 total flags

*= M: metallic casing / NM: non-metallic casing / AP: anti-personnel / AT: anti-tank

The obvious problem resulting from the gradient maps presented in this chapter, is the occurrence of false positives in the data that either pad the detection possibilities or corrupt the plots themselves. In combating false positive sources it is important to complete an encompassing catalog of possible contributors. The next chapter investigates magnetic phenomenon that lead to false positive detections and provides examples of sources encountered during this research project.

Chapter 6
Discussion: Possible Sources of False Positives

6.1 False Positive Sources

In the detection of unexploded ordnance and land mines, the ability to distinguish between true targets and false targets becomes increasingly important due to the high cost and limited man-power of demining projects. As the number of false positive detections seen in the maps of Chapter 5 indicate, this is a common problem associated with single detection method surveys. For example, in the magnetic gradient map shown in Figure 6.1 there appears to be 13 shallow buried objects possessing gradiometric signatures comparable to ordnance. In actuality only three anomalies on the map are land mines, the rest are false positives. Thus it is important to consider possible false target sources that may be encountered during a detection survey. These sources can be complex and numerous, with the most common being magnetic rocks. The mechanisms by which geological structures become magnetic, either induced or remnant, depends on the thermal, chemical, and mechanical history and mineral assemblage of the rock or soil in question.

During a magnetic detection survey for land mines or UXO these factors must be addressed. The following sections of this chapter deal with possible sources of falsely identified targets. These sources fall into two main categories of magnetism, induced magnetization and remnant magnetization. Both geologic structures and buried artifacts behave magnetically via one, or both, of these two mechanisms.

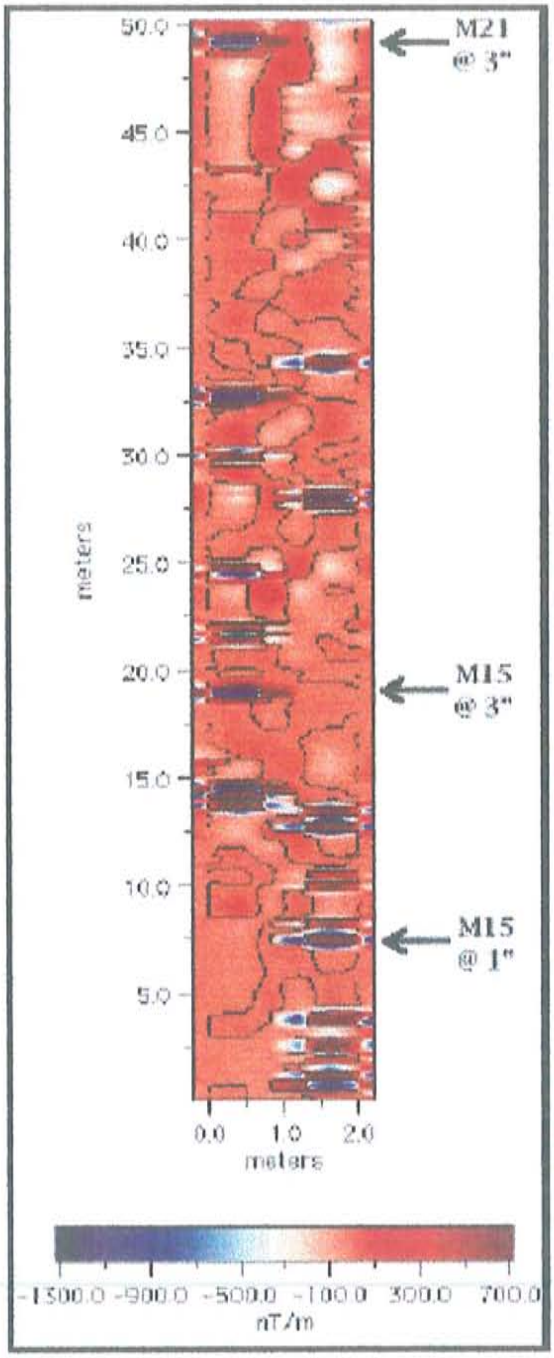

Figure 6.1: Magnetic vertical gradient contour map of CTS land mine track showing the occurrence of false positive detections. Of the 13 shallow source anomalies visible on the map, only the three indicated with arrows are land mines. The mine types, approximate locations, and depths of burial are indicated in the map.

6.2 Induced Magnetization Sources

6.2.1 Properties of Induced Magnetism

The most common source of false positive detections associated with magnetic survey techniques are sources of induced magnetization. Induced magnetization refers to the action of the Earth's ambient magnetic field on the material. As a result of induced magnetization, the material in an object causes the magnetic field to be enhanced and the object itself acts as a magnet. The magnetization of the material is directly proportional to the intensity of the ambient field and to the ability of the material to enhance the local field (Steiner, 1977). This ability is the object's magnetic susceptibility and determines the magnitude, or intensity of the materials induced magnetization. Without the inducing field the material would not behave magnetically. The induced intensity of magnetization (I) is equal to the product of the magnetic susceptibility (k) and the earth's ambient field strength (H) or

$$I = k\ H$$

Induced magnetization is common both in geologic structures and in man-made objects. The sources of induced false positives in the sub-surface include magnetic clasts or rock structures, buried metallic or magnetic artifacts, and accumulations of soil with a high magnetic susceptibility.

6.2.2 Induced Magnetic Anomalies from Rock

The magnetic susceptibility of a rock containing magnetite is simply related to the amount of magnetite it contains as well as the form of the magnetite found. Solid pieces of magnetite can have susceptibilities 10 to 30 times greater than pulverized magnetite grains of the same total mass.

Generally magnetite is uniformly distributed throughout a rock and is higher for igneous and metamorphic rocks than for sedimentary rocks (Sanford, 1994). During a magnetic survey for ordnance it will be igneous and metamorphic rock clasts that will produce the highest instances of false positives. An example of an anomaly produced by magnetism induced in a rock in the shallow subsurface is shown in Figure 6.2.

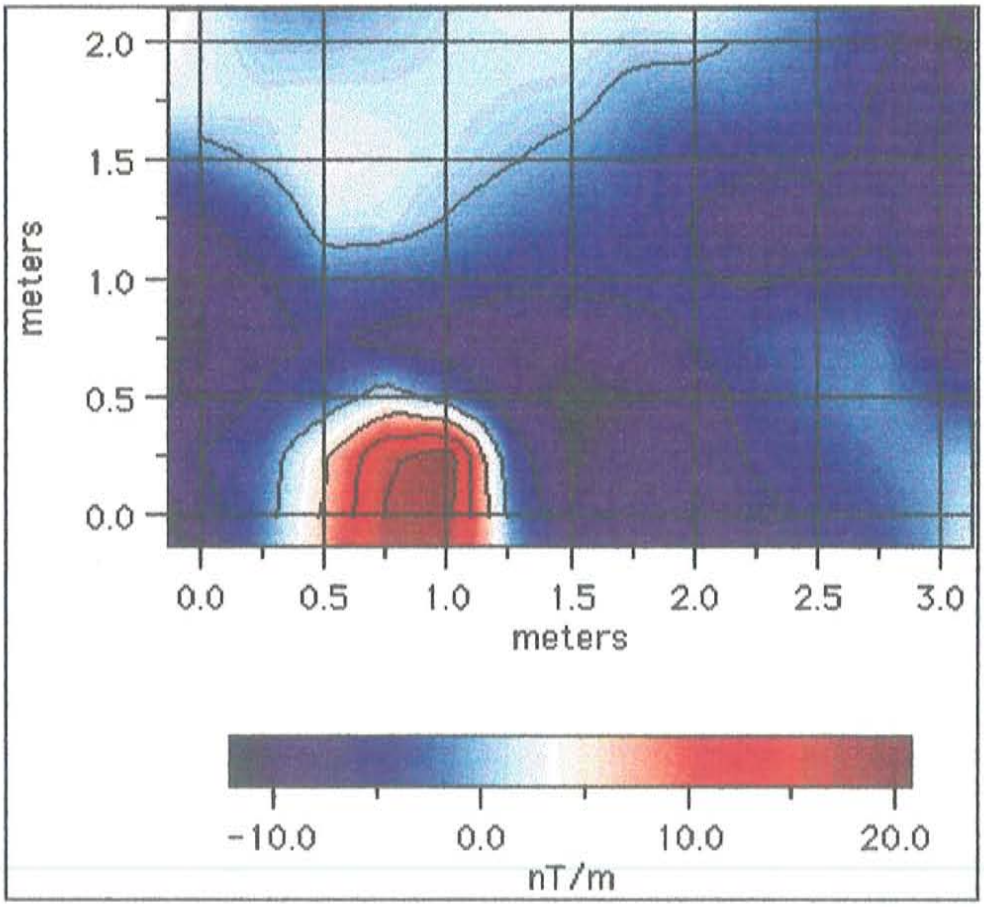

Figure 6.2: Magnetic gradient map of induced magnetism in a rock 10 cm in diameter and partially exposed on the surface. This survey was performed at desert site north of the EMRTC building. Station spacing was 0.5 meters, sensor separation was 0.7 meters, and gradient height was 0.65 meters. The data were recorded on 9/24/96.

The anomaly produced by the rock is 20 nT/m in magnitude and 1 meter wide. The rock was igneous, 10 cm in diameter, and partially exposed on the surface. Its anomaly is consistent for rocks possessing induced magnetization. Generally for objects exhibiting induced magnetism, the direction of the object's magnetization is the same as the Earth's field, 11.5 degrees North. The magnitude, or intensity of the object is determined by the amount of magnetite, and the proximity to the surface.

6.2.3 Induced Magnetic Anomalies from Buried/Surface Artifacts

Most soil types have a range of magnetic susceptibilities between 0.000001 to 0.1 cgs. However, magnetic susceptibilities of iron and steel are about 1 to 10^6 cgs (Steiner, 1977). Thus iron and steel objects generate the highest magnetic gradients associated with near surface objects. During a gradiometric survey for ordnance in a battlefield or habitational environment, surface and buried iron is probably the most common source of induced false positives. Anomalies resulting from these sources are characteristically have a sharp peaked profile, high in magnitude, and narrow in width. Figure 6.3 shows the gradient profile of a steel survey spike encountered along the boundary of a CTS test track. The spike was approximately 0.3 meters in length, 10 mm in diameter, and partially driven into the soil vertically.

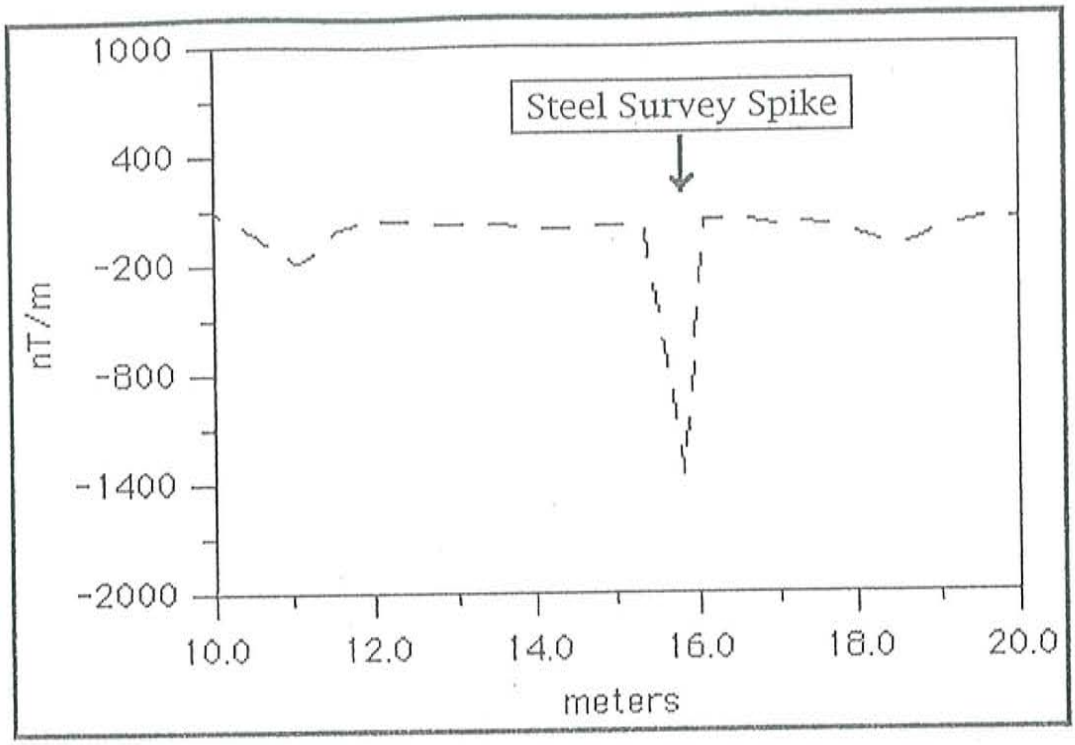

Figure 6.3: Magnetic gradient curve of induced magnetism in a steel survey spike 0.3 meters in length and partially buried vertically. The survey was performed at a CTS test track boundary. Station spacing was 0.5 meters, sensor separation was 0.7 meters, and gradient height was 0.65 meters. The data were recorded on 6/22/96.

6.2.4 Induced Magnetic Anomalies from Top Soil

As with all types of induced magnetic objects, the degree to which soil behaves magnetically depends on the magnetic properties of its constituent particles. Soil possesses a magnetic susceptibility that is dependent on its percent composition of magnetic minerals such as magnetite and other iron and titanium oxides (Steiner, 1977). Generally the magnetite concentration is depth dependent, inversely proportional to depth beneath the surface. The upper soil horizon, or A horizon, has a higher magnetic susceptibility than the horizons beneath it or of its parent rock. The susceptibility decrease with

depth is generally linear with typical loess soils having an order of magnitude change in susceptibility between the surface and 1 meter (Scoller et al., 1990)

The degree to which soil may contribute to false positives is dependent on the magnetic susceptibility contrasts between the uniform background soil magnetism and that of localized magnetic sediment accumulations. An area may possess highly magnetic soil but if it is uniformly distributed a survey would not generate a point source anomaly consistent with buried ordnance. However if in the process of inserting the ordnance, magnetic soil was removed, agitated, and partially replaced, then a detectable anomaly is probable. There are soil conditions that may mimic this tale-tell sign including animal borrows, ground water sink holes, surface water run-off patterns, and soil volcanoes caused by liquefaction, as well as man-made soil alterations. All of these mechanisms cause accumulation of foreign soil in relatively small pockets within native soil. Independent of whether it is the native or foreign soil possessing the greatest magnetism, a magnetic anomaly may result.

Anomalies resulting from surface accumulations of high susceptibility soil are generally broad in width and low in magnitude. Desert soils and sand lack significant magnetite concentrations to produce these types of anomalies. Agricultural and woodland terrain possess soils conducive to this false target phenomenon.

6.3 Remnant Magnetization Sources

6.3.1 Properties of Remnant Magnetism

Another common source of false positives associated with buried or surface objects within a magnetic survey are those possessing a permanent, or remnant magnetization. Remnant magnetization is often the predominant magnetization in igneous rocks and metal alloys (Steiner, 1977). Permanent magnetization depends on the metallurgical properties and the thermal, mechanical, and magnetic history of the object and is independent of the field in which it is measured. The high values of remnant magnetization are related to the effects of heating. Prior to heating the small domains within the magnetite crystal are randomly oriented. During heating at high temperatures the domains reorient themselves in the direction of the ambient field and are thus parallel to each other creating a net magnetization fixed within the object on cooling (Steiner, 1977).

Remnant magnetism is generally dissimilar to induced magnetism in the character of its mapped anomaly. While objects with induced magnetism maintain a direction of magnetization parallel to the Earth's field, objects with permanent magnetism need not. The dipole nature of the anomaly shown in Figure 6.4 indicates that its direction of magnetization is northwest to southeast as the survey lines are parallel to magnetic North. This implies the source of the anomaly is permanent magnetism with a direction different from the Earth's field.

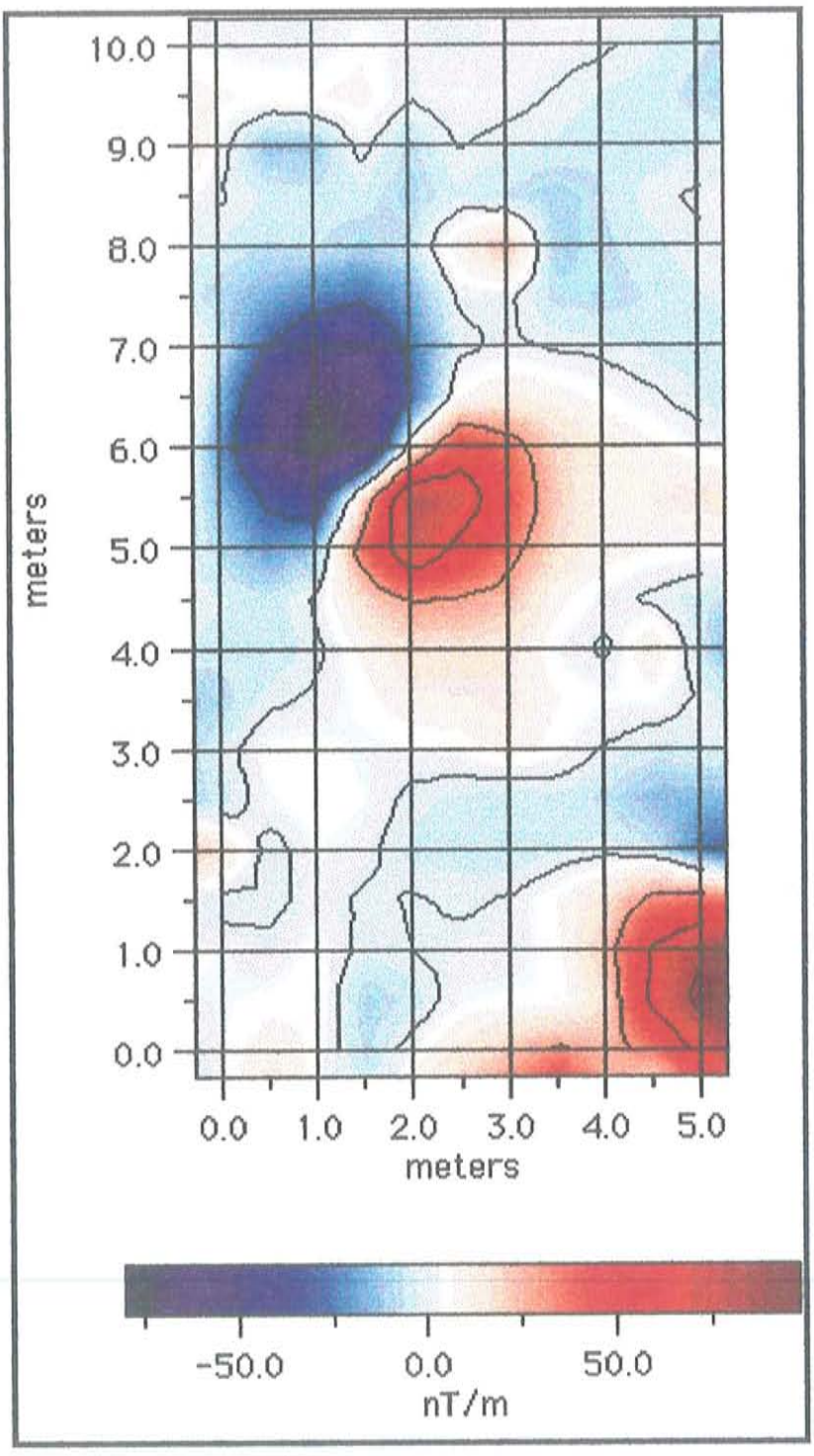

Figure 6.4: Magnetic gradient map of a remnant magnetization source. Survey performed at desert site north of the EMRTC building. Station spacing is 0.5 meters, sensor separation is 0.7 meters, and gradient height is 0.65 meters. Vertical gradients have had a local average subtracted. The data were recorded on 9/24/96.

6.3.2 Magnetic Anomalies from Thermo-Remnant Magnetism

The most common mechanism for producing remnant magnetism in rocks is thermal remnant magnetization or TRM. This mechanism is the primary source of permanent magnetism in igneous and metamorphic rocks. TRM is acquired when a rock is cooled from above the Curie temperature in the Earth's magnetic field. Initially the rock is above the maximum temperature at which its susceptibility causes magnetic behavior, and as the rock cools it becomes permanently magnetized at intensities several times greater than its original state of induced magnetism. For some extrusive basaltic rocks the magnetic intensity caused by TRM may be 100 to 200 times greater than its magnetization due to susceptibility induced magnetism (Sanford, 1994).

Sub-surface basalt clasts possessing TRM may produce anomalies similar to metallic permanent magnets, and are the chief source of false positives in areas of volcanic dominated petrology like the Counter-Mine Test Site. Figure 6.5 shows the magnetic anomaly produced by rock clasts possessing thermal remnant magnetism.

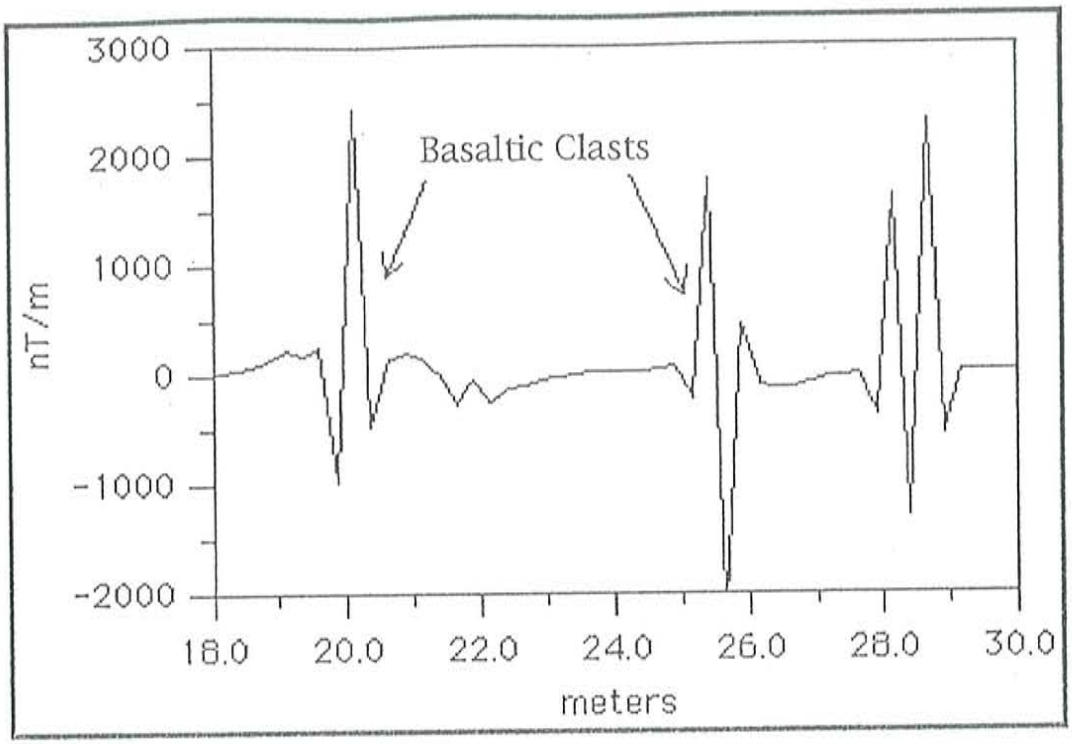

Figure 6.5: Vertical gradient profile of basaltic rock clasts possessing thermal remnant magnetism. Approximate locations of sub-surface rocks are indicated. Recorded during a land mine survey of CTS On-Road Track 2. Sensor separation is 0.7 meters and gradient height is 0.65 meters.

The clasts responsible for the 2000 nT/m anomalies in Figure 6.5 are worse case examples of TRM in the volcanic fields surveyed at the CTS.

6.3.3 Magnetic Anomalies from Isothermal Remnant Magnetism

Isothermal Remnant Magnetism (IRM) is a possible source of false positives in the detection of UXO. The chief mechanism for IRM is lightning strikes. The occurrence of lightning induced magnetic anomalies is possibly underestimated during magnetic prospecting in areas prone to that specific meteorological phenomenon.

A lighting strike problem in the search for UXO is not readily apparent until some basic statistical theory is applied. Most exposed rock outcrops and soil horizons do have a mathematical chance of being magnetically affected by lightning. If a strike does exist on a rock outcrop or soil surface its intensity might be great enough that no practical magnetic detection procedures could be carried out in that area. The intensity may also be weak enough that the fulgurite (soil structure caused by lightning) could be mistaken for a buried metallic object. The relative numerical probability that one, or multiple strikes, might occur is calculated based on the area of the terrain, the absolute age of the soil horizons down to some depth beyond which the lightning stroke's current ceases to flow (which may be significant), and the lighting stroke distribution density in the area as determined through meteorological studies.

For the purposes of probabilistic conservatism, it will be assumed that the soil age used in the calculation is the maximum depositional age of any horizon within the effective range of the stroke's penetrative current. Also considered a conservative assumption, is that the stroke distribution in an area is uniform both temporally and spatially. Thus if a terrain is y years old and possesses a stroke distribution of N strokes per year per area. Then the probability of finding a stroke in any area is:

$$\frac{strokes}{unit\ area} = \frac{N\ strokes}{area\ \ year} \circ y\ \ age\ \ in\ \ years$$

For example, in the Socorro area lightning may strike with a distribution density of once every year per square kilometer, thus for surfaces containing a soil layer or rock outcrop of age 10,000 years old, there is a probability that a lightning strike exists every 100 square meters. If the

surface is 100,000 years old there might be a strike every 10 m^2, that is just over 3 meters on a side. The upper meter of artificial soil on test tracks at the Counter-mine Test Site are only several months or years old, thus the density of lightning strikes is statistically negligible. However, country mine fields, jungles, and deserts can possess soils of considerable age and are more susceptible to these statistical discussions.

Isothermal Remnant Magnetism (IRM) creates magnetic anomalies as a result of lateral variations in the intensity of permanent magnetism in rock outcrops and soil deposits. During the formation of IRM a sample of rock or soil containing ferromagnetic minerals such as iron oxides, magnetite, and maghemite, is subjected to a magnetic field of intensity and direction other than that of the ambient field. The rock will then acquire an intensity of magnetism that is dependent on the strength of the applied field. As the applied field is removed or reduced back to ambient the increased intensity of the material's magnetism does not go to zero, but rather retains a small residual magnetism of intensity I_R which is a small fraction of the total applied field I_T (Sanford, 1994). The entire application of residual magnetism occurs at a constant temperature and is thus independent of Curie-effect Thermal Remnant Magnetism. Figure 6.6 shows the hysteresis curve by which the materials magnetic intensity behaves during the application and removal of the applied field. The final intensity of the object is incremented by I_R.

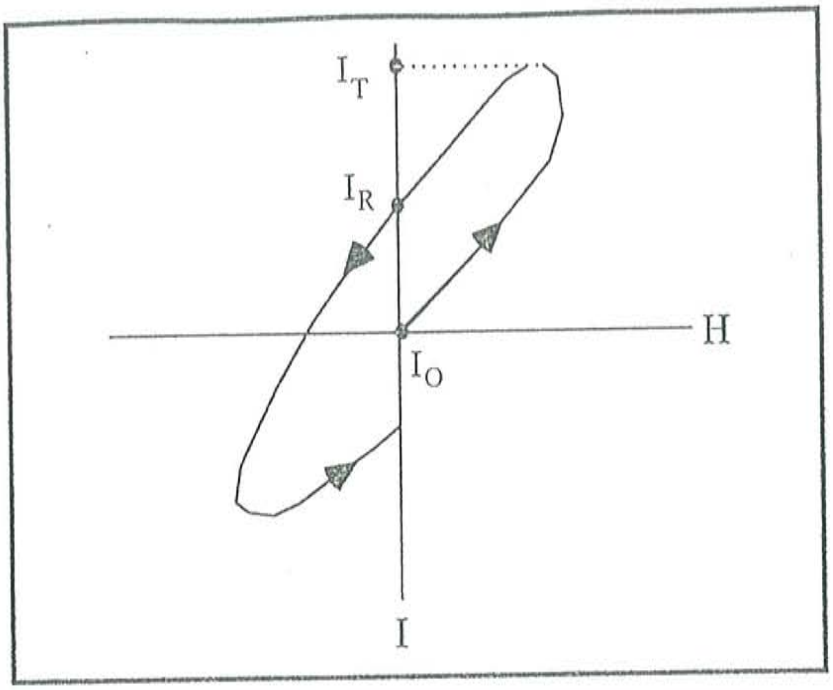

Figure 6.6: Hysteresis curve by which a rock's magnetic intensity behaves during the application and removal of the applied field I_T. The final intensity of the object's initial state I_o is incremented by I_R.

Lightning strikes produce IRM anomalies with magnetic intensities varying from significant (tens of nT) to tremendous (thousands of nT). About 90% of all lightning carries a negative charge to the earth, mostly discharged in 40-50 microseconds. The temperature of the plasma in a lightning strike can be as high as 2×10^4 °C, but any thermal remnance is localized and is negligible compared to the magnetic effect of the current discharge. Although half of all strikes discharge less than 25 kiloamps (kA), it is often several hundred kA (Lopez, 1987). The electrical energy is carried in a wide variety of frequencies, mostly in the 10-12 kHz range, but these frequencies are variations of a unidirectional current so the rocks only respond to the magnetization associated with the peak direct current (Fisher, 1993). The main current usually travels horizontally from the strike, passing through the

higher conductivity soil and surface water, but decays exponentially with depth so that the magnetic effects are restricted mainly to the top 20 meters. Rocks along the path of maximum current may become magnetically saturated, but at greater distances from the strike they acquire an IRM which is superimposed on their pre-existing remnant.

Measured fields at the base of triggered lightning channels may be used to estimate magnetic intensity associated with IRM. The situation in which peak amplitude currents are measured for return strokes from triggered lightning can be used to calculate azimuthal magnetic fields for each stroke. The simplest relationship applicable to the situation is Ampere's law equaling the magnetic field resulting from a propagating current.

$$H(t) = \frac{I(t)}{2\pi r}$$

where H(t) is the magnitude of the azimuthal component of the magnetic field, I(t) is the current flowing in the channel, and r is the radial distance from the strike point. Studies have shown that the magnetic fields at ground level out to a range of 20 meters from the base of a lightning channel are well described by Ampere's law (Fisher, 1993).

Typical current amplitudes associated with moderate lightning strokes range in value from 5 to 50 kA. Thus within a radius of 1 to 2 meters of a strike, applied magnetic fields may be as high as 8000 Ampere per meter (50 kA over 1 m radius). Since the H-field varies inversely proportional to distance, the field at a 0.5 m radius would be 16,000 A/m for the same current. 16,000 A/m is over 2×10^7 nT. This is 3 orders of magnitude greater than the ambient H-field of the Earth.

Resulting residual remnant magnetism is of course dependent on the characteristic magnetic susceptibilities of the rock or soil. Volcanic rocks, gray reduced clay, black soil, and ferrous-rich minerals will retain the most remnant magnetism, while average top soil, limestone, granite, gravel and oxidized clay will retain the least magnetism upon being struck by lightning (Aitken, 1974).

A magnetic survey of a volcanic outcrop mesa southwest of Socorro provides insight into possible lightning stroke magnetic anomalies. Black Mesa is a relatively old volcanic surface upon which the Sled Track Facility of EMRTC is built. Figure 6.7 shows a vertical magnetic field strength profile of a 100 meter strip of Black Mesa. Apparent in the profile is the huge magnetic fluctuation at the north end of the traverse. The amplitude of the peak is nearly 4000 nT and may represent the IRM of a lightning stroke. The soil and vegetation make it difficult to examine the surface for a scorch or fulgerite structure, however there was some discoloration over several large clasts in about a 0.5 meter radius.

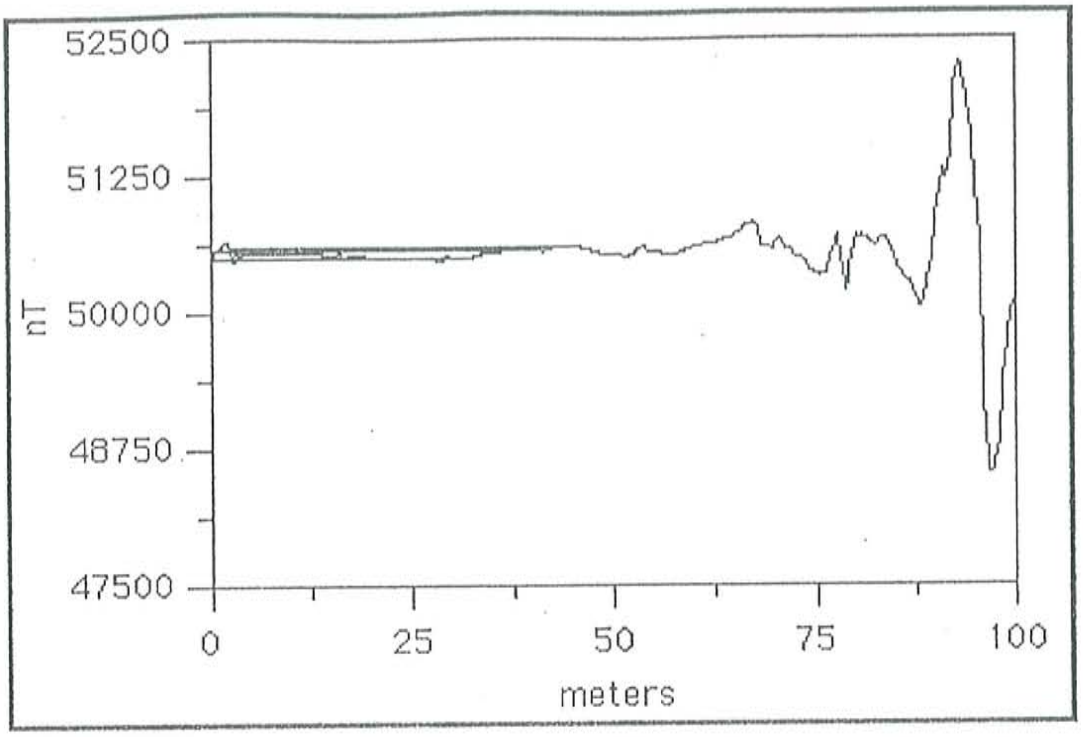

Figure 6.7: Vertical magnetic field strength profile of a 100 meter section of Black Mesa. The sensor height is 1.1 m and the meter marks begin south and progress north The large peak may represent a lightning strike.

Figure 6.8 shows a vertical magnetic field strength profile of a 200 meter strip of Black Mesa. This strip has a North-South orientation like the first but is approximately 30 meters west of it. Also apparent in the profile is the huge magnetic fluctuations near the center of the traverse. The amplitude of the peaks are nearly 6000 nT and may represent the IRM of one or more lightning strokes.

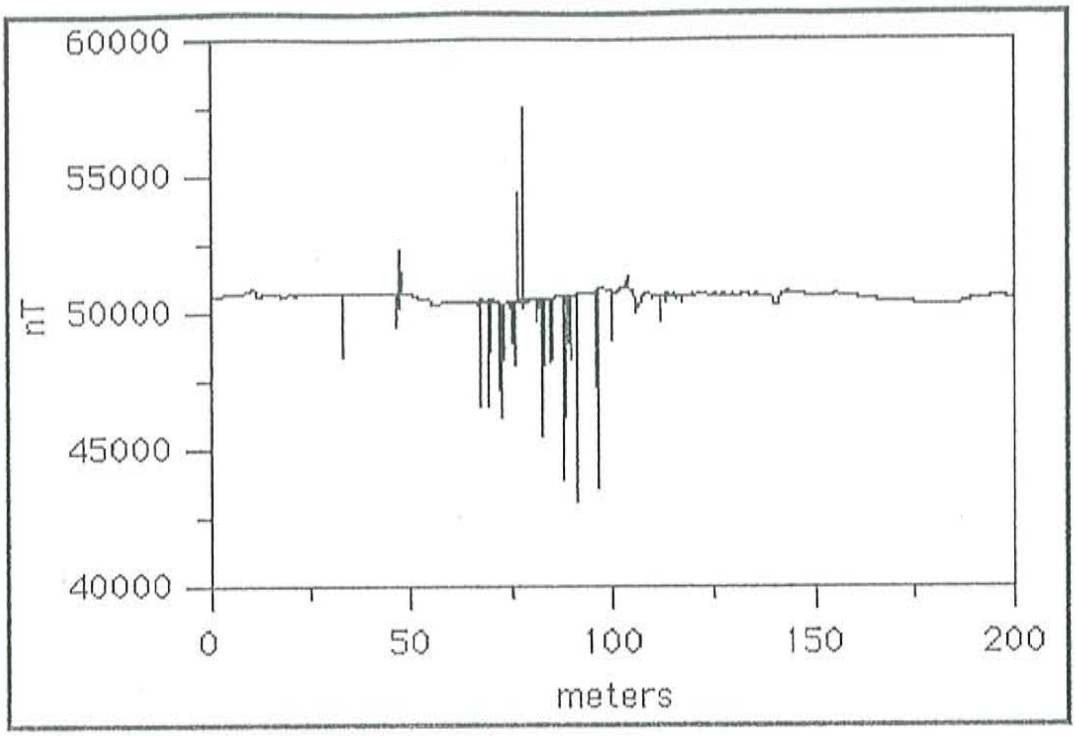

Figure 6.8: Vertical magnetic field strength profile of a 200 meter section of Black Mesa. The sensor height is 1.1 m and the meter marks begin south and progress north. The large peak may represent a lightning strike.

Although lightning produced soil structures are rare along roads and agricultural areas due their lack of aging and continued disturbance, open field areas may contain strike distributions of some significance. A meteorological understanding of an area to undergo demining with magnetometers is an important tool to avoid confusion and reduce false positives.

6.4 Equipment and Environmental Sources

6.4.1 Atmospheric Magnetic Storms

Magnetic storms are transient disturbances in the Earth's magnetic field caused by solar activity and the ionic bombardment of the Earth's magnetosphere. These storms may create magnetic fluctuations in the Earth's field with amplitudes exceeding several thousand nT at most latitudes (Sanford, 1994). Although erratic, magnetic storms often occur at 27 day intervals (solor rotation period) and thus correlate with the distribution of sunspot activity. Anomalies caused by magnetic storms in the atmosphere are not likely to be confused with a UXO signature; they are simply detrimental to a UXO search. Generally the fluctuations in the Earth's field caused by magnetic storms are erratic and cause the magnetometer's field readings to sporadically change, give null values, or cause signal loss in the sensors. Therefore, it becomes impossible to use the magnetometer in ordnance detection surveys during magnetic storms.

6.4.2 Sensor Malfunction

The magnetometer may produce spurious readings that could be interpreted as false positives. High magnetic gradients result when one sensor malfunctions or gives a null reading, leading to a large gradient computation. A null reading may be caused by a power loss to the sensor, a faulty cable connection, or a dead zone sensor reading. Dead zones are common to cesium sensors and result from insensitivity to magnetic fields in certain directions (Geometrics, 1995). If the magnetic field direction is within 15 degrees of the optical centerline of the sensor, or within 15 degrees of the

plane perpendicular to that plane, the sensor will read a 0.00 magnetic field value. If this occurs a gradient of zero will appear.

Thus during a land mine or UXO survey the sensors must be oriented to ensure a non-null reading. This orientation is dependent on the magnetic inclination at the survey site. Knowing this inclination, the software option CSAZ in the Geometrics MAGMAP application will help to determine the optimal sensor orientation. During the course of this study the vertical sensor orientation used was sensitive to fields with dip angles between 15 and 75 degrees from the horizontal (Geometrics, 1995). The local 61 degree inclination safely fell within this range avoiding dead zone readings.

During a gradiometer search for land mines or UXO it is vital that data quality be monitored either visually or by some automated technique. To establish that an anomaly reading is valid, it may be necessary to repeat a measurement several times. Successive readings in the same location should not vary by more than the gradient sensitivity, 0.14 nT per meter for a 0.7 meter sensor separation. Extreme variations of tens of nT per meter are indicative of a degradation in the signal to noise ratio and are caused by either a sensor power fluctuation or a magnetic storm (Steiner, 1977).

Cesium sensors are sensitive to extremely high magnetic gradients that may cause the magnetometer to lose signal indefinitely until the computer is restarted. These high gradients result from proximity to large metallic objects such as fences, vehicles or buildings, AC power lines or transformers, or massive iron ore bearing rocks. In the case where only one sensor signal is lost, the resulting gradient measurement is easily identified in the data stream as a gradient equal to the local field strength divided by the sensor separation, i.e. 50,760 nT minus zero nT divided by 0.7 meters equals 72,514 nT/m.

Fortunately the Geometrics Magnetometer monitors the signal and data quality and gives quality control warnings based on programmable parameters. Warnings are given both graphically and via audio tones if signal quality or sporadic fluctuations occur. It is the small scale anomalies caused by atmospheric or equipment based fluctuations that may create false positives in ordnance surveys. The gradient fluctuations that escape the instrument or operator quality controls may show up in the data as anomalies with amplitudes and dimensions similar to ordnance signatures.

Chapter 7
Conclusion: Magnetic Applicability To Counter-mine Efforts

7.1 Geometrics G-858 Magnetometer Performance

The use of differential measurements from two closely spaced sensors made it possible to detect magnetic disturbances arising from small objects, including voids, in the presence of a great deal of magnetic noise. The nearly instantaneous response of the cesium magnetometer, combined with rapid sampling rates, allowed for surveys to be done in a fraction of the time required by predecessing magnetometers. The instrument capabilities that aided in data quality and object detection were the cadence beats for pacing, signal quality warnings, and real time analog display of the magnetic field on the LED viewer screen. The G-858's dual lithium cell battery belt packs allowed for continuous field operation of the magnetometer for 3 to 5 hours daily, as well as efficient storage and transfer of the recorded data. Using the G-858 in the vertical gradiometer mode added additional weight and maneuverability constraints to field use, however, only a short period was needed to develop an efficient technique for maintaining control of the sensor staffs during surveys. Following all surveys, the data were transmitted via high-speed RS-232 data link to a PC computer for further analysis and map generation. The magnetometer to PC interface software, MAGMAP, allowed for the downloading of the magnetometers' binary data and conversion into the ASCII format, and also for significant data review and editing capabilities.

The gradiometer was essentially a first derivative operator that resolved composite or complex anomalies into individual components. The vertical gradients computed through the use of this survey technique reflected no long period absolute magnetic deviatoric phenomenon such as diurnal (temporal) and regional (spatial) fluctuations. For two-dimensional contour

maps, the gradiometer technique accentuated the small scale anomaly images of land mines and UXO, and reduced long-wavelength geologic anomalies contributing to the magnetic noise in the data.

A standard 0.7 meter sensor separation and 0.65 to 0.7 meter sensor midpoint height was adopted for land mine detection. Sensitivity increased with sensor separation and the 0.3 meter separation curve was nearly a flat response at zero nT/m. Gradient sensitivity increased with sensor separation, while the sensor's measurement was affected by the cube of the distance to the object. Considering the magnetic noise levels, expected depth of targets, and the limitations of the sensor staff assembly, the lower sensor was needed to be close to the ground while preserving maximum separation with the upper sensor.

7.2 Magnetic Exploration Results

7.2.1 Control Test Pad

The Control Test Pad (CTP) allowed for the systematic investigation of magnetic signatures associated with an array of magnetic and non-magnetic targets. The pad provided a near homogenous half-space layer that lacked large surface rocks and vegetation. The thick, homogenous, and relatively non-magnetic nature of the soil overburden provided a well defined medium with which to conduct magnetic surveys. The areas of magnetic investigation at the CTP were divided into four categories: soil magnetism, void detection, detection thresholds, and buried target mine signatures. Within the CTP were 5 test grids containing background vertical gradients in the ±10 nT/m range. A gradient of zero indicated that the field strength was constant within a

meter above the surface and thus the soil had no lateral changes in magnetic susceptibility.

The magnetic anomalies produced by 7.6 liter voids in the CTP soil averaged an absolute gradient of about -7 nT/m. The lack of soil magnetism yielded an insufficient susceptibility contrast for void detection based on gradient values alone within this soil type as the anomaly strengths were at or below background levels. Removing the background magnetism from the void anomaly isolated the gradient signature of the void. The resulting gradient curves showed small positive peaks above the void location. While these positive peaks were low amplitude (less than 5 nT/m) their small widths were distinguishable from the background levels.

The detectability limits for a vertical iron pin with the standard gradiometer sensor configuration and background magnetism was found to be 1.0 gram. The 1.0 gram iron pin had a mass and dimensions similar to mine fuse mechanisms and was buried 2 cm below the surface.

The CTP experiments provided magnetic anomaly signatures for metallic and non-metallic targets. The amplitudes and anomaly curves shown for each target were one of many possible non-unique signatures depending on soil conditions, target orientation and depth, sensor configuration, and target construction. However, the clues provided in the experiments lent much needed boundary conditions to the problem of mine and UXO detection

7.2.2 Counter-Mine Test Site

The majority of magnetometer data was gathered at a dedicated counter-mine testing facility coordinated by the Energetic Materials Research and Testing Center (EMRTC). The Counter-mine Test Site (CTS) contained test track lanes prepared with a number of buried foreign and domestic anti-personnel mines, anti-tank mines, and sources of unexploded ordnance. The testing environment at the CTS consisted of road-like tracks within which the mines and ordnance were buried. The tracks where created upon natural mesas within the volcanic outcrops and sedimentary fans of the southwest side of Socorro Peak. The top soil consisted of weathered tuft sediments and thin accumulations of silts and clays derived from adjacent alluvial fans. After the emplacement of a land mine or UXO, the soil was raked, saturated, and dried repeatedly to ensure the targets anonymity. Thus the only sources of magnetic anomalies expected in the testing lanes other than the buried ordnance were from volcanic clasts, survey stakes, and metallic debris resulting from previous inhabitation or testing programs in the area.

An in-field test for mine detection using the gradiometer in SEARCH MODE yielded a detection rate of 3 targets found out of 7 possible mines and 8 false positives. Immediately following the SEARCH MODE portion of the blind test, a standard recorded MAPPED SURVEY was performed. Processing of the test lane data increased the signal to noise ratio and enhanced the detection rate. This processing included spatial Laplacian filtering and amplitude scaling and yielded a detection ratio of 6 targets found out of 7 possible mines and 3 false positives.

The UXO surveys also had better detection rates after filtering of the data. The original gradient plot contained 10 UXO detections out of 25 possible sources, and 7 false positives. The filtered plot revealed 16 detections out of 25

sources with 5 false positives. By additionally scaling the amplitude the detected sources increases to 20 detections out of 25 sources but the number of false positives increases to 7.

Detection surveys during land mine deployments at the CTS also produced a catalog of individual magnetic anomalies associated with several foreign and domestic land mine types. Each mine produced a characteristic, though highly non-unique, magnetic gradient signature. The M15 was the first of the U.S. mines analyzed. The M15 anti-tank mine possesses a 3.9 kg circular metallic casing 0.34 meters in diameter. Its high degree of metallic construction made it a relatively simple mine to detect using the gradiometer. For most mine track scenarios, the mine's anomaly signature had a peak negative gradient of -490 nT/m and a detection radius of 0.85 meters at a burial depth of 2.54 cm. Anti-tank mines may often be buried significantly deeper, however this particular mine would probably generate a detectable anomaly to depths near a meter.

The M16 anti-personnel mine possessed a 3.1 kg cylindrical metallic casing 10.3 cm in diameter and 19.9 cm in height. Although it was volumetrically smaller than the M15, it contained nearly the same metallic components. The anomaly signature of the M16 had a peak negative gradient of -90 nT/m and a detection radius of 0.70 meters at a burial depth of 7.62 cm.

The M19 anti-tank mine was encased in a 3.2 kg square non-metallic container 0.33 meters in width. The mine's size aided in its detection when the background magnetic noise was not too great. The signature of the M19, for most mine track scenarios, had a negative gradient of -60 nT/m and a detection radius of 0.50 meters at a burial depth of 7.62 cm. Compared to a metallic anti-tank mine, the M19 was much more difficult to detect.

The M21 was the final U.S. mine analyzed at the CTS. The M21 anti-tank mine had a metallic casing but detailed physical characteristics were not available. The M21 signature had a dipole structure with a peak to peak gradient amplitude of ±250 nT/m, and a detection radius of 0.95 meters at a burial depth of 2.54 cm.

The two foreign land mines analyzed were the Italian made Valmara 69 and VS2.2. The Valmara 69 (VAL69) anti-personnel mine had a 2.7 kg cylindrical non-metallic casing 13.0 cm in diameter and 20.5 cm in height. Although it had a plastic casing and fuse cover, the VAL69 had internal metallic shrapnel which aided in its detection. The gradiometric signature of the VAL69 had a peak negative gradient of -220 nT/m and a detection radius of 0.35 meters at a burial depth of 7.62 cm.

The VS2.2 anti-tank mine had a circular non-metallic casing. Its anti-personnel version, the VS50, contains no metallic components and it is assumed that the VS2.2 possesses the same basic fuse mechanism, with only increased RDX main charge mass. The best detection signature of the VS2.2 had a gradient of -25 nT/m and a detection radius of 0.35 meters at a burial depth of 2.54 cm

The mass of the mines given in the previous conclusions considered only the casings. The land mines were often 3 to 4 times heavier because of the mass of the main and booster charges. Also, it should be noted that the land mines used at the CTS test tracks had been made inert for safety reasons. Thus any fuse modification that involved removal of metallic components resulted in lower signature strengths.

The anomaly signatures for each mine had a characteristic amplitude and shape, but the curves were not unique. The signatures' characteristics, although based partly on sensor orientation and direction, were dependent on

the position of the mine itself. All objects exhibiting induced magnetism have vector components of magnetization. Thus the orientation of the mine, i.e. radial position and angle of inclination, within the Earth's field effected the measured gradiometric signature. However, a range of peak gradients and detection radii were intrinsic properties for each mine. Anomaly characteristics given in this text were based on average negative gradient peaks as measured from the initial survey plots. The detection radii were average horizontal distances from the mine's center of magnetization where the gradients were measurably higher than the background noise level.

The local geology was the greatest source of magnetic noise as large volcanic clasts were abundant within the surface layer of the test tracks. Also present was the magnetic noise of metallic objects associated with surveying equipment, metal survey stakes, metal culverts. The soil, of variable magnetic susceptibility, created local field strength variations within a meter of the surface. Thus it is assumed that the data generated during the surveys were representative of actual land mine and UXO contaminated areas.

7.2.3 False Positive Target Realities

The number of false positives discovered during testing revealed the importance of considering possible false target sources encountered during a detection survey. These sources were complex and numerous, with the most common being magnetic rocks. The mechanisms by which geological structures became magnetic, either induced or remnant, depended on the thermal, chemical, and mechanical history and mineral assemblage of the rock or soil. These sources fall into two main categories of magnetism, induced magnetization and remnant magnetization.

During the magnetic surveys for land mines and ordnance at the CTS it was igneous and metamorphic rock clasts that presented the highest instances of induced false positives. During a gradiometric survey for ordnance in a battlefield or habitational environment, surface and buried iron is probably the most common source of induced false positives. Anomalies resulting from these sources were characteristically of a sharp peak profile, high in magnitude, and narrow in width.

An area may possess highly magnetic soil but if it is uniformly distributed a survey would not generate a point source anomaly consistent with buried ordnance. However if in the process of inserting the ordnance, magnetic soil was removed, agitated, and partially replaced, then a detectable anomaly is probable. There are soil conditions that may mimic this tale-tell sign including animal borrows, ground water sink holes, surface water run-off patterns, and soil volcanoes caused by liquefaction, as well as man-made soil alterations. All of these mechanisms cause accumulation of foreign soil in relatively small pockets within native soil. Independent of whether it is the native or foreign soil possessing the greatest magnetism, a magnetic anomaly may result. Anomalies resulting from surface accumulations of high susceptibility soil are generally broad in width and of low magnitude. Desert soils and sand lack significant magnetite concentrations to produce these types of anomalies. Agricultural and woodland terrain possess soils conducive to this false target phenomenon.

Sub-surface basalt clasts with CTS test lanes possessed Thermal Remnent Magnetization (TRM) resulting in anomalies similar to metallic permanent magnets, and were the chief source of false positives in the volcanic dominated petrology of the Counter-mine Test Site. Isothermal Remnant Magnetism (IRM) was also a possible source of false positives in the detection

of UXO. The chief mechanism for IRM upon a surface was lightning strikes. The occurrence of lightning induced magnetic anomalies was possibly underestimated during magnetic prospecting in this area which has been prone to that specific meteorological phenomenon. Although lightning produced soil structures are rare along roads and agricultural areas due their lack of aging and continued disturbance, open field areas may contain strike distributions of some significance. A meteorological understanding of an area to undergo demining with magnetometers is an important tool to avoid confusion and reduce false positives.

References

Aitken, M.J. (1974). Magnetic Prospecting. *Physics and Archaeology.* Oxford University Press. pp 207-240

Cameron, D. (1967) Magnetic Detection of Certain Light Weapons, Mines, Grenades and Equipment. Quantum Electronics Division Technical Report. Varian Associates. Palo Alto, CA.

Dunlop, N.(1995). Cambodia: An Exhibition of Photographs By Nic Dunlop. In *Oneworld Online Landmines Special Report Gallery.* [Online] . Oneworld Online. Available: http:/www.oneworld.org/landmines /gallery [1997, March 20].

Energetic Materials Research and Testing Center EMRTC (No Date). Countermine Test Facility. In *EMRTC Field Laboratories* [Online]. Available: http:/www.emrtc.nmt.edu/countermine.html [1996, December 22].

Environmental Security Technology Certification Program (ESTCP) (1996). Draft ESTCP Test Plan: Remote Controlled Surface/ Near Surface UXO Detector. Energetic Materials Research and Testing Center. Socorro, NM.

Fisher, R. (1993). Measured Fields and Earth Potentials at 10 and 20 meters from the Base of Triggered Lightning Channels. SNL, Albuquerque, N.M Government Microfiche. NMT #E 1.99:SAND-93-2735C. 1993.

Fowler, C.M.R. (1990). *The Solid Earth, An Introduction to Global Geophysics.* Cambridge University Press, New York, NY.

Fyfe, K. (1996). Present Detection Methods. In *A Mechanical Means of Landmine Detection* [Online]. Mechanical Engeneering Department, University of Alberta. Available: http:/faramir.mece.ualberta.ca/ landmine/present.html [1997, March 10].

Geometrics (1995). Geometrics G-858 Magmapper Operations Manual. Geometrics, Inc. Sunnyvale, CA.

Geometrics (1997). G-858 Portable Cesium Magnetometer. In *Land Magnetometers*,[Online]. Available:http:/www.geometrics.com/858.html [1996, December 22].

Geyer, R.G. (1988). Magnetostatic Measurements for Mine Detection. Technical Report. Electromagnetic Fields Division, National Institute of Standards and Technology. Boulder, CO.

Hurley, G. (1996). The Perfect Soldier: Stealing a glimpse of Angola. In *Oneworld Online Landmines Special Report* [Online] . Oneworld Online, Oxfam Press. Available: http:/www.oneworld.org/landmines [1997, March 10].

Lopez, R. E., Holle, R.L. (1987). The Distribution of Summertime Lightning as a Function of Low-level Wind Flow in Central Florida. NOAA Technical Memorandum. ERL-ESG-28. July.

Oneworld Online (1997). Landmines: A Special Report. In *Landmines Home Page* [Online] , Oneworld Online. Available: http:/www.oneworld.org/ landmines [1997, March 10].

Parker, R.L. (1994) *Geophysical Inverse Theory.* Princeton University Press, Princeton, New Jersey.

Sanford, A. (1994) Magnetic Method. Geop 445 Class Notes, pp 87-109

Scollar, I., et al. (1990) *Archaeological Prospecting and Remote Sensing.* Cambridge University Press. Cambridge New York, NY.

Steiner, C. (1977) Applications Manual for Portable Magnetometers. Geometrics, Inc. Sunnyvale, CA.

Telford, W.M., Geldart, L.P. and Sheriff, R.E. (1990). *Applied Geophysics, Second Edition.* Cambridge University Press, New York, NY.